63 3 4

CT AF 61(052) 7

JAN 1963

403 765

AFCRL - 63 - 401

403765

AS AD NO.

CF. ASTIA

TECHNICAL REPORT

VARIATIONS OF THE SEA LEVEL MUON FLUX

F. ASHTON, B.Sc., Ph.D.,

J.B.M. PATTISON, B.Sc.,

and A.W. WOLFENDALE, B.Sc., Ph.D., F.Inst.P.

DEPARTMENT OF PHYSICS,

DURHAM COLLEGES,

UNIVERSITY OF DURHAM,

DURHAM, ENGLAND.

D D C

MAY 14 1963

TISIA B

AD

TECHNICAL REPORT

VARIATIONS OF THE SEA LEVEL MUON FLUX

F. ASHTON, B.Sc., Ph.D.,

J.B.M. PATTISON, B.Sc.,

and A.W. WOLFENDALE, B.Sc., Ph.D., F.Inst.P.

DEPARTMENT OF PHYSICS,

DURHAM COLLEGES,

UNIVERSITY OF DURHAM,

DURHAM, ENGLAND.

ABSTRACT

Studies of cosmic ray muons have been made with a spectrograph comprising a solid iron magnet, Geiger counters and neon flash-tubes. The characteristics of the instrument are described.

Time variations in the vertical direction have been studied and are attributed to variations of meteorological parameters.

Momentum spectra have been measured in the range 2 - 500 GeV/c for zenith angles between 77.5 and 90°. The results are interpreted as showing that most muons in this range come from pions; an upper limit of 0.55 is placed on the K/π ratio for proton-air nucleus collisions of 700 - 30,000 GeV.

The positive-negative ratios confirm a near constant value of 1.2 over the range of muon energies 10 - 200 GeV; a likely explanation is that there is an increase in the fluctuations of multiplicity in high energy collisions.

CONTENTS

List of Figures

1. INTRODUCTION

1.1 General Summary

The Cosmic Ray Group of the Department of Physics, Durham Colleges, is undertaking a programme of research concerned mainly with measurements on the muon component of the cosmic radiation at Durham. To date the measurements have included the interactions of muons in local absorbers, the momentum spectrum of muons as a function of zenith angle and the time variations of low momentum muons in the vertical direction. Associated studies have included the momentum spectra of near-vertical protons and pions.

That part of the work supported by the European Office, Aerospace Research, USAF, comprises the variations of the muon flux with respect to time and zenith angle. Accordingly, this report deals mainly with these studies but reference will be made to the associated studies where this is necessary.

Much of the early work has been described in Technical Notes (Nos. 1 to 4) and will not be repeated in detail. Instead, attention will be given to the more important aspects of the techniques developed and the results of the later work.

The work carried out falls naturally into four stages, as follows:

Stage I The Solid Iron Magnet

The magnetic lens technique used by early workers in cosmic rays was examined and from it was evolved a device, the solid iron magnet, which could be used to deflect cosmic ray muons in a well defined manner. A programme of research was initiated in which experiments on model magnets were carried out by colleagues at Nottingham University and the

College of Advanced Technology, Brighton and design studies were made at Durham. Eventually a full scale magnet was constructed at Durham and its characteristics were studied in detail. This work has been described by the Senior Investigator and his colleague (O'Connor and Wolfendale, 1960). In view of the importance of the technique, (several other solid iron magnets have since been constructed by other groups) a brief description of the earlier work is given, in Chapter 2, in addition to more recent work.

Stage II Time Variations of the Vertical Muon Flux

A spectrograph was constructed embodying the solid iron magnet, with Geiger counters as detectors, and the variation of the muon flux with time was studied for various momentum bands. A description has been given in Technical Notes 1 and 2 and a brief summary is given in Chapter 3.

Stage III The Low Momentum Spectrum at a Zenith Angle of 80°

The Geiger counter spectrograph was turned on its side and measurements were made of the momentum spectrum and charge ratio in the range 1.5 to 40 GeV/c for zenith angles close to 80°. The results of this work were reported briefly at the Kyoto Conference on Cosmic Rays (Ashton and Wolfendale, 1962) and a more extended account by the same authors is in the press. A detailed account is given in this report in Chapters 4 and 7.

Stage IV The Momentum Spectrum in the Zenith Angle Range $80-90^{\circ}$

More recently, the spectrograph has been considerably improved by the addition of neon flash-tubes and the geometrical arrangement has been changed so that a range of large zenith angles is covered. The resulting instrument has potentialities for studies of the interactions of muons in detectors placed at the output end of the 'machine' and a consideration of this aspect is given in Chapter 5.

The results of preliminary experiments on the momentum spectrum and charge ratio are given in Chapter 6 where some discussion is also made of accompanied events.

The interpretation of the results on the inclined spectrum measurements, in terms of the nature of the particles whose decay gives rise to the muon flux, is given in Chapter 7.

1.2 Staff employed on the Contract
Scientific Staff

Senior Investigator : Dr. A.W. Wolfendale, from start of Contract,

January 1, 1958,

Investigator :   Dr. F. Ashton, from October 1, 1960,

Research Students: P.V. O'Connor, July 1958 - September 1960.

J.B.M. Pattison, from October 1, 1961.

(In addition graduate students have been

employed for short periods during vacations).

Technical Staff

Junior Technicians: K. Richards, February 1958 - July 1958.

E. Anderson, August 1958 - September 1960.

P.J. Finley, from October 1961.

1.3 Objectives of the Research

The objectives have been to derive information about the cause of time variations of the vertical muon flux as a function of momentum, and to study the characteristics of high energy nuclear interactions through a comparison of momentum spectra and charge ratios in the vertical and inclined directions.

2. THE SOLID IRON MAGNET

2.1 Introduction

A variety of techniques are available for determining the momenta (or energies) of ionizing particles but of these the most widely used is that of magnetic deflexion. The most common arrangement is to deflect the particles in the air gap of an electromagnet; in the early cosmic ray experiments cloud chambers were used to determine the particle trajectories but more recently electrical detectors, mainly Geiger counters and neon flash-tubes, have been adopted, with a consequent increase in the efficiency with which the field volume is used. With the increasing emphasis on higher intensities and higher upper limits to momentum determinations, the size of magnet needed has increased. A further increase by an order of magnitude is almost out of the question with conventional methods and some other approach is necessary.

If attention is confined to non-interacting particles, in particular to muons, the immediate possibility arises of deflecting the particles in magnetised iron as distinct from the air gap of an air-cored magnet. With a magnetised iron system ('solid iron' magnet) the magnet can be of simple form and can be highly efficient. Thus, high inductions and large volumes can be achieved for low powers of excitation.

Although the probability of a muon suffering a large deflexion through it short-range interaction with nuclei is small, there will be a finite deflexion in a thick absorber resulting from multiple Coulomb scattering. This results in a limit being set to the accuracy with which the momentum of a single particle may be determined. Although the r.m.s. angle of scattering increases with length of trajectory, L, as $L^{\frac{1}{2}}$, the magnetic deflection increases at a faster rate, αL, and the fractional error in momentum determination falls

accordingly as z^{-4}. In practice, then, L is made as large as possible.

The use of magnetised iron for deflecting cosmic ray particles is not a new idea; Rossi (1931), Bernadini et al. (1945) and Conversi et al. (1945) have all used magnetic lenses for partial separation of positive and negative mesons, but the present work appears to be the first to develop the technique for the precise determination of particle momenta.

2.2 The Design of the Magnet

The design of the full-scale magnet used at Durham was mainly the result of theoretical studies; the model experiments, which were carried out at the same time as those on the full-scale magnet, were carried out mainly to give measurements which could not be made on the full-scale magnet.

The linear dimensions chosen were the result of a compromise between the conditions for high signal to noise ratio, large collecting power and tolerable cost. The height chosen for the magnet was 25 in., for which the theoretical signal to noise ratio is 3.74 at an excitation current of 16 A, the magnetic deflexion is 1.68° for a particle of momentum 10 GeV/c and the momentum loss in penetrating the iron is 0.89 GeV/c.

2.3 The Construction of the Magnet

The magnet consists of 50 horizontal laminations, of nominal thickness 0.5 in. and weight 4.2 cwt per plate. A diagrammatic view is shown in Fig. 2.1. (The magnet is there shown in the position for deflecting vertical particles).

The constitution of the iron is shown in Table 2.1.

Coils were wound on two sides of the magnet (B and C of Fig. 2.1); in the first arrangement, used for measurement of the field distribution, the

Table 2.1 Chemical Composition of iron used in the Magnet

Element	C	S	P	Mn	Si	Cr	Ni	Cu
% by weight	.07	.026	.01	.36	.01	.021	.11	.20

Element	Sn	Co	As	V	Al	Mo	Fe
% by weight	.026	.017	.031	.01	.038	015	remainder

(B.S.S. 24 Part 6, Spec. 18).
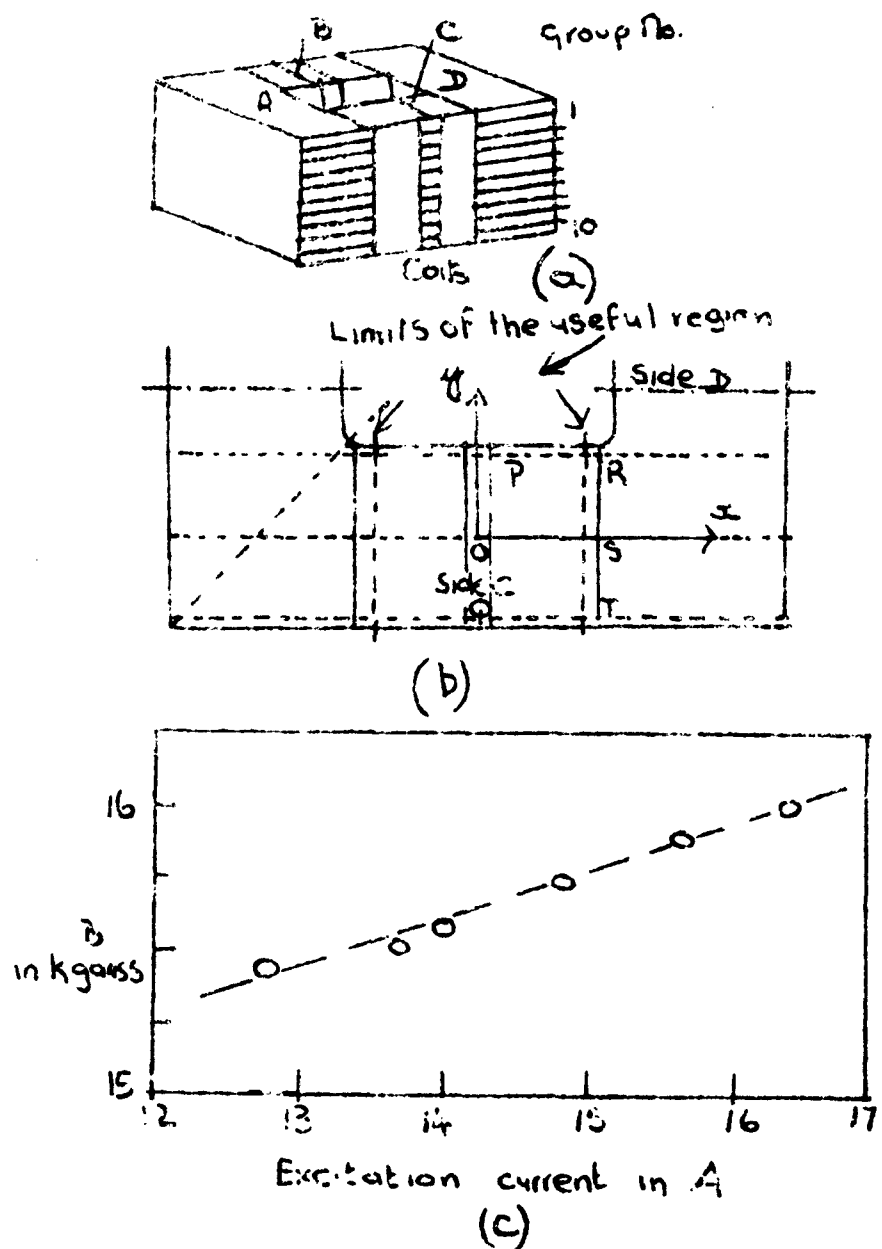
Fig. 2.1 The Durham full scale magnet and the variation of induction with excitation current.

coils were split to enable 'stored coil' wires to be inserted at the centre of the deflecting volume, but in the most recent application the coils are continuous. The coils consist of 150 turns of 14 S.W.G. copper wire on each yoke, the total resistance of the whole coil being 5.25 ohms and the self-inductance 150 mH (These figures relate to the magnet as set up at the present time).

Current is supplied to the coils by a mains rectifier and a reversing switch to incorporate for field reversals.

2.4 The Magnetic Measurements of the Full-scale Magnet

Insulated wires were inserted between successive groups of five plates (Fig. 2.1) in the first arrangement and the variation of $\int BdA$ from one group of plates to the next was determined. These measurements, and all successive measurements, were made using a calibrated fluxmeter and current reversal.

The mean induction in each group was found from $\int BdA$ by dividing by the area and the results are plotted in Fig. 2.2. Although not of practical importance, there is a remarkable sinusoidal variation. It is interesting to note that a similar variation, although not as marked, was found by Bennett and Nash in their actual experiment (see Fig. 2.5). The origin of this variation is not known.

The variation of $\int BdA$ over the whole magnet, with respect to excitation current and position on the sides was found very simply from measurements with a single search-coil wrapped around the whole of the side. The measurements with the first arrangement are shown in Figs. 2.1 and 2.2, where the mean value of B is plotted. It is seen that the variation over the area occupied by the coils is not serious.
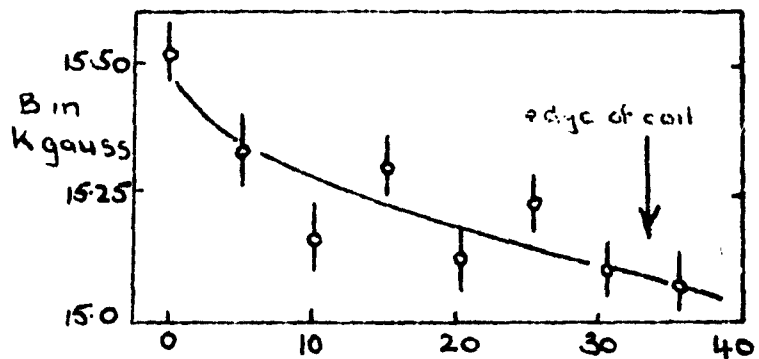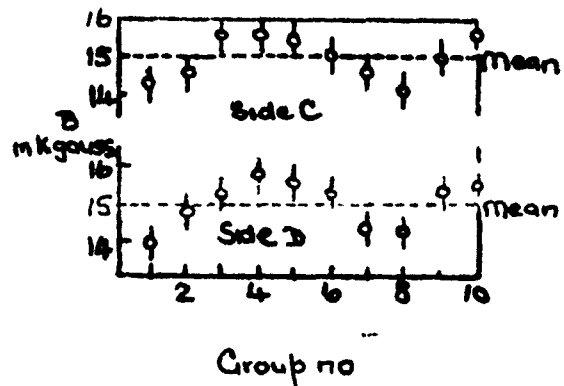
Fig. 2.2 Variations of induction with group number and position
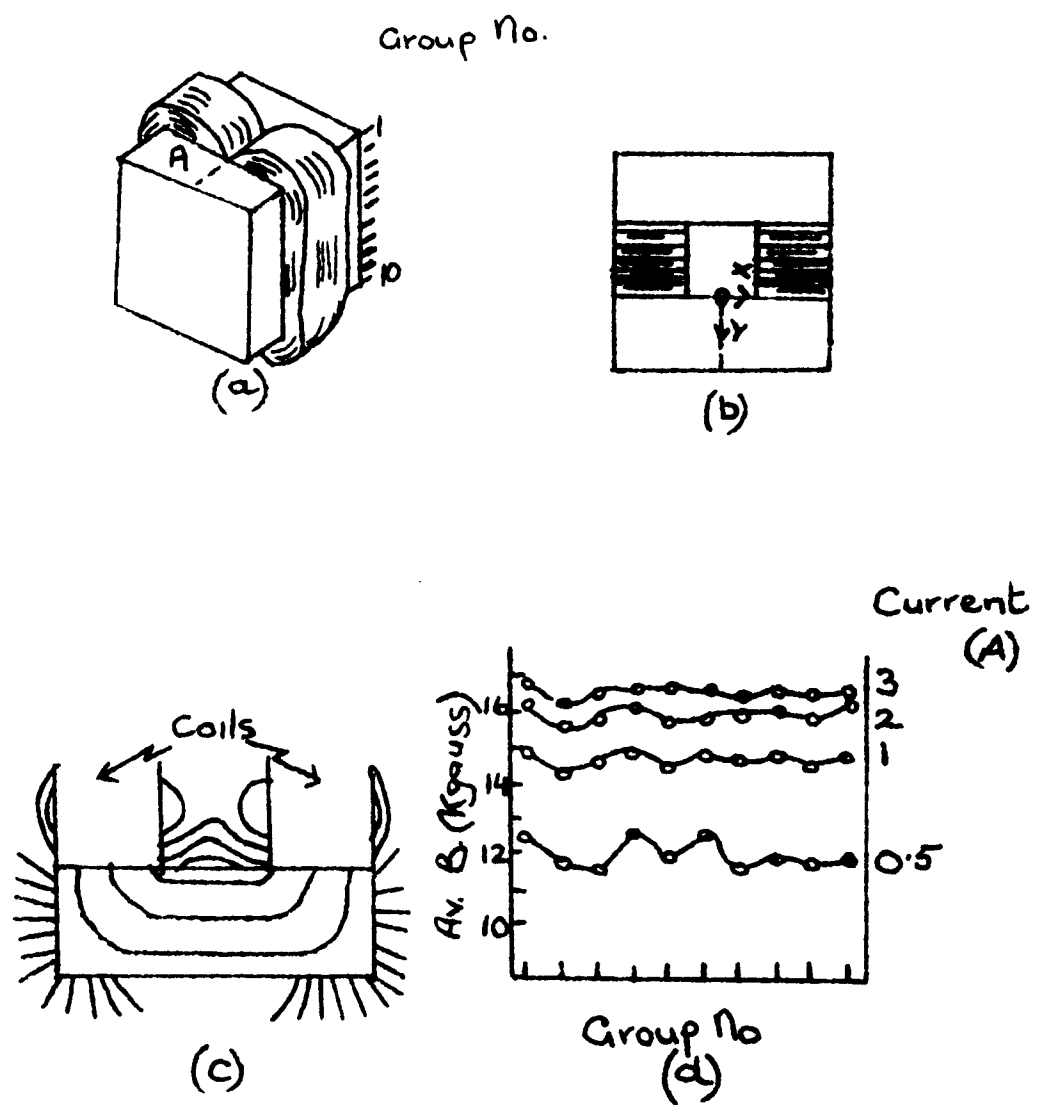
Fig. 2.3 The Nottingham model magnet and the results on the leakage
flux and the variation of induction with group number.

Fig. 2.1(c) enables the stability of the magnetic induction to changes in excitation to be studied; the resulting value for the ratio of the fractional change in induction to that in current, viz. $\left(\frac{I\partial B}{B\partial I}\right)$ is 0.178 at an excitation current of 1 A. Such a degree of stability is eminently satisfactory.

2.5 The Measurements on the Model Magnets

The main use of the measurements with the model magnets made by Bennett and Nash (1960) with regard to the present studies has been in the predictions they give about the induction in regions of the magnet inaccessible in the full-scale magnet

One of the models is shown diagrammatically in Fig. 2.3, where some of the results of measurements are also shown. Fig. 2.3(c) shows the leakage flux over the surface and confirms the limits set to the 'useful region' adopted in the full-scale magnet (see Fig. 2.1(b)). Fig. 2.3(d) shows that, as would be expected, variations in induction from group to group diminish as the excitation current increases.

The most important of the measurements concerns the variation in induction from point to point in the direction Oy. These measurements were made with what was essentially a two-dimensional model: a section of thickness 0.5 in.and linear dimensions as shown in Fig. 2.4. The coils contained 510 turns. Search coils were located in fine holes, as shown. The results give the variation of $\int B\,dl$ with y and show that over the region adopted as the useful region in the full-scale magnet, which corresponds to the region AC reflected about A (in Fig. 2.4), the variation is tolerable.

The net result of all the measurements is that the r.m.s. variation of $\int B\,dl$ for vertical trajectories over the whole of the useful region of the full-
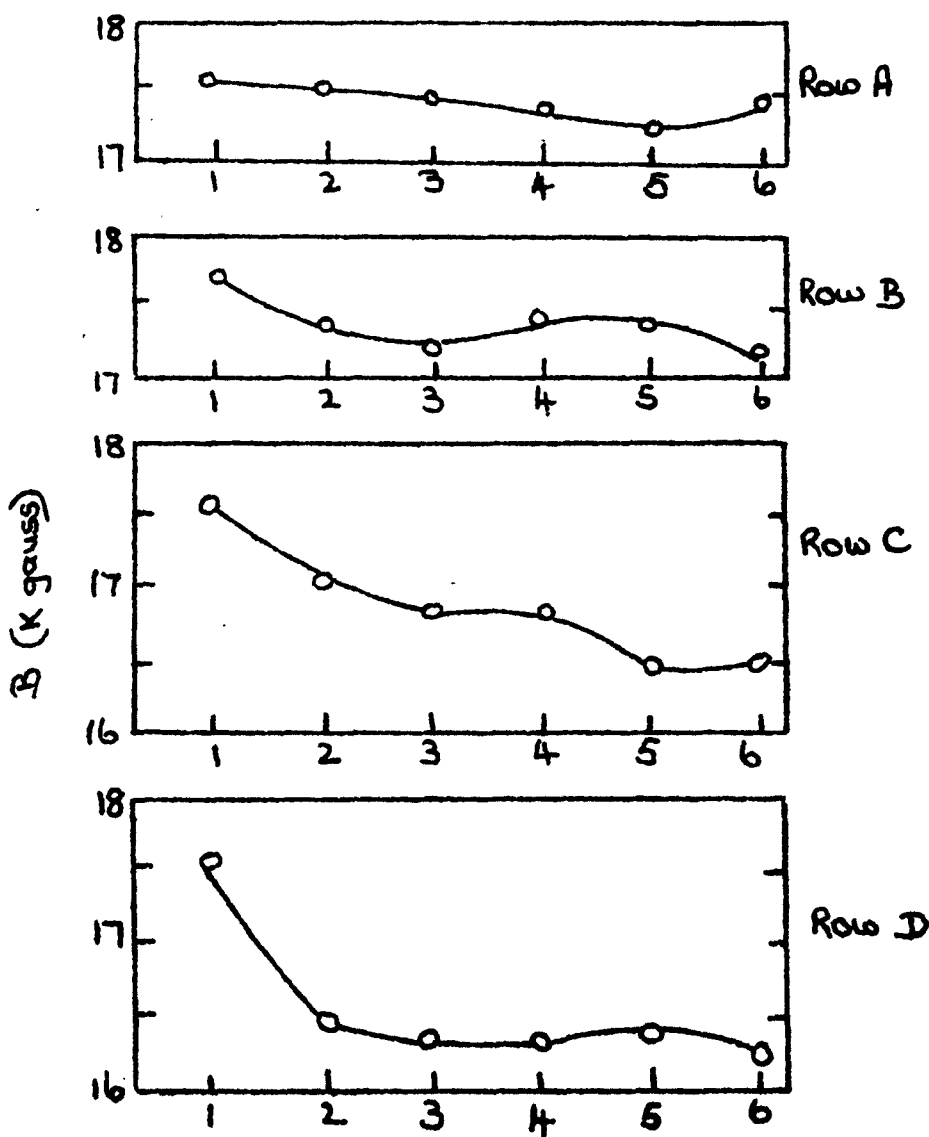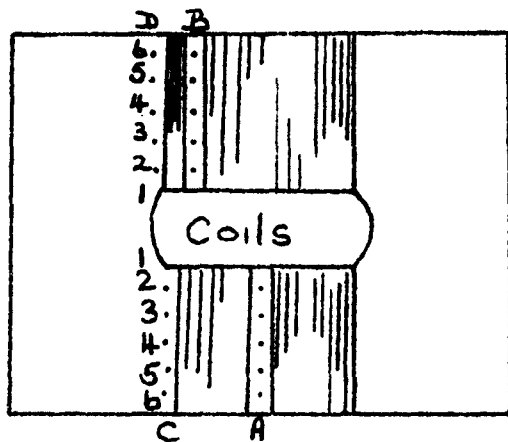
Fig. 2.4 Variations of induction with position for the Nottingham model magnet.
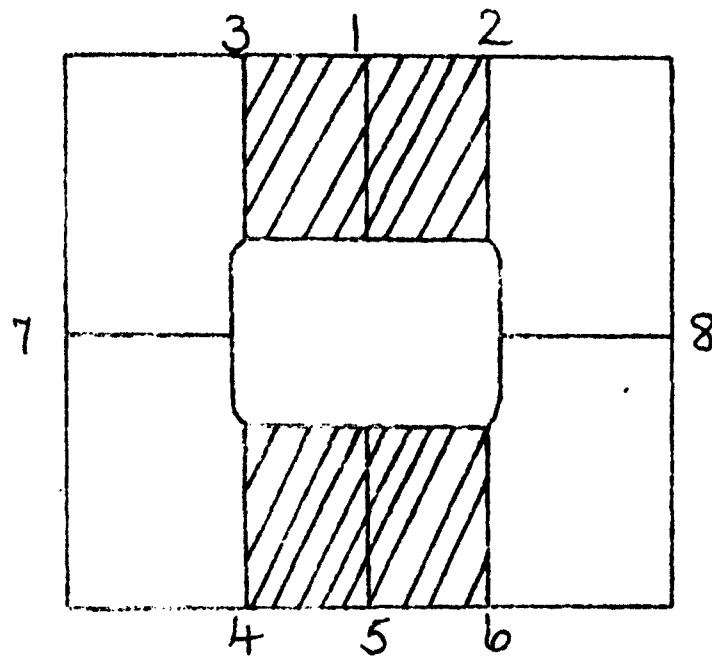
POSITION	B (kgauss)
1	15·48
2	14·97
3	15·04
4	15·37
5	15·38
6	15·32
7	14·92
8	15·09

Fig. 2.5 Precise results for the full scale magnet.
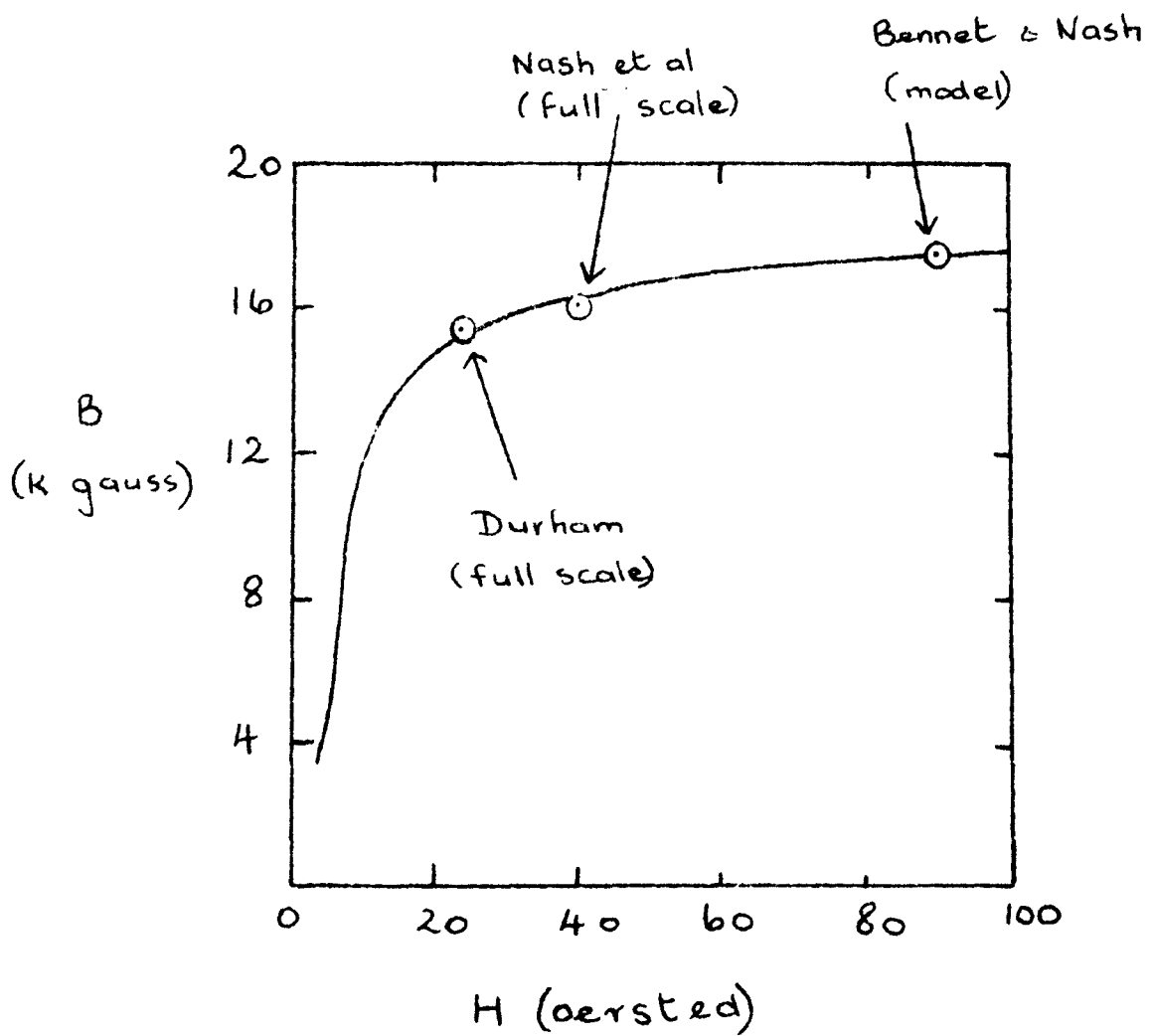
Fig. 2.6 Comparison of the operating values for the various solid iron magnets.

scale magnet is ~3%. This variation can, along with the scattering error,
be allowed for if very accurate measurements are to be made.

2.6 Precise Measurements with the Latest Arrangement

As has been pointed out already, the magnet has been re-assembled and
is at present being used to study horizontal measurements. A particularly
precise set of measurements of $\int BdA$ over the whole magnet has been made and
the results are shown in Fig. 2.5. These measurements were made by two
methods involving Fluxmeters calibrated using standard mutual and self-
inductances. Corrections were applied for the finite time of decay of the
excitation current.

Measurements have also been made of the ripple in the excitation current
in normal operation; the r.m.s. variation is 3.4%. The corresponding varia-
tion in induction is 0.6%.

3. TIME VARIATIONS OF THE VERTICAL MUON FLUX

3.1 Introduction

3.1.1 Historical Introduction

Exhaustive review papers on the flux variations in general have appeared (Elliot, 1952; Sarabhai and Nerurkar, 1956; Dorman, 1957) and these all show that the largest variations are due to variations in the meteorological parameters. It is these variations that will be discussed here.

The existence of a correlation between the intensity of sea-level cosmic rays and meteorological factors appears to have been first pointed out by Myssowsky and Tuwin in 1928. These workers found that a change in barometric pressure of 1 mm Hg produced a change in intensity of 3.45 %, the changes being in opposite directions. This variation was correctly interpreted as being due to the increased absorption and therefore lower intensity at higher atmospheric pressure and vice versa at lower pressure.

With the development of cosmic ray detectors having high counting rates, and improvements in the collecting of meteorological data, particularly with regard to regular measurements of upper atmosphere data with balloons, further correlations became apparent.

3.1.2 The Equation of Duperier

These correlations can be most conveniently understood from the early work of Duperier (1949). Duperier showed, by analysis of the day to day changes in the intensity at sea-level, that the changes could be correlated with the following meteorological factors.

1. The barometric pressure - P.

2. The height of the 100 mb level in the atmosphere - H.

3. The average temperature of the atmosphere between the 100 mb

   and 200 mb levels - T.

Thus, considering the fractional change in intensity $\Delta I/I$ at sea-level
and the parameters P, H and T, they may be related by the following equation.

$$\frac{\Delta I}{I} = \alpha_P \, \Delta P + \alpha_H \, \Delta H + \alpha_T \, \Delta T$$

where ΔP, ΔH and ΔT represent the changes in the respective parameters, the
α's being their respective coefficients

Considering the physical significance of the various parameters it can
be seen that α_P represents the mass absorption effect; an increase in
pressure will cause more low energy μ-mesons to be absorbed by the atmosphere
before they reach sea-level with a corresponding decrease in intensity.
α_H represents the decay coefficient, and may be interpreted as the change in
survival probability arising from a change in height of the meson formation;
an increase in H causes more μ-mesons to decay into electrons before reaching
sea-level, thus again the intensity falls. The third parameter, α_T, is the
positive temperature coefficient due to the competition between π-μ decay and
nuclear capture of the parent π-meson near the production level; a rise in
temperature gives a corresponding fall in density and consequently more
π-mesons decay and fewer interact since the average interaction distance will
increase. At sea-level this will result in an increase in intensity of
μ-mesons with increasing temperature of the upper atmosphere.

3.1.3 More accurate analyses of the Meteorological Effects

Many over-simplifications of physical processes involved have been made
in deriving the regression formula; for example, μ-mesons are not in fact genera-
ted at a unique height but have a probability of generation which varies with
height, T and P are not independent etc. In practice therefore it is found
that the coefficients are not strictly constant but vary with time, for each
experimental arrangement, and inconsistencies appear between the results from

different arrangements. In particular, widely differing values of α_T have been found by different workers, ranging from -0.023 ± 0.027 to $+0.193 \pm 0.024\%$ per $^{\circ}C$ (Bachelet and Conforto (1956) have summarized the discrepancies). Much more elaborate regression formulae have in consequence been developed to take account of these factors, demanding a knowledge of the physical conditions over the whole of the atmosphere instead of at a few selected points. These treatments have been carried out by a number of authors, notably Olbert (1953, 1955) and Dorman (1957), and have resulted in more satisfactory agreement between theory and experiment (e.g. the results of Matthews, 1959). A more detailed discussion will be given later.

A further important point that can be considered here is that the coefficients in the simple regression formula represent the aggregate effect summed over particles having a wide range of momenta, over the whole of the sea-level momentum spectrum in fact. Now the theoretical analysis, as distinct from the empirical analysis of Duperier (1949), considers the expected variations as a function of momentum. Referring to the simple regression formula we should expect the coefficients to vary with momentum as follows:

1. α_r should fall with increasing momentum since, as the momentum rises, the amount lost in traversing the atmosphere (~ 2 GeV/c) becomes less and less important.

2. α_H should fall with increasing momentum because at the higher momenta the probability of μ-e decay becomes progressively smaller.

3. α_T should become more important at high momenta since it is only at high momenta (>20 GeV/c) where there is significant loss of π-mesons by interaction rather than decay.

3.1.4 Experimental studies of the Variations as a Function of Momenta

Systematic experimental studies of the intensity variation as a function of momentum have not been made. Some relevant work has been carried out however. For example, measurements have been made using counter telescopes under absorbers so that the data refer to particles having energy greater than some minimum value, E_{min}. Thus, measurements were carried out during the International Geophysical Year using counter telescopes at sea-level, with a thin absorber to give $E_{min} \approx 0.4$ GeV, and at various depths underground: 25 metres water equivalent (M.W.E.), giving $E_{min} = 6.4$ GeV and at 55 M.W.E., giving $E_{min} = 14.4$ GeV. These measurements have shown that there are no gross discrepancies between experiment and theory but a more detailed experimental study of the momentum (or energy) dependence is still desirable.

3.2 Properties of the Spectrograph

The general characteristics of the instrument were described in an early report (Technical Report No. 1) and a more detailed account of accurate momentum determinations was given in a later report (Technical Report No. 3).

Briefly, the instrument comprised three trays of geiger counters mounted two above and one below a solid iron magnet (Fig. 3.1). Coincidence circuits selected particles which were confined to a narrow angle of incidence (near the vertical) and a restricted range of momentum. The configurations of counters used allocated particles to 'momentum categories' for which the median momenta were as given in Table 3.1.

3.3 Treatment of the Experimental Data

3.3.1 The basic data on particle rates

The number of particles traversing the spectrograph was recorded automatically every 25 minutes. The spectrograph was operated for an extended

TABLE 3.1

CATEGORY	Median Mom. in GeV/c.	Rate of Particles in counts/hr.
111	9.1	72.7
110, 112	5.0	60.6
220, 113	3.4	43.3

Categories 110 and 112 select particles having the same momentum distribution but opposite signs, similarly for categories 220 and 113.

TRAY A (10 G.M.)

Momentum Category

← 111
← 110
← 113

107.6 cm.

TRAY B (10 G.M.)

9.7

Magnet

64.9

TRAY C (10 G.M.)

12.0
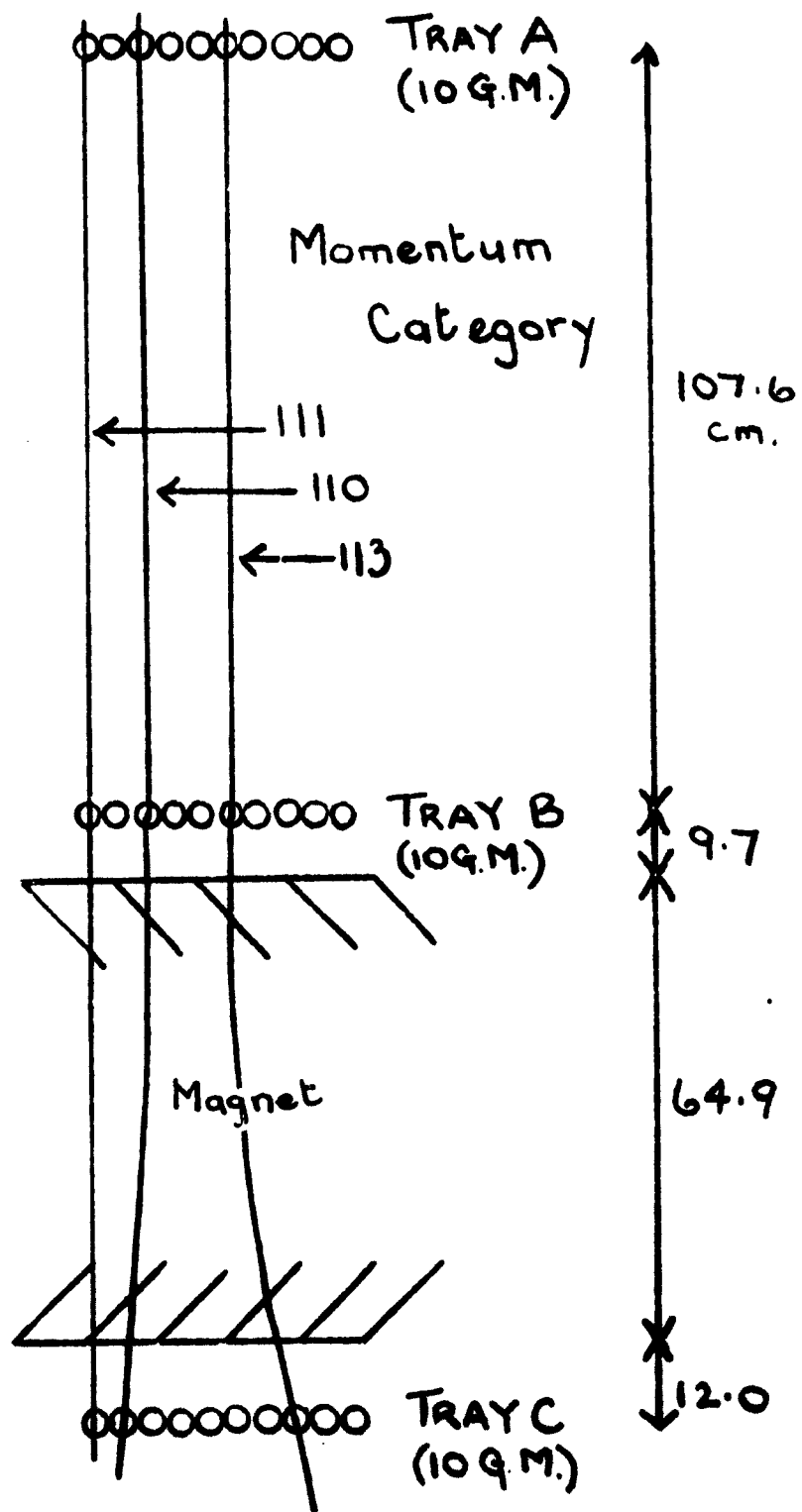
Fig. 3.1 Arrangement of the Vertical Spectrograph

period on each of the categories (Table 3.1), some 70,000 particles being recorded for category 111 and about 10,500 particles for each of the other categories.

The magnet current was monitored using a recording milliammeter and alternate records were obtained with the direction of the magnet current reversed.

A check on the performance of the instrument was carried out by examining the distribution in the interval of time between successive particles. This was found to be accurately consistent with a Poisson distribution, indicating satisfactory operation.

3.3.2 The Meteorological Data

The meteorological data used in the analyses was obtained from the Meteorological Office, who publish data found from radiosonde observations from a number of stations in Britain. The nearest station to Durham is Leuchars, some 120 miles to the north.

Before the data obtained from Leuchars could be used, however, it was necessary to study the effect that this distance would have on the accuracy of the data, as applied to Durham. To enable this to be done the data from 3 Meteorological Stations was studied and compared; Leuchars, Hemsby about 130 miles south-west of Durham, and Aughton about the same distance to the south-east. Thus Durham lies roughly equidistant from these 3 stations, in the centre of the triangle formed by them.

A close study of the data from the 3 stations, carried out over a period of days, and including the variations of temperature and pressure levels up through the atmosphere, revealed little significant change from station to station; thus it was concluded that for the present study the data obtained

from Leuchars was satisfactory, and that a detailed study of the variation
in intensity of μ-mesons with the atmospheric parameters could be carried
out.

The meteorological data extracted for use in the analysis comprised
the following:

    (i) the sea level pressure

    (ii) the heights of the 100 mb and 150 mb levels

    (iii) the atmospheric temperatures at sea level and at the

        500 mb, 200 mb, 150 mb and 100 mb levels.

The rate of particles was found for 4-hourly periods and was plotted
against time, along with the meteorological parameters given above.

3.4 <u>The Results on Correlation with Pressure Changes</u>

    3.4.1 <u>The single correlation treatment</u>

The results of the simplified analysis, in which the correlation between
intensity and pressure alone was studied, were described in detail in
Technical Report No. 1. The result was that the form of the variation of
the pressure coefficient with momentum was similar to that expected but that
its magnitude was some 70% higher than expectation.

    3.4.2 <u>The correlation treatment of Dorman</u>

As was mentioned in 3.1.4 a comprehensive treatment of the correlation
problem has been given by Dorman (1957). This author has pointed out that the
atmospheric temperature is intimately connected with the barometric pressure.
Thus, most of the troposphere is usually warmer under high pressure and colder
at low pressure; in both cases the result is an enhanced variation in cosmic
ray intensity and an apparent increase in the pressure coefficient.

Following Dorman, the effect of temperature variations (at constant pressure) canbe considered as follows: The relative variation in the intensity of μ-mesons, $\frac{\delta N_\mu}{N_\mu}$, due to variations in air temperature $\delta T(h)$ in the region from the top of the atmosphere to the level of observation, h_o, may be represented in the form

$$\frac{\delta N_\mu}{N_\mu} = \int_0^{h_o} W_T(h) \, \delta T(h) dh.$$

where $W_T(h)$ is a function indicating the role of the various layers of air in the production of the temperature effect on a $1^o C$ variation in the air temperature. $W_T(h)$ therefore represents the 'density' of the temperature coefficient.

Dorman shows that $W_T(h)$ varies strongly with the level of observation, h_o, the π-meson production spectrum and the minimum energy of recorded μ-mesons $\Delta\varepsilon$.

It is now necessary to find the value of this integral for the periods of time for which data for each pressure range were accumulated and to correct each intensity. The result will then be a corrected mean intensity for each pressure range, from which the corrected pressure coefficient may be found directly.

The variation of $W_T(h)$ with h was calculated by Dorman for $\Delta\varepsilon = 0.4$, 6.4 and 14.4 GeV, with the result shown in Fig. 3.2. For the present work the variation is required for other values of $\Delta\varepsilon$ and the equivalent minimum values for each of the momentum categories are given as follows:

2.0 GeV for categories 113 and 220,

2.3 GeV for categories 112 and 110,

and 3.5 GeV for category 111.

$W_T(h)$, $\%$ $^{O}C^{-1}$ atm^{-1}

+0.4

+0.3 — 4.4

+0.2

+0.1

0.0 ———— 0.2 ——— 0.4 —— 0.6 —— 0.8 —— 0 ——— h(atm.)

6.4

3.5 (111)

-0.1

2.3 (112)

2.0 (113)

-0.2

Minimum
energy

0.4

-0.3
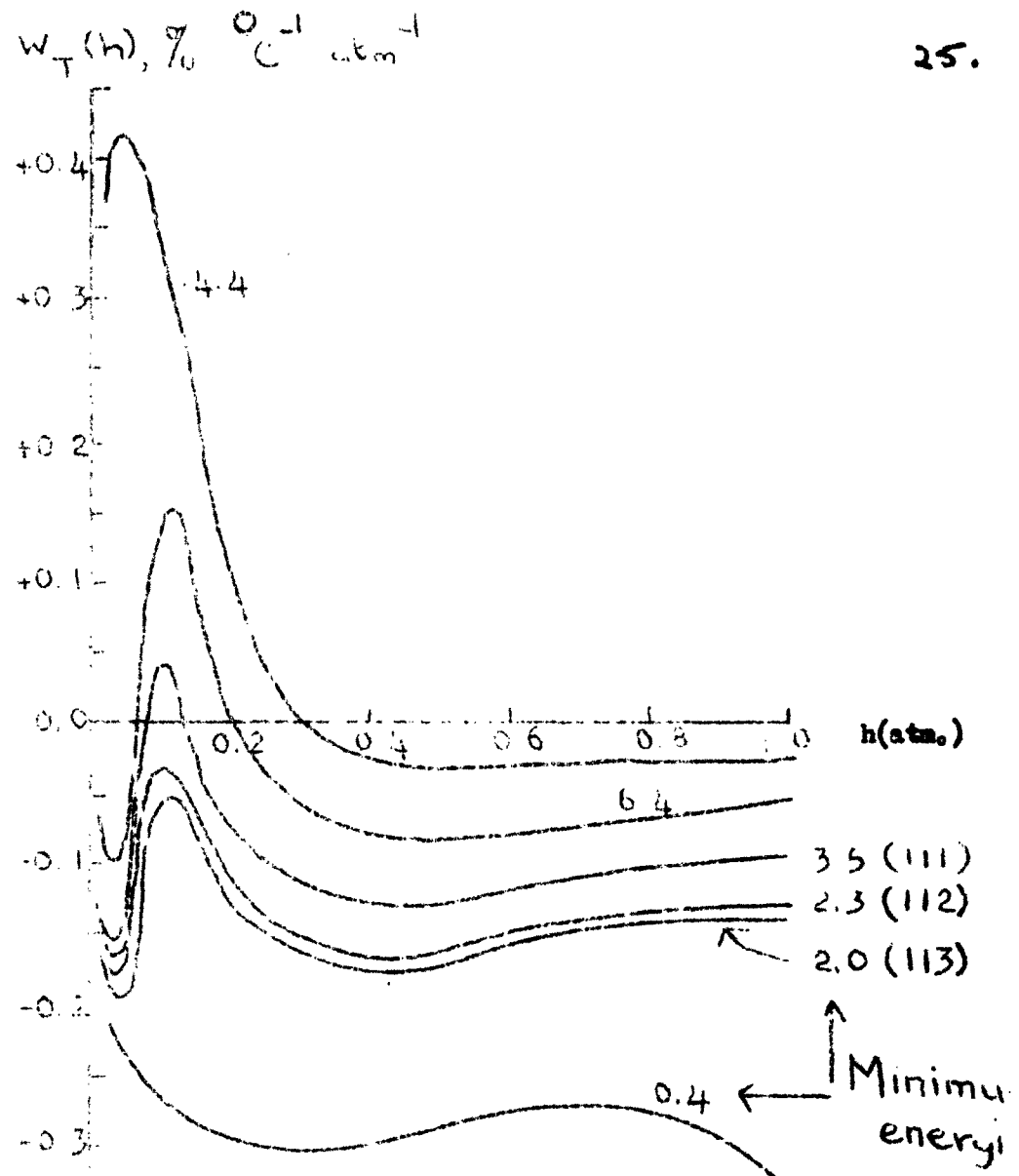
Fig. 3.2 The Variation of $W_p(h)$ with h

Values of $W_t(h)$ were found by interpolation on a graph of $W_t(h)$ against $\Delta \epsilon$ with h as parameter and the results are also shown in Fig. 3.2.

The integral can be rewritten, to sufficient accuracy, as

$$\frac{\delta N}{N} = \sum_{h=0.1}^{h=1.} W_h(h) \, \Delta T \Delta h = \phi$$

where $\Delta h = 0.1$ atrosphere and ΔT is the difference in temperature of the layer (h) from its mean value. Applying this to the present experiment ϕ was computed from the meteorological data, interpolating the temperature values where necessary, for each category. The intensities were then plotted against ϕ for narrow bands of pressure. A range of values of ϕ was then taken and the mean intensity was plotted against ϕ for each pressure band. These curves were then normalized to the same mean value to give a master curve of 'mean' intensity against ϕ for each category.

It was found that the resulting 'curve', composed of normalized intensities, showed large fluctuations from one value of ϕ to the next. In many cases the fluctuations were greater than could be accounted for by statistical errors and it was not possible to verify the predicted variation of ϕ.

However, an approximate corrected pressure coefficient was computed for each category, as follows. The data referred to above, on the range of value of ϕ for each pressure band, was taken and the intensities were normalized so that intensity was the same for each band of ϕ. The mean of these corrected intensities was then taken for each pressure band and plotted against pressure and the 'corrected' coefficient determined. This method is not exact, but is thought to be more accurate than the first approximation. Essentially, it assumes that the temperature effects have the form predicted by Dorman but that the magnitude may be different. The resulting values of α_p, which show
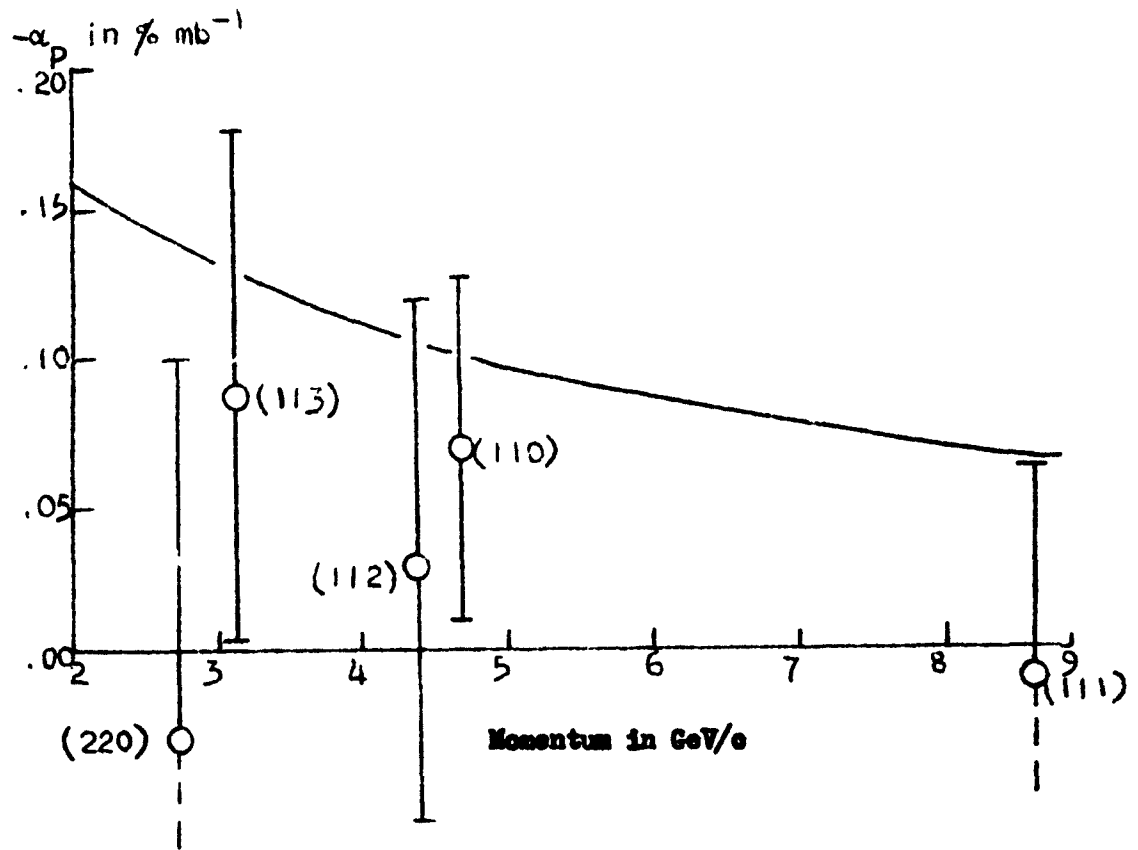
Fig. 3.3 Corrected values of α_p as a function of momentum

rather large errors, are given in Fig. 3.3. It will be seen that they are systematically below the theoretical curve.

It is reassuring to see that this treatment, which would be expected to give an underestimate, does in fact give low values, whereas the simple method, as expected, gives high values. It is perhaps fortuitous that an average of the two sets of values is very close to the expected curve.

3.4.3 Conclusions

It must be concluded from these experiments of rather low statistical accuracy that there is no evidence in favour of any great discrepancy between the experimental and theoretical values of the pressure coefficient of μ-mesons at ground level in the momentum range 2 - 10 GeV/c.

4 THE MOMENTUM SPECTRUM AT $80°$ TO THE ZENITH

4.1 Introduction

Cosmic rays which arrive at large zenith angles (the term 'zenith angle' will be used throughout to mean angle with the vertical) at sea level are of interest for two reasons: firstly, because they give information about the parent particles from which they are derived; and secondly, because they consist mainly of muons of very high average energies.

Measurements of the intensity of particles at large zenith angles have been made by Jakeman (1956), Wilson (1959), and Sheldon and Duller (1962) but the only previous determinations of momentum spectra are the experiments of Moroney and Parry (1954), Pak et al. (1961) and Allen and Apostolakis (1961).

In the experiment to be described a magnetic spectrograph, comprising the "solid iron" magnet with counter recording, has been operated at Durham (200 ft. above sea-level) and the momentum spectrum of muons incident at a zenith angle of $80°8' \pm 1°40'$ has been measured in the range 1.5 - 40 GeV/c.

4.2 The Spectrograph

The apparatus (Fig. 4.1) consisted of 3 trays of Geiger counters, A, B and C and the magnet. Each tray contained 8 counters, each of sensitive length 60 cm and internal diameter 3.3 cm, and an assembly of three-fold coincidence circuits permitted "parallel" telescopes to be selected. Particles were accepted with zenith angles between $81°48'$ and $78°28'$, the axis of the apparatus pointing in a direction $55°36'$ east of magnetic north. The opening angle of the telescopes projected on to a horizontal plane was $29°$.
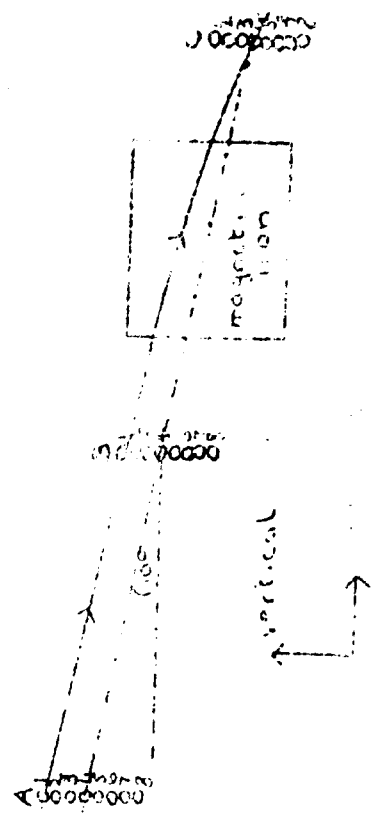
Fig. 4.1 The horizontal spectrograph (with counter recording)

Extensive air showers were rejected by requiring that only one counter in each of the trays A, B and C was discharged. This selection also caused the loss of those muons which were accompanied by other particles or which produced knock-on electrons in the iron and hence gave rise to two particles traversing tray C; the loss (about 7%) has been measured in a subsequent experiment (§5 and §6) using trays of neon flash-tubes placed close to the geiger counter trays. The most serious spurious rate came from low density air showers which triggered the apparatus but only discharged one counter in each tray. This rate was found by measuring the 'background rate' with tray B displaced and has been subtracted from the measured rate.

4.3 The Measured Rate.

The three-fold counting rates, and the associated background rates, were measured for telescopes of the types $A_1 B_1 C_1$ (8 channels), $A_1 B_1 C_2$ (7 channels) $A_1 B_1 C_3$ (6 channels) and $A_1 B_1 C_4$ (5 channels), for each direction of the magnetic induction, and the results are given in table 4.1; H^+ and H^- refer to the field directions by which positive and negative muons were selected.

A relaxation method is used to derive the form of the momentum spectrum from the measured rates, that is, incident spectra are assumed and the expected rates calculated and compared with observation. The main problem is to determine the trajectory of a particle which loses energy and is subject to Coulomb scattering as it passes through magnetized iron.

4.4 Theory of the Spectrograph

4.4.1 The magnetic displacement of a particle undergoing energy loss

Consider a muon of momentum p, incident on a block of magnetized iron at a small angle θ_1 with the normal to the surface and in the plane perpendicular to the lines of magnetic flux, as shown in figure 4.2. Let α be the mean
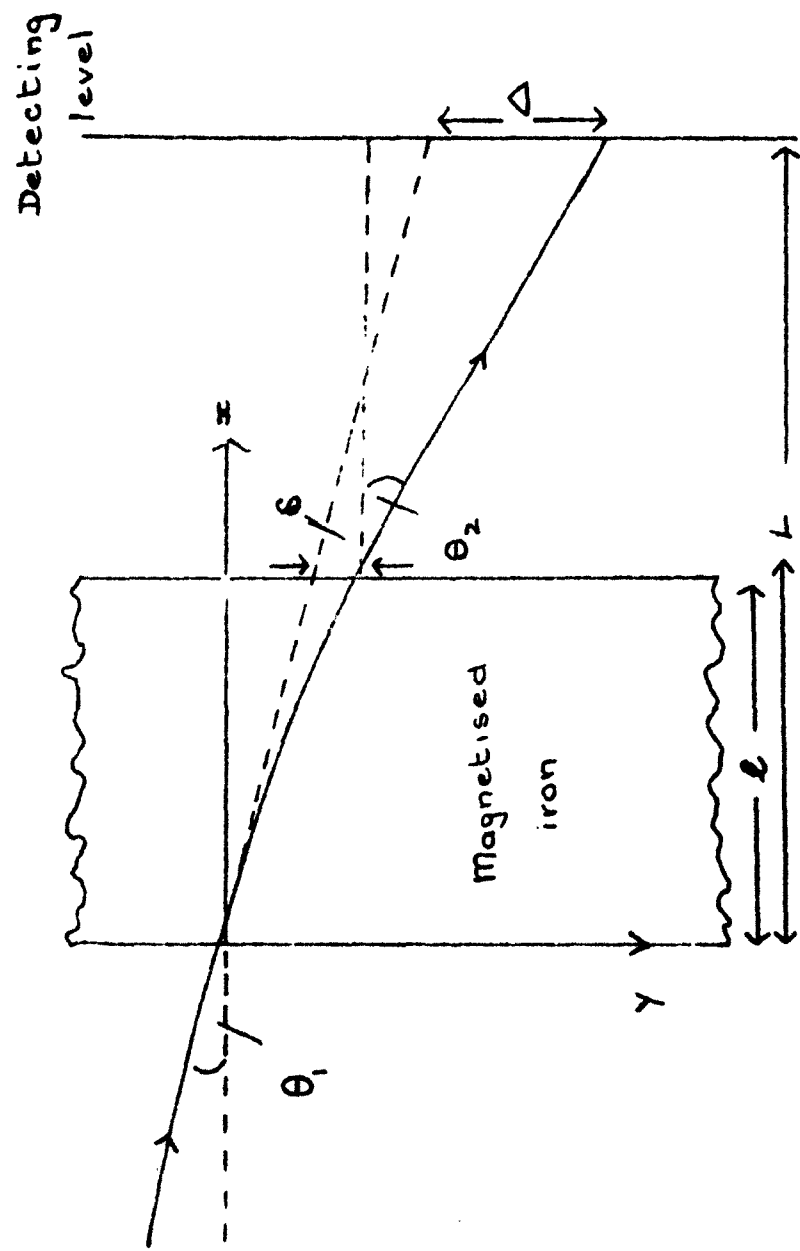
Fig. 4.2 Trajectory of a particle traversing the magnet in the vertical plane.

Table 4.1   The particle rates

Configuration of counters	Magnetic field	No. of channels	Rate of single particles for all channels, corrected for background* (hr^{-1})
$A_1 B_1 C_1$	H^+	8	$2.85 \pm .15$
	H^-		$2.89 \pm .17$
$A_1 B_1 C_2$	H^+	7	$1.630 \pm .086$
	H^-		$1.507 \pm .072$
$A_1 B_1 C_3$	H^+	6	$.59 \pm .037$
	H^-		$.347 \pm .043$
$A_1 B_1 C_4$	H^+	5	$.080 \pm .027$
	H^-		$.117 \pm .025$

*Background rate: $(.0158 \pm .0032) hr^{-1}$ channel^{-1}.

momentum loss per unit path length in the iron (assumed constant over the trajectory) and B the magnetic induction. The equation of the trajectory is

$$p_1 = \alpha \int_0^x \sqrt{1 + \left(\frac{dy}{dx}\right)^2} \, dx = 300 \, B \left(1 + \left(\frac{dy}{dx}\right)^2\right)^{3/2} \left(\frac{d^2y}{dx^2}\right)^{-1}$$

For most cases of interest the angles with the normal are small and the solutions for the angular reflexion and the displacement, δ, at the point of emergence from the magnet are

$$\theta_2 - \theta_1 = -\frac{300 \, B}{\alpha} \ln\left(1 - \frac{\alpha\ell}{p_1}\right) \qquad \cdots \quad 4.1$$

$$\delta = \frac{300 \, B \, \ell^2}{2 p_1} \left\{ 1 + \frac{1}{3}\left(\frac{\alpha\ell}{p_1}\right) + \frac{1}{6}\left(\frac{\alpha\ell}{p_1}\right)^2 + \frac{1}{10}\left(\frac{\alpha\ell}{p_1}\right)^3 + \cdots \right\} \cdots \, 4.2$$

Hence from 4.1 and 4.2 the magnetic displacement, Δ, at a detecting level a distance $L(>\ell)$ from the front of the magnet (Fig. 4.2) is

$$\Delta = \delta + (L-\ell)(\theta_2 - \theta_1) \qquad \cdots \quad 4.3$$

4.4.2 The Scattering Displacement

The mean square projected angle of scatter, $\langle d\theta^2 \rangle$, suffered by a particle of momentum $p_1 - \alpha x$ in travelling between x and $x + dx$ from the front of the magnet is given to sufficient accuracy by the equation

$$\langle \theta^2 \rangle = \frac{K^2}{2} \frac{1}{(p_1 - \alpha x)^2 \beta^2} \frac{dx}{X_0}$$

where $K = 21$ MeV/c, $\beta = v/c$ and X_0 is the radiation length in iron.

The mean square projected displacement, $\langle y^2 \rangle$, at the detection level, for $\beta \to 1$, is given by

$$\langle y^2 \rangle = \int_0^\ell (L-x)^2 \langle d\theta^2 \rangle$$

$$= \langle y_0^2 \rangle + \frac{K^2}{2X_0 p^2} \sum_{n=2}^\infty \left(\frac{\alpha\ell}{p}\right)^{n-1} 2\left\{(L-\ell)^2 + \frac{2(L-\ell)\ell}{n+1}\right.$$

$$\left. + \frac{2\ell^2}{(n+1)(n+2)}\right\} \qquad \dots\ 4.4$$

where $\langle y_0^2 \rangle$ is the mean square projected displacement for no energy loss. It
will be noticed that all the results reduce to the familiar ones for $\alpha = 0$.

4.4.3 Application to the present spectrograph

The mean energy loss per unit path length in iron has been evaluated
by making appropriate modifications to the theoretical formula for the rate
of energy loss of muons in rock given by Ashton (1961) and is given, as a
function of muon energy in Fig. 4.3. Equations 4.3 and 4.4 have been
evaluated for the dimensions of the present spectrograph and the results
are given in fig. 4.4; the curves give the systematic displacement, Δ, due to
magnetic deflexion and the r.m.s. value of the projected scattering displace-
ment about the systematic value.

4.5 The expected spectrum at large zenith angles

4.5.1 The method of calculation

In this section attention is directed only to the case of pions being
the source of muons, the effects of kaons and other particles are considered
later, in §7.

The method adopted is to use the vertical muon spectrum as measured by
Hayman and Wolfendale (1962) and from it to determine the muon production
spectrum and from it the pion production spectrum. The adopted pion produc-
tion spectrum is shown in Fig. 7.1.
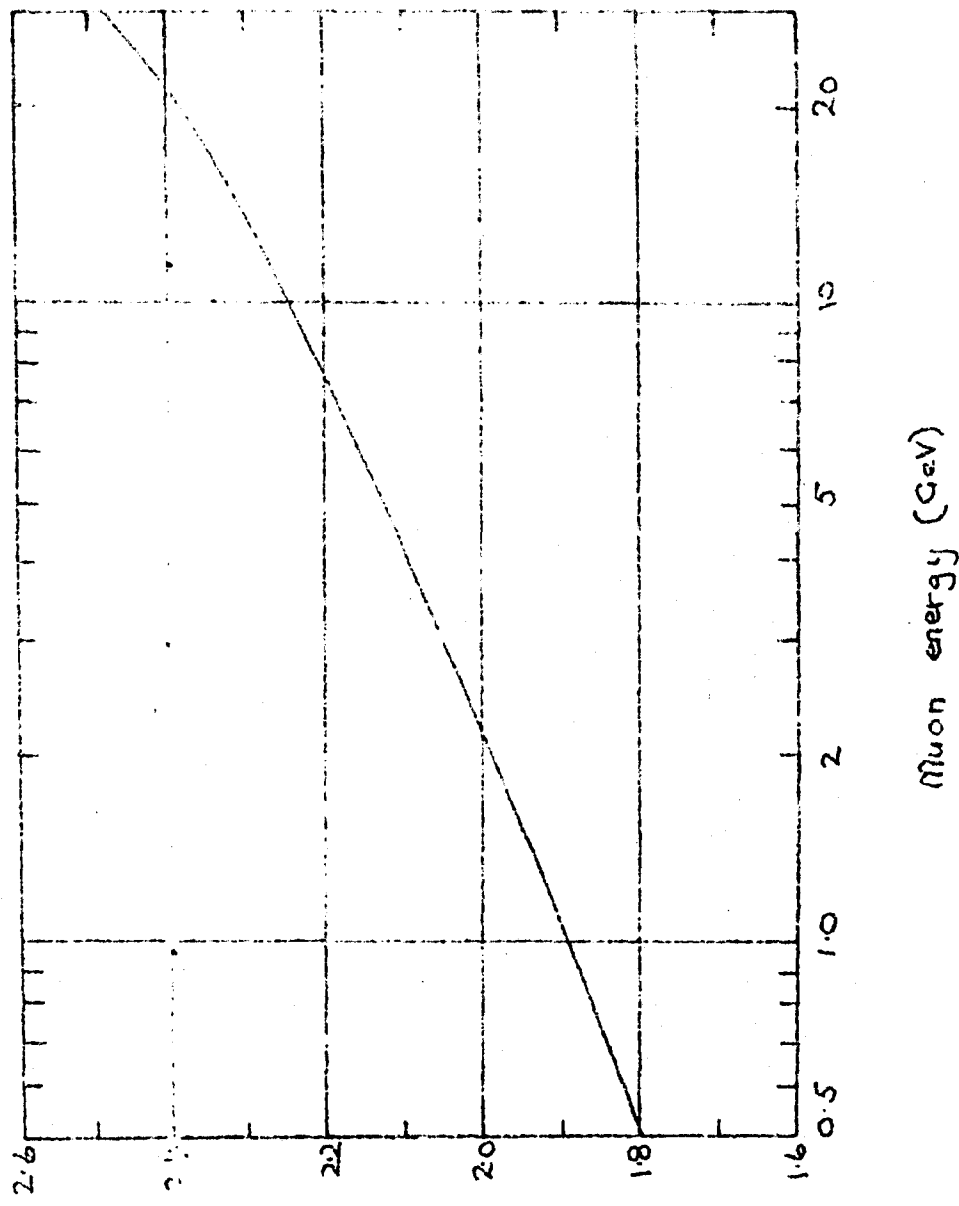
Fig. 4.3 The rate of energy loss of muons in iron as a function of energy.
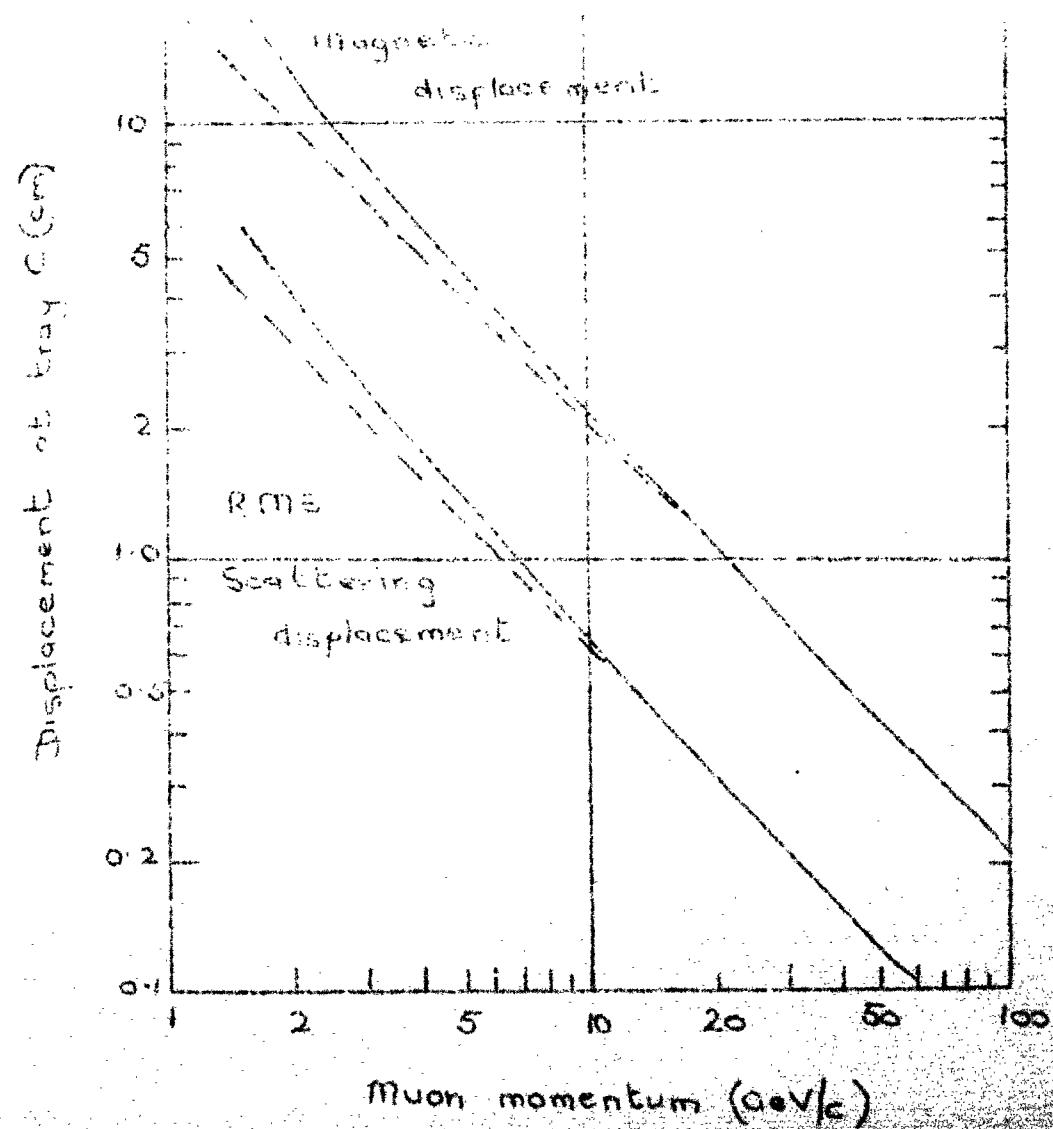
Fig. 4.4 The magnetic a.u r.m.s. projected scattering displacements at tray C as a function of momentum. The dashed curve corresponds to the case where energy loss is not able to neglected.

4.5.2 The muon spectrum at 80° to the zenith at sea level

The muon production spectrum, $M_{\mu}(E,80^{\circ}) = F_{\pi}\left(\dfrac{E}{r_{\pi}}\right) \cdot \dfrac{1}{r_{\pi}} \cdot \dfrac{1}{1 + E/B_{\pi}(80^{\circ})}$

has been taken as the starting point and corrections have been applied for energy loss and $\mu-e$ decay, using the data given in Appendix 2, to give the expected muon spectrum at sea level. At low momenta corrections have also been applied for scattering in the atmosphere and the effect of geomagnetic deflexion, the latter correction arising because the axis of the apparatus was at an angle to the magnetic meridian. The vertical component of the earth's field affects both positive and negative muons equally but the horizontal component causes negative muons of a given momentum at sea level to have a lower momentum at production but greater survival probability than positive muons of the same momentum. The effect of this is to introduce a negative excess of low momentum muons. (see § 4.6).

The corrected spectrum is given in Fig. 4.5. This spectrum has been used as a trial spectrum and the expected rate of events has been determined for each of the counter channels of the spectrograph. The calculations have made use of the data in Fig. 4.4 to convert the momentum spectrum into a deflexion spectrum and allowance has been made for the effect of scattering in the iron and the variation in rate of particles of a given momentum over the acceptance angle of the apparatus. The experimental points, also shown in Fig.4.5, are plotted at the median momenta of the counter channels and the ordinates bear the same relation to the predicted spectrum as do the measured rates to the predicted rates.
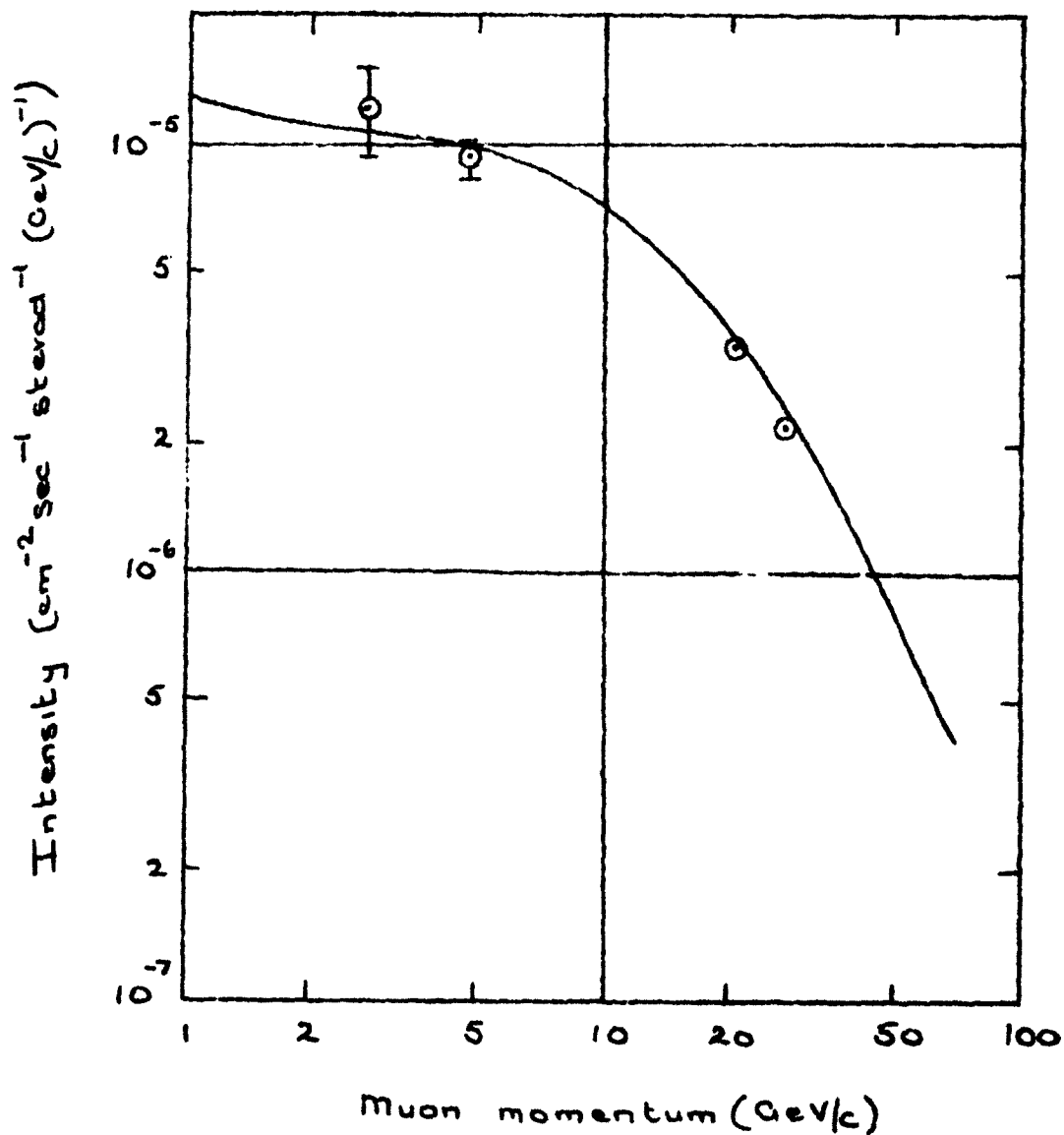
Fig. 4.5 The measured muon spectrum at 80° and the predicted spectrum based on pions as the sole parents of the observed muons.

4.6 The charge ratio

The median momenta of muons traversing the two low momentum channels are 2.5 GeV/c and 4.5 GeV/c respectively. Using the momentum dependence of the positive-negative ratio at production given by Pine et al. (1959), and allowing for geomagnetic deflexion by tracing the trajectories of positive and negative muons through the atmosphere, the expected positive to negative ratios for these two channels are 0.42 and 0.33 respectively. The measured values are 0.68 ± 0.29 and 0.75 ± 0.12. The two high momentum channels record mainly high energy muons which suffer little magnetic deflexion and thus count both positive and negative muons. Little change in the counting rate on reversing the field is therefore expected, as is, in fact, observed (table 4.1).

.7 Discussion of the results

Examination of figure 4.5 shows that the measured spectrum is close to that expected on the basis of a pion source for the sea level muons. In this respect the results are in good agreement with those of Pak et al. (1961) and Allen and Apostolakis (1961). The question of the relevance of this result to the determination of the relative abundances of parent particles of various masses is deferred until after the results at greater inclinations have been described.

5 THE HORIZONTAL SPECTROGRAPH

5.1 The General Arrangement

Diagrammatic views of the spectrograph are given in Figs. 5.1 and 5.2 and a photograph of the instrument is shown as the frontispiece. The spectrograph comprises the solid iron magnet, six trays of Geiger counters and four trays of neon flash-tubes. The Geiger counters used are 20th Century Electronics, type G60, each of sensitive length 60 cm and diameter 3.28 cm. The flash-tubes used are ~60 cm in length and 1.5 cm in diameter.

The requirements for an event to be accepted are a four-fold coincidence pulse ABCD without a coincidence pulse from E or F counters. The E and F counters are located above the magnet and their function is to reduce the frequency of events due to extensive air showers.

After the coincidence arrangements are satisfied, a high voltage pulse is applied to the flash-tube electrodes and a photograph of the flashed tubes is taken by the camera through the mirror system (Fig 52). The mirrors are so arranged that the camera lens 'sees' all four trays of flash-tubes. At the same time a cycling system is triggered which firstly illuminates a clock under tray C and two fiducial marks on each flash tube tray, and secondly moves on the film.

5.2 The Neon Flash-Tube

The characteristics of the flash-tubes have been described in detail by Coxell (1961) and briefly by Coxell et al. (1962). A summary will be given here.

The tubes contain 'neon' (98% Ne, 2%He, <200vpm A, O_2, N_2) to a pressure of about 60 cm. The glass is soda (G.E.C., X8) and the tubes are painted black, except for the plane end window, with a lower white layer over the 20 cm nearest the window.

Fig 5.1 Plan view of the horizontal spectrograph

A

B

ELECTRONICS

MAGNET

CAMERA

OPTICAL SYSTEM

C

D

Scale

20 cm → 20cm
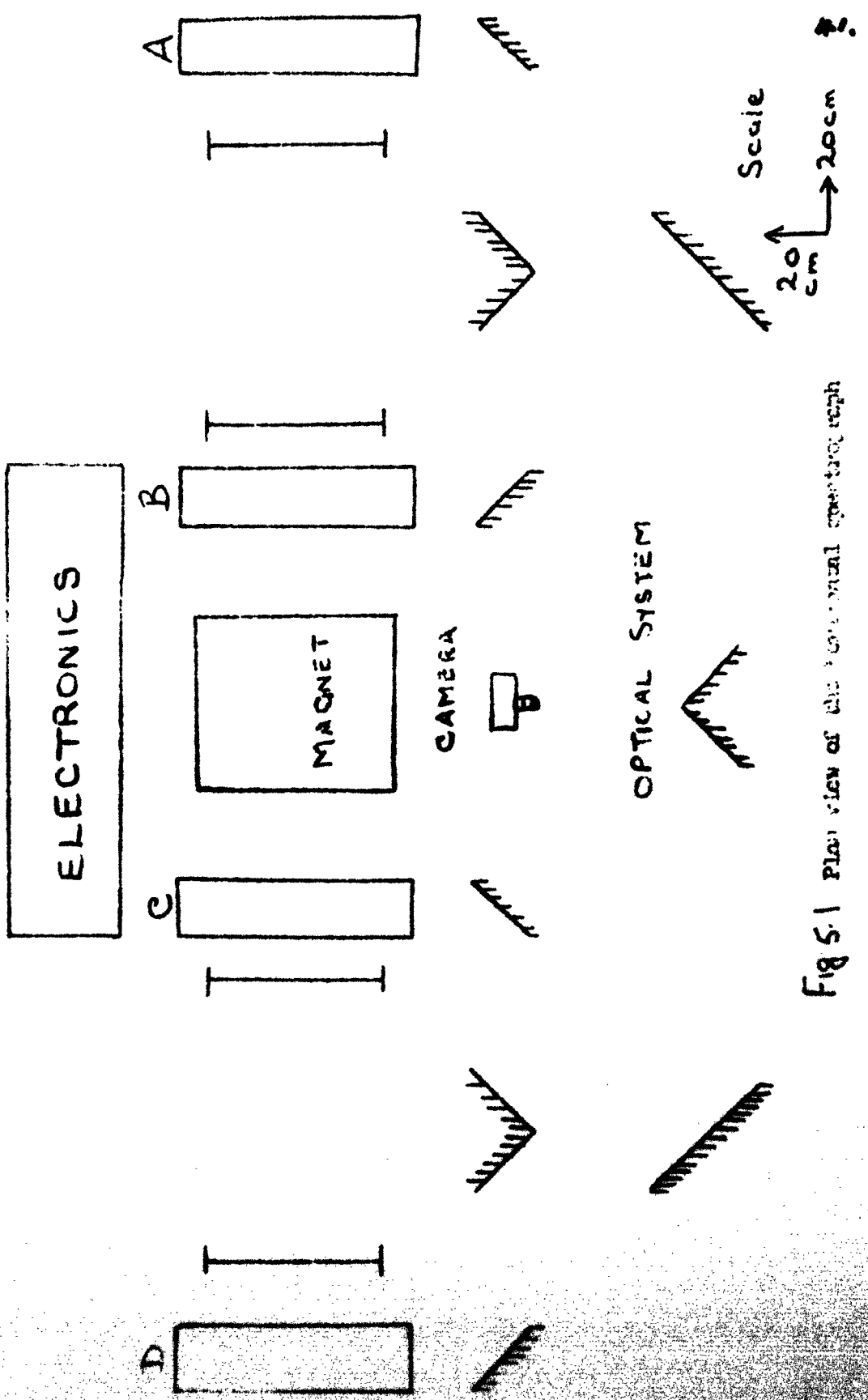
42.
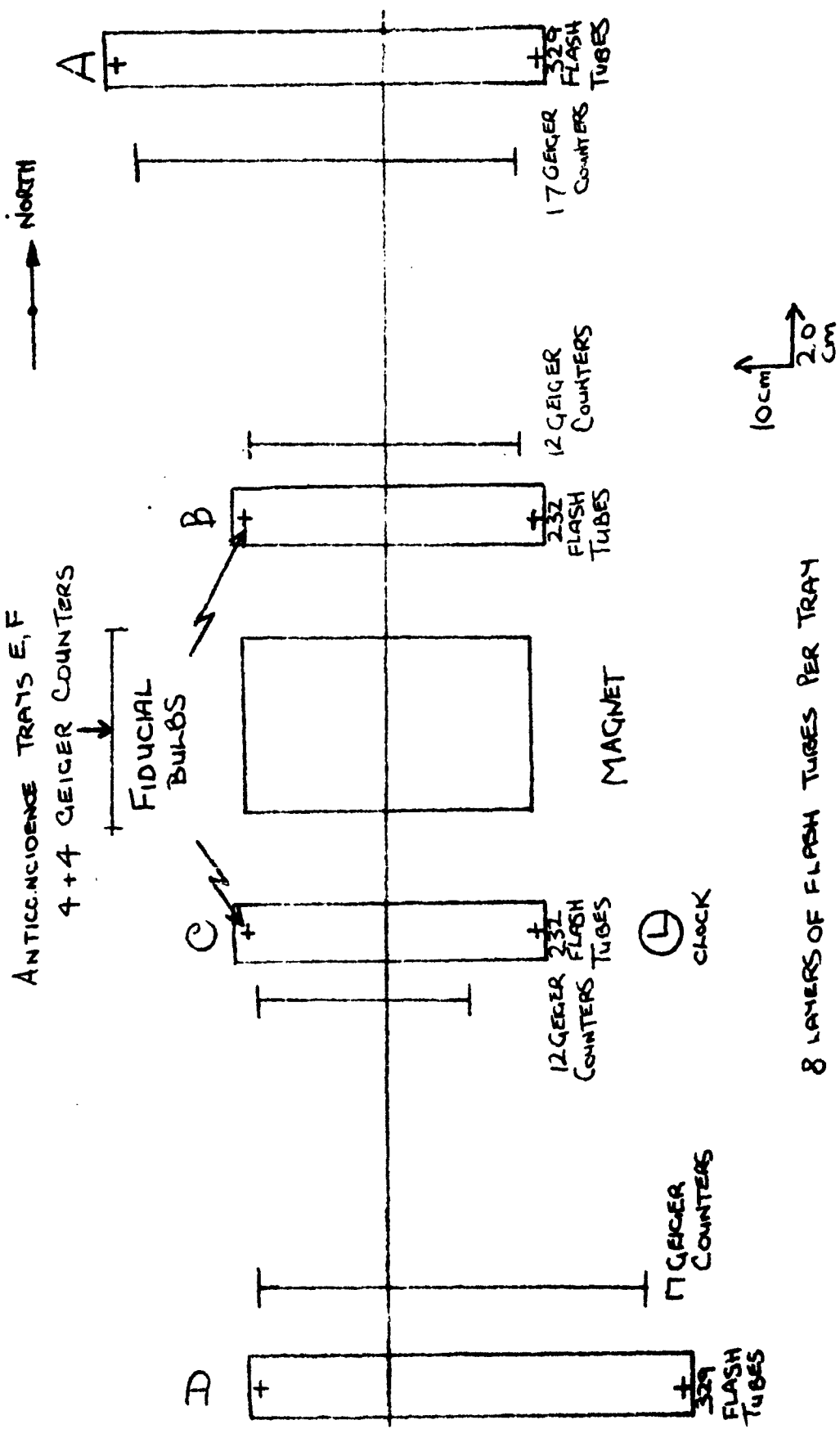
Fig. 5.2. Side elevation of the horizontal spectrograph

8 LAYERS OF FLASH TUBES PER TRAY

The variation of efficiency of flashing with respect to the parameters of the electrical pulse and other important characteristics are shown in Figs. 5.3 - 5.5 and table 5.1. From these figures it is seen that the necessary conditions for maximum efficiency and visibility are:

(i) The highest voltage pulse consistent with an insignificant rate of spurious flashing

(ii) Short rise time of the applied pulse

(iii) Short delay between passage of the particle and application of the pulse

(iv) Direction of photography making the smallest possible angle with the axes of the flash-tubes.

The method of satisfying these conditions will be considered in later sections.

The geometrical arrangement of flash-tubes in a tray is shown in Fig. 5.6(a). It will be seen that each tray consists of eight layers of tubes staggered in such a way that a single particle accepted by the instrument cannot pass through a tray without flashing at least one tube. Electrodes formed by thin aluminium sheets are placed between successive layers of tubes. The tubes are supported in slots milled in 'Tufnol' square section rod (Fig. 5.6(b)) and positioned in such a manner that any small bowing of the tube is in the horizontal plane. All the tubes are accurately parallel to one another within a tray and the trays are aligned (§5.4) so that all the tubes in the whole instrument are parallel.

The vertical distance between adjacent tubes is (1.905 ± 0.001) cm. This dimension is referred to as the 'tube separation' or 't.s.'. The horizontal distance between layers of tubes within one tray is 2.8 cm.
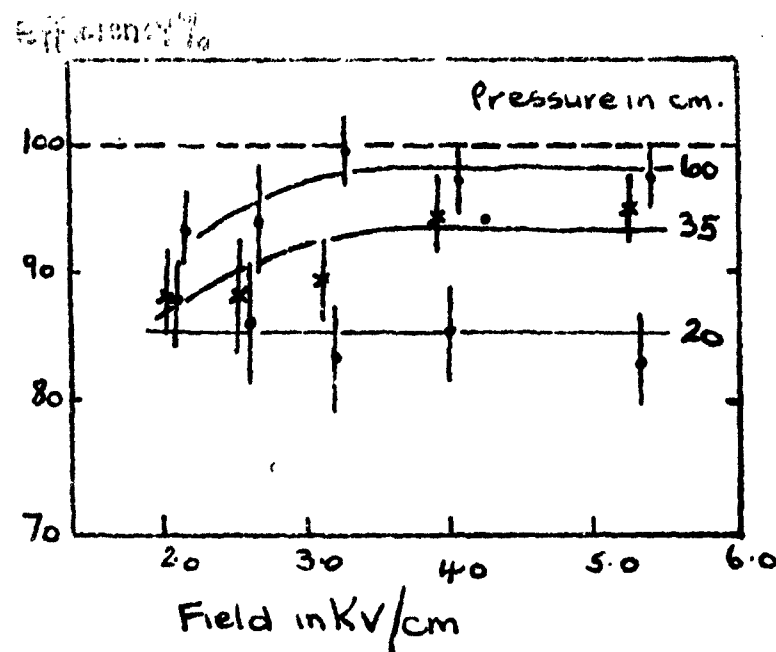
Fig. 5.3(a) The efficiency, field characteristics, with gas pressure as parameter. T_D = 3.2 µsec, T_R = 0.5 µsec, τ = 4 usec.
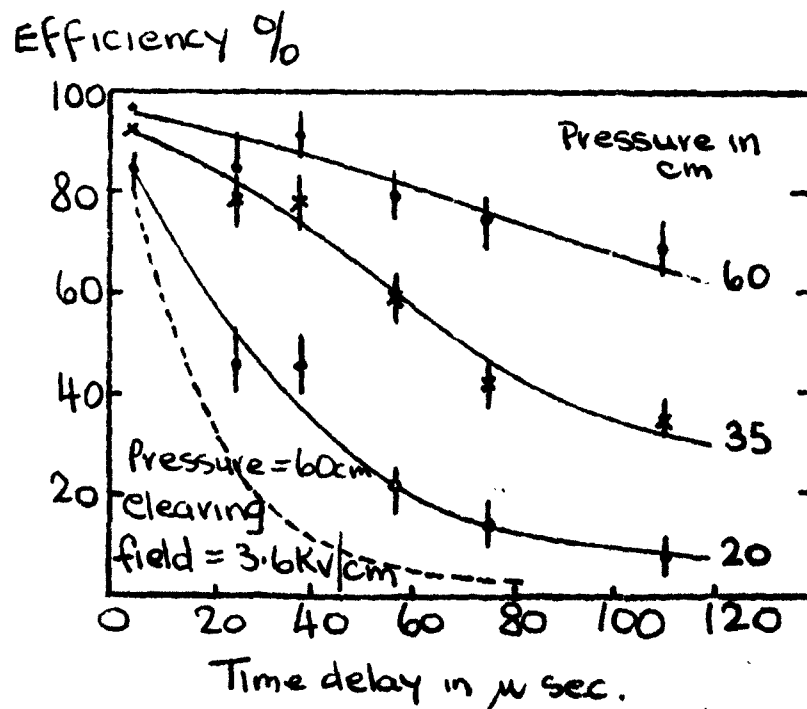
Fig. 5.3(b) The efficiency, time delay characteristics, with gas pressure as parameter. E_{max} = 3.7 KV/cm, T_R = 0.5 µsec, τ = 4 µsec.

Efficiency %

Rise time in μ sec
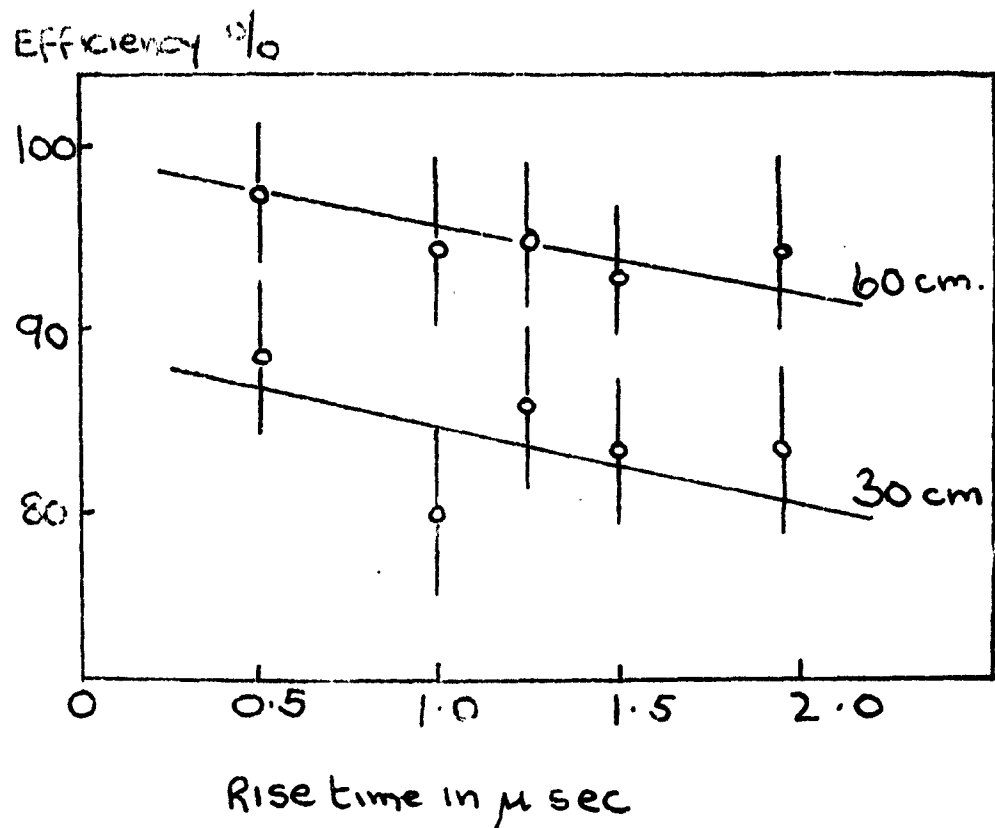
Fig 5.4 (a) The efficiency, rise time characteristic, with gas pressure as parameter, E_{max} = 3.0 KV/cm, T_D = 3.2 μsec, T = 4 sec.

Layer efficiency %

Field in kv/cm
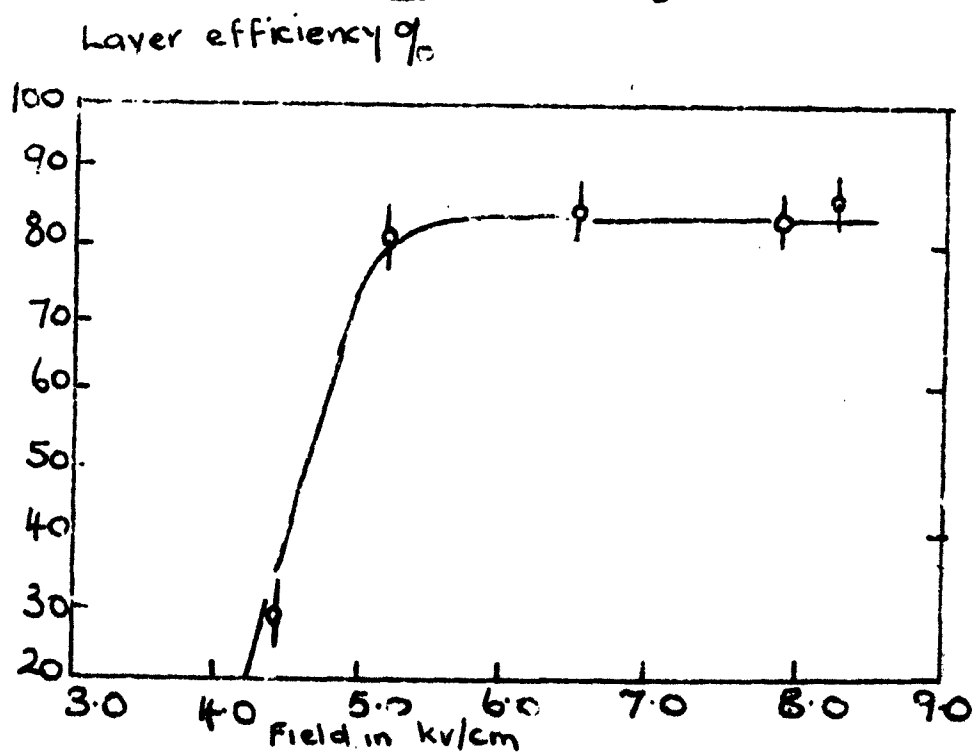
Fig 5.4 (b) The efficiency, field characteristic for the tubes used in the horizontal spectrograph.

Layer efficiency %

Time delay in μ sec.
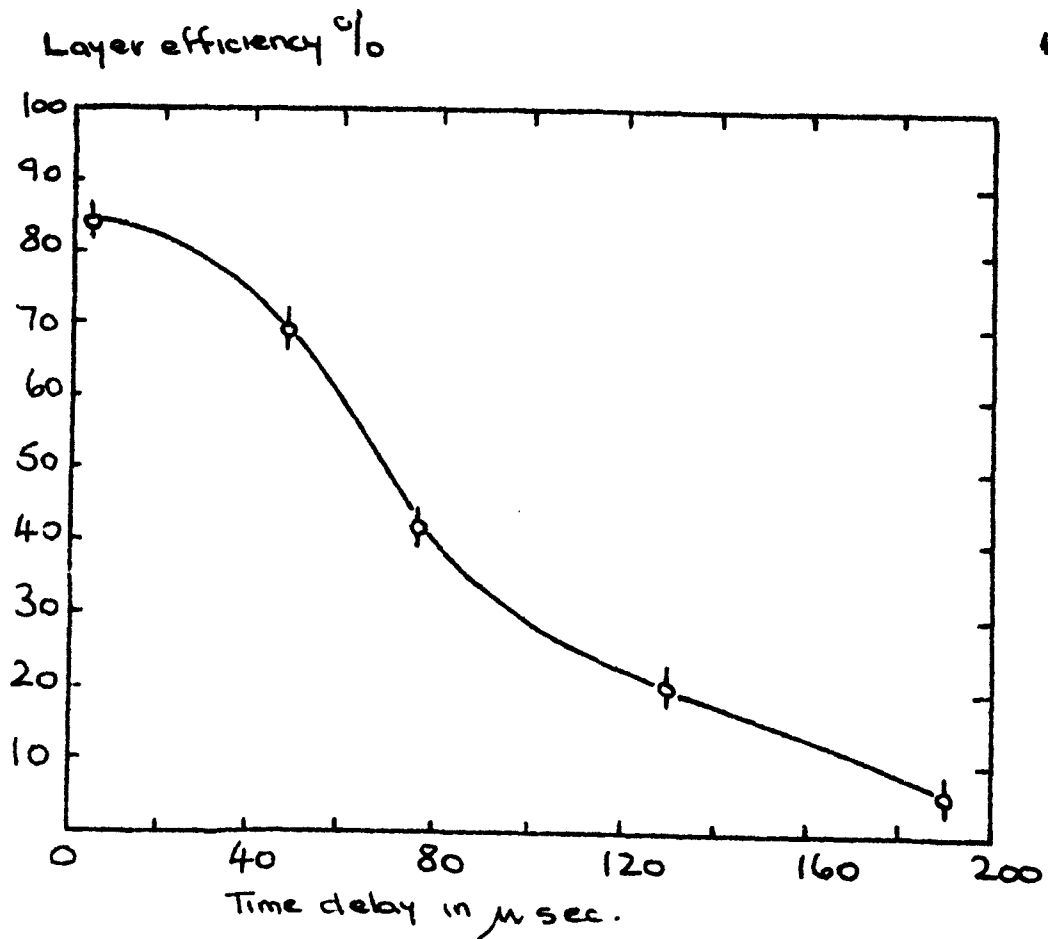
Fig 5.5(a) The efficiency, time delay characteristic for the
tubes used in the horizontal spectrograph.

EXPERIMENTAL ARRANGEMENT
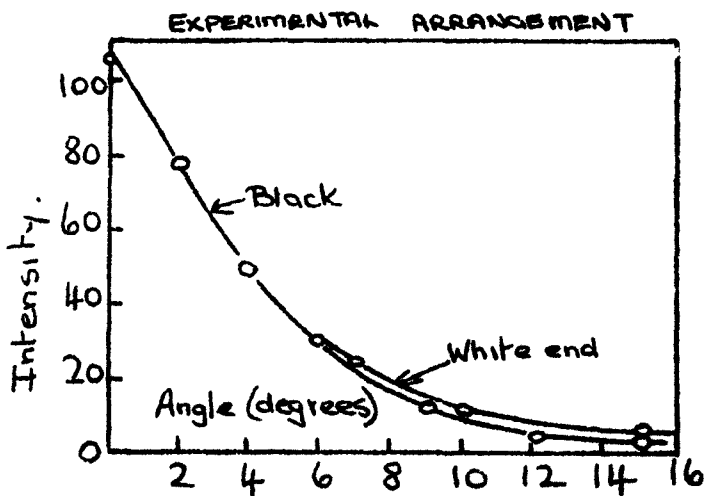
Fig .5.5(b) Polar diagram for light output from the flash-tubes.
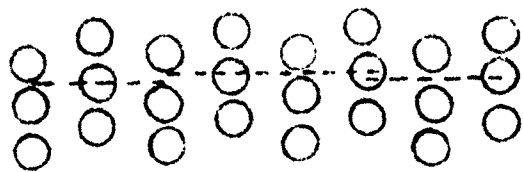
(a) A section of a flash-tube array

(b) Flash-tube support

Tufnol Bar

PARTICLE

Rossi 4-fold coincidence

Anticoincidence Gate Pulse

KV

8

4

0 1 2 3 4 5 6 7 8 9 10 11 12

TIME (μsec)
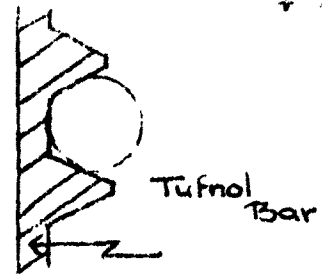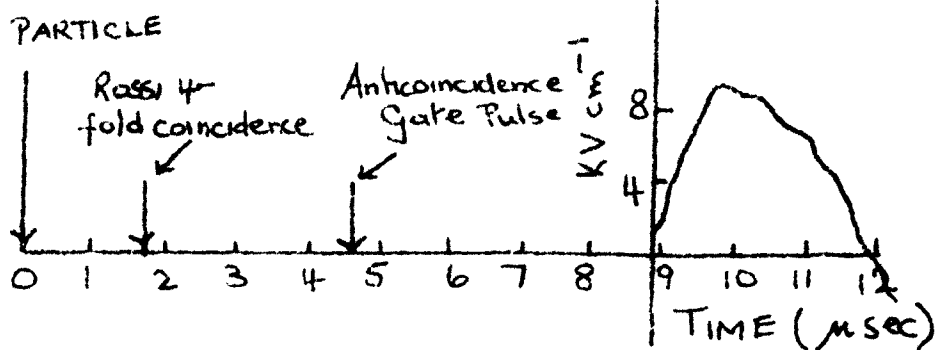
(c) Time sequence from passage of a particle to the application of the high voltage pulse.

D   C   MAGNET B   A

θ_2 θ_1

l

d c b a

l_4 l_5 l_2 l_1

d_0 c_0 b_0 a_0
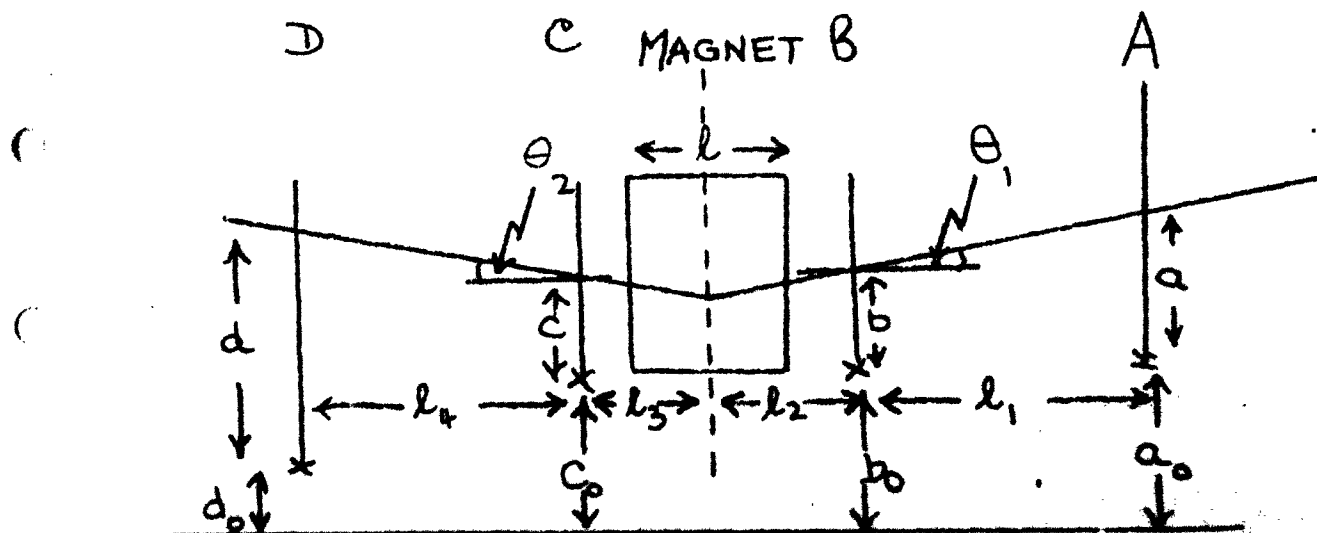
(d) The experimental arrangement.

Fig 5.6

Table 5.1

Spurious Flashing

The ratios are per tube per 1000 pulses

Field Pressure	2.1	2.8	3.5	4.2	4.9	5.6	Kv/cm
60 cm Hg	0.18	0.54	0.37	0.6	0.6	0.6	
35 cm Hg	0.0	0.18	0.0	0.18	0.2	0.8	
20 cm Hg	0.18	0.18	0.18	0.2	1.2	4.0	

5.3 The Electronic Circuits

A block diagram of the electronic system is shown in Fig. 5.7. As has already been mentioned, the coincidence requirement is ABCDEF. The output of the anti-coincidence unit trigger a thyratron which in turn triggers the high voltage unit consisting of an XP hydrogen thyratron and pulse transformer. This unit triggers four further units, each comprising an enclosed spark gap (trigatron type) and another pulse transformer. The output of each of these units is applied to a flash-tube tray (the circuits are shown in Fig. 5.8).

The time sequence for the pulses is shown in Fig. 5.6(c). It is seen that a pulse of rise time 0.5 μsec is applied to the electrodes 8.8 μsec after the passage of the ionizing particle through the apparatus. The measured rate of spurious flashes, i.e. flashes not associated with a (selected) particle is ~6 x 10⁻⁴ per tube per pulse.

From a typical sample of 500 events the layer efficiency was found to be 78%. This figure and that for the rate of spurious flashes are in good agreement with the values reported by Coxell (1961) for the same conditions of applied pulse.

5.4 Alignment of the Spectrograph

The alignment of the instrument and the determination of the geometrical constants are subjects of great importance and a detailed description will be given.

Each flash-tube tray is fitted with four plates through which a single hole is bored, the plates being in identical positions on each tray. The trays B and C are supported on arms fixed to the pillars of the magnet framework and the trays C and D are supported on frames bolted to the laboratory floor
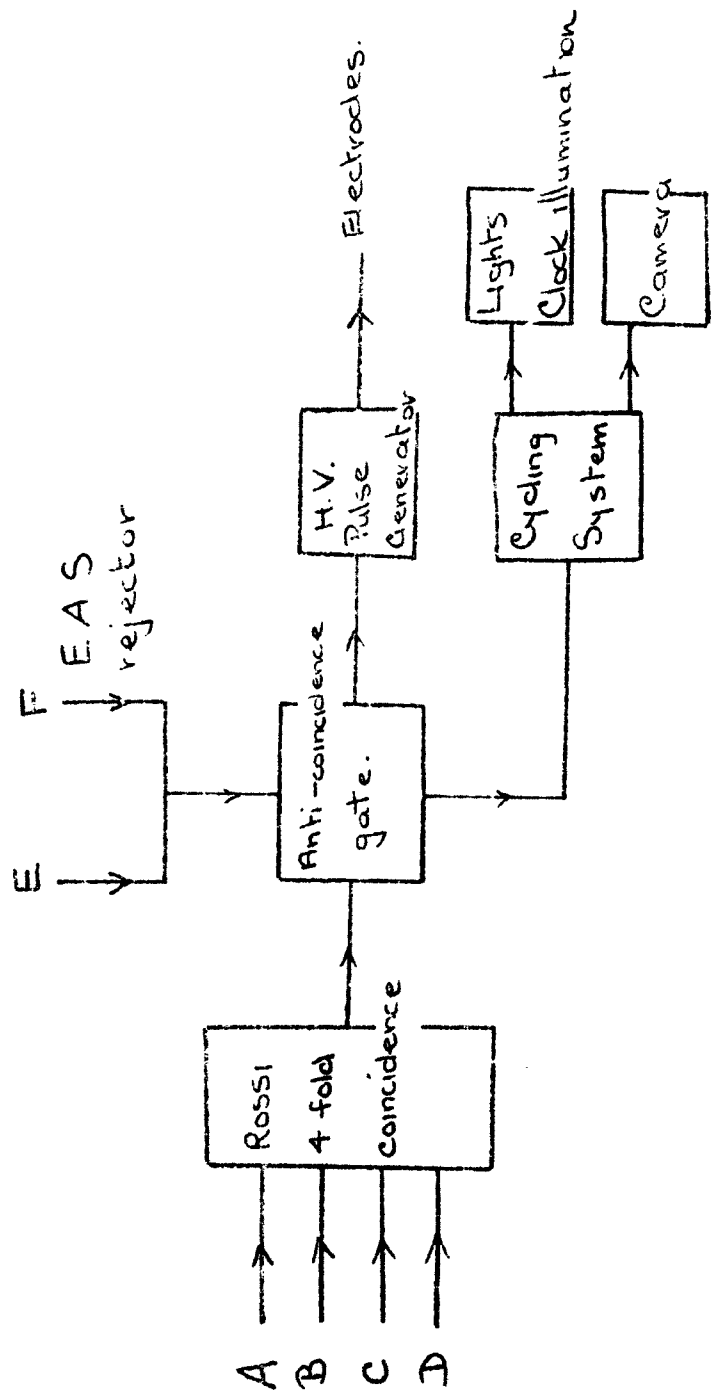
Fig 5.7 Block diagram of the electronic circuits.
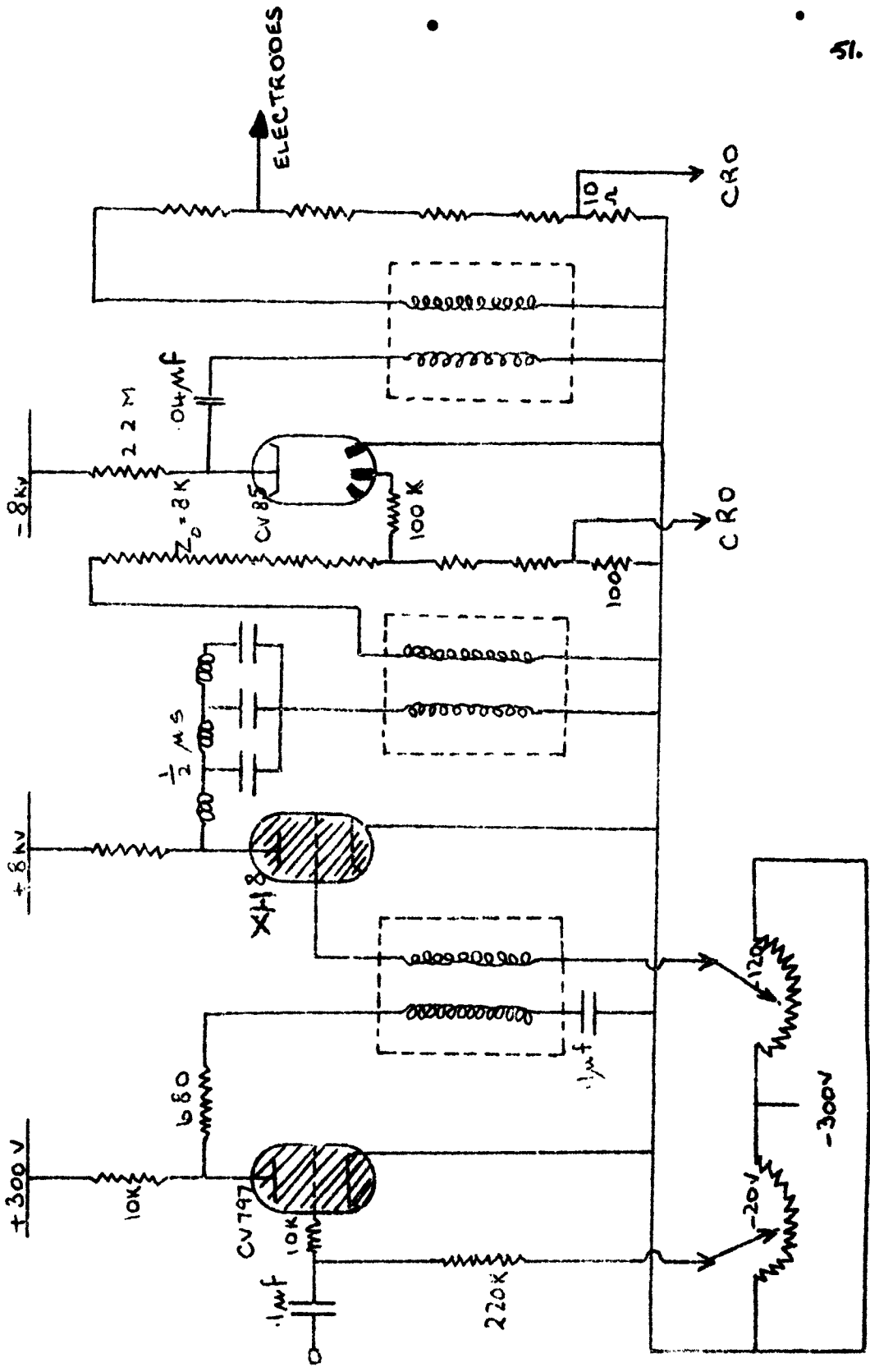
FIG 5.8 The high voltage pulsing unit.

52.

In the alignment process all four trays were adjusted so that

a) cotton fibres were able to pass through the centre of the hole in each place on both sides, an

b) each tray was in the vertical plane and the tubes in it were horizontal. The degree of horizontal levelling was checked in three ways:

i) optically, using a cathetometer and telescope

ii) directly, using a sensitive spirit level

iii) by using a straight tube of glass of the same diameter as the flash-tubes, containing a small amount of mercury (effectively a large spirit level).

The constants of the spectrograph (Fig. 5.6(d)) were determined using cotton (or nylon) fibres stretched along the length of the spectrograph from knife edges at each end, one pair on the east side and one on the west. A cathetometer was then used to set the knife edges in the horizontal plane and to measure the vertical distance from a reference tube in each tray to the fibre. The vertical separation of the tubes was also measured in this way. The horizontal dimensions were measured with an accurate steel tape.

Corrections were applied to the (vertical) measurements for the catenary effect and all the measurements were repeated by two other observers. The final adopted values are given in Table 5.

The relation between the spectrograph constants, the measured quantities for a particle and the momentum of the particle, can be considered by examining Fig. 5.6(d). The alignment measurements give the quantities a_o, b_o, c_o, d_o and the various ℓ's, and the measurements on the photographs (§5.6) give a, b, c and d.

If the momentum of the particle is p (eV/c) then p = 300 $H\rho$, where H is the field strength in gauss and ρ is the radius of curvature in cm. It follows that

Table 5.1

Adopted Values of Geometrical Constants (c.f. fig. 5.6(d))

Dimension	a	t.s.	
ℓ_1	149.15 ± 0.02	78.29 ± 0.01	
ℓ_2	74.54 ± 0.04	39.13 ± 0.02	
ℓ_3	71.95 ± 0.03	37.77 ± 0.02	
ℓ_4	150.44 ± 0.05	78.97 ± 0.03	
ℓ	53.5	33.33	
a_0	25.643 ± 0.003	13.461 ± 0.002	Normalized
b_0	25.864 ± 0.002	13.577 ± 0.001	to $d_0 = 0$
c_0	25.512 ± 0.002	13.392 ± 0.001	
d_0	0 ± 0.002	0 ± 0.001	

1 t.s. = 1.905 cm.

$$p\theta = 300 \ \text{Hd}\ell$$

$$= 17.3 \ \text{GeV/c} \times \text{degrees} \quad \text{for B} = 15.85 \ \text{gauss.}$$

The deflexion, θ, is determined from the measurements in a straightforward way. Thus:

$$\theta = \left\{(a + a_0) - (b + b_0)\right\}\ell_1^{-1} + \left\{(d - d_0) - (c + c_0)\right\}\ell_4^{-1}$$

in the small angle approximation

It is convenient to work with the linear dimension $\ell_1\theta = \Delta + \Delta_0$, where

$$\Delta = (a - b) - \ell_1\ell_4^{-1}(c - d) \text{ and } \Delta_0 = (a_0-b_0)-\ell_1\ell_4^{-1}(c_0-d_0)$$

Thus, Δ_0 is a constant of the instrument and Δ is determined directly from the measured quantities for each accepted particle.

The resulting relation is $p(\Delta + \Delta_0)\ell_1^{-1} = 17.3$ GeV/c.

5.5 The Measured Rates of Events

It is useful to examine the frequencies of events of different types. These are as follows:

Coincidences ABCD : $55.6 \pm 1.0 \ \text{hr}^{-1}$

Coincidences ABCDEF : $16.4 \pm 0.4 \ \text{hr}^{-1}$

Rate of single particle events observed on film : $7.9 \pm 0.4 \ \text{hr}^{-1}$

These figures demonstrate the large contribution to the counting rate (ABCD) from extensive air showers. The overwhelming majority of the showers comprise electrons and have an angular distribution which varies with zenith angle as $\cos^8\theta$(e.g. Coxell et al., 1962); the number of muons lost through their being accompanied by showers at very large zenith angles is considered to be very small. Even with the anti-coincidence arrangement it is found that about one half of the events consist of extensive air showers; these showers have a low density and do not trigger the counter trays E and F.

5.6 The Measurement Technique

The quantity required for each particle is the angular deflexion in the magnetic field. However, as has already been mentioned (§5.4) it is more convenient to work with the quantity $\Delta + \Delta_o$ since the measurements then required are the distances a, b, c and d.

Each photograph is projected on to a screen on which is marked the outline of each flash tube in each tray together with the pairs of fiducial marks. A cursor is then adjusted over the images corresponding to the passage of the particle through a single tray and the best estimate of the position of the track is made. Also marked on the screen is a scale, in units of tube spacings (t.s.), at the centre of the fourth row of flash-tubes in each tray. The appropriate values of a, b, c and d are read off the scales

The accuracy in these measurements is 0.15 cm at each level.

5.7 The Basic Data

The data under analysis were collected over a running time of 169 hours 4 minutes during the period 5 July 1962 to 17 August 1962. In this time some 1283 particles were recorded photographically. To obviate any bias introduced by the experimental arrangement the magnetic field was reversed for half the running time. The mean magnet current was 15.50 A giving a mean value for the magnetic induction of 15.85 kgauss.

From the measured data, comprising a, b, c and d for each particle, the displacement $\Delta + \Delta_o$ and the discrepancy, x, (Fig. 5.) at the centre of the field were calculated. Accidental coincidences of separate tracks were eliminated by rejecting events with x > 0.575 t.s. or $|\Delta + \Delta_o|$ > 15.1 t.s.

Fig. 5.9. The discrepancy, x, at the centre of the magnet.
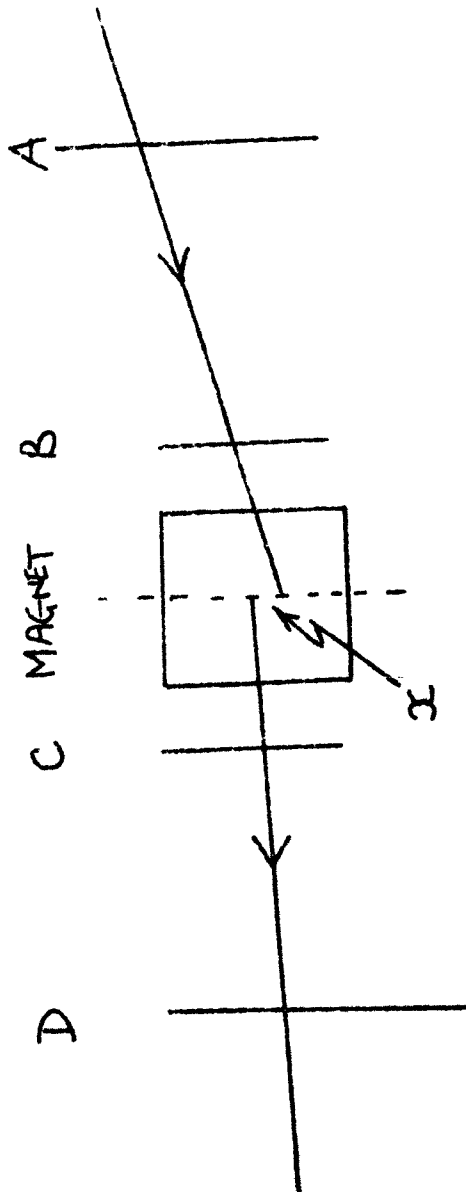
Table 5.3 gives the number of accepted events for the various momentum and zenith angle ranges.

Although the accuracy of track measurement resulting from the simple observations on the projected images is sufficient for particles of comparatively low momentum ($p \lesssim 100$ GeV/c), at higher momenta an improved technique is necessary to give the necessary higher accuracy. Consequently, the fast particles were re-examined using another method. This method involved noting the positions of the flashed tubes in each tray and putting this information on a scale diagram (track simulator). The scales of the diagram are dissimilar to improve the accuracy of location (enlargement of a factor of 2.5 in the vertical direction and 0.716 in the horizontal direction). Information used in this method, but not in the less precise method, is the inclination of the track at each tray and the accurate positions of both the flashed and unflashed tubes.

In order to provide a wide overlap with the projector data, all particles having $\Delta + \Delta_o < 0.46$ t.s. were re-measured.

The most sensitive indicator of the accuracy with which the measurements are made is the magnitude of the discrepancy, x, at the centre of the magnetic field. The frequency distributions for x for the two methods are shown in Fig. 5.10. The improvement in accuracy for the projector data shows up as a reduction in the width of the distribution.

The magnitude of x arises both from errors in track location and the effect of Coulomb scattering. It can be shown (e.g. Ashton et al., 195?) that the relation between the root mean square value of x, $\langle x_{\Delta \Delta_o} \rangle$ and the magnetic displacement $(\Delta + \Delta_o)$ is:

Table 5.3 The basic data for the projection measurements

Deflection Interval (c.a.)	Momentum Interval GeV/c	Mean Momentum GeV/c	observed number of particles as a function of total angular ranges					
			78° - 90°	82° - 82°	83° - 83°	85° - 87°	87° - 87°	87° - 90°
13.1 - 6.5	1.6 - 3.7	2.6	30	23	2	2	2	2
6.5 - 4.1	3.7 - 5.8	4.7	28	26	23	1	1	1
4.1 - 2.4	5.8 - 9.8	7.8	28	41	20	13	13	6
2.4 - 1.2	9.8 - 20.0	14.9	65	84	52	2	2	11
1.2 - 0.8	20.0 - 31.0	25.5	49	52	56	28	28	15
0.8 - 0.5	31.0 - 51.3	41.2	31	56	51	37	37	15
0.5 - 0.3	51.3 - 73.8	62.5	14	24	30	20	20	12
0.3 - 0.1	73.8 - 215	144	26	34	42	38	38	33
0.1 - 0.0	>215	524	5	17	15	19	19	5
		Total	270	367	320	152	152	108

Grand Total 1257

Fig. 5.10. The distribution of x for fast particles.

$$\langle x_{S,A_0}\rangle^2 = x_0^{\,2} + K^2(\Lambda + \Delta_0)^2$$

where K is a constant which contains the effect of scattering and x_0 is the contribution from errors of track location (see Appendix 4 for the determination of the scattering constant). The quantity x_0 is related to the r.m.s. uncertainty in track location at each tray, c, through the geometrical constants of the instrument $x_0^{\,2} = 4.(13\sigma^2$.

For small displacements $\langle x_{S,A_0}\rangle^2 = x_0^{\,2}$ and the value of x_0 can thus be found from Fig. ... The resulting values of σ follow as

(.... for the projector method

and (0.047 ± 0.002) mm. for the track simulator method

An important quantity, the maximum detectable momentum, follows from the value of σ (or, more usually, from the value of the probable error, p, given by $p = 0.674\sigma$).

The corresponding maximum detectable momenta (probable error values) are:

$(204 \pm ...)$ GeV/c for the projector method

$(359 \pm ...)$ GeV/c for the track simulator method.

5.8 Accelerator Characteristics of the Spectrograph

Apart from measuring the spectrum of muons at large zenith angles the horizontal spectrograph is designed to act as a "source" of very fast particles (i.e. muons) so that experiments investigating the interactions of these particles with matter can be carried out. It is thus necessary to know the momentum and spatial-distribution of the emergent particles. The overall momentum distribution is given in Table 5.4, where the total number of particles in the running time of the experiment and the particle rates are given.

Table 5.4 The Overall Momentum Distribution of Particles

Momentum Interval GeV/c	Total Number of particles	Rate (day^{-1})
1.6 - 3.7	78	11.1
3.7 - 5.8	82	11.6
5.8 - 9.8	113	16.0
9.8 - 20.0	250	35.5
20.0 - 31.0	202	28.7
31.0 - 51.3	190	27.0
51.3 - 73.8	100	14.2
73.8 - 215	173	24.6
>215	69	9.8
Total	1257	179

The spatial distribution has been examined by analyzing the events with respect to angle of trajectory on emergence from D, as a function of position in D. The data are given in Figs. 5.11 and 5.12, where division has been made between particles with momentum above and below 25 GeV/c. The sign convention is negative for downward directed tracks and positive for upward tracks, and distances y are measured upwards in the reference level of tray D.

Fig. 5.13 shows the total distribution of exit angle for the whole tray, and Table 5.5 shows how the total is achieved as one progresses up tray D.

It is evident that the majority of particles emerge with angles between -1° and $+2^{\circ}$, and leave tray D between flash-tube numbers 8 and 28. The angular spread on emergence both in the plane under consideration and in the perpendicular plane indicates that a detector used to study interactions must be placed as close to tray D as possible.

For studies of the interactions of particles of the highest energies as long a path length in the cascade detectors as possible is required: with the present arrangement some 5 metres is immediately available, with a possible extension to about 6 m if a temporary partition is removed.
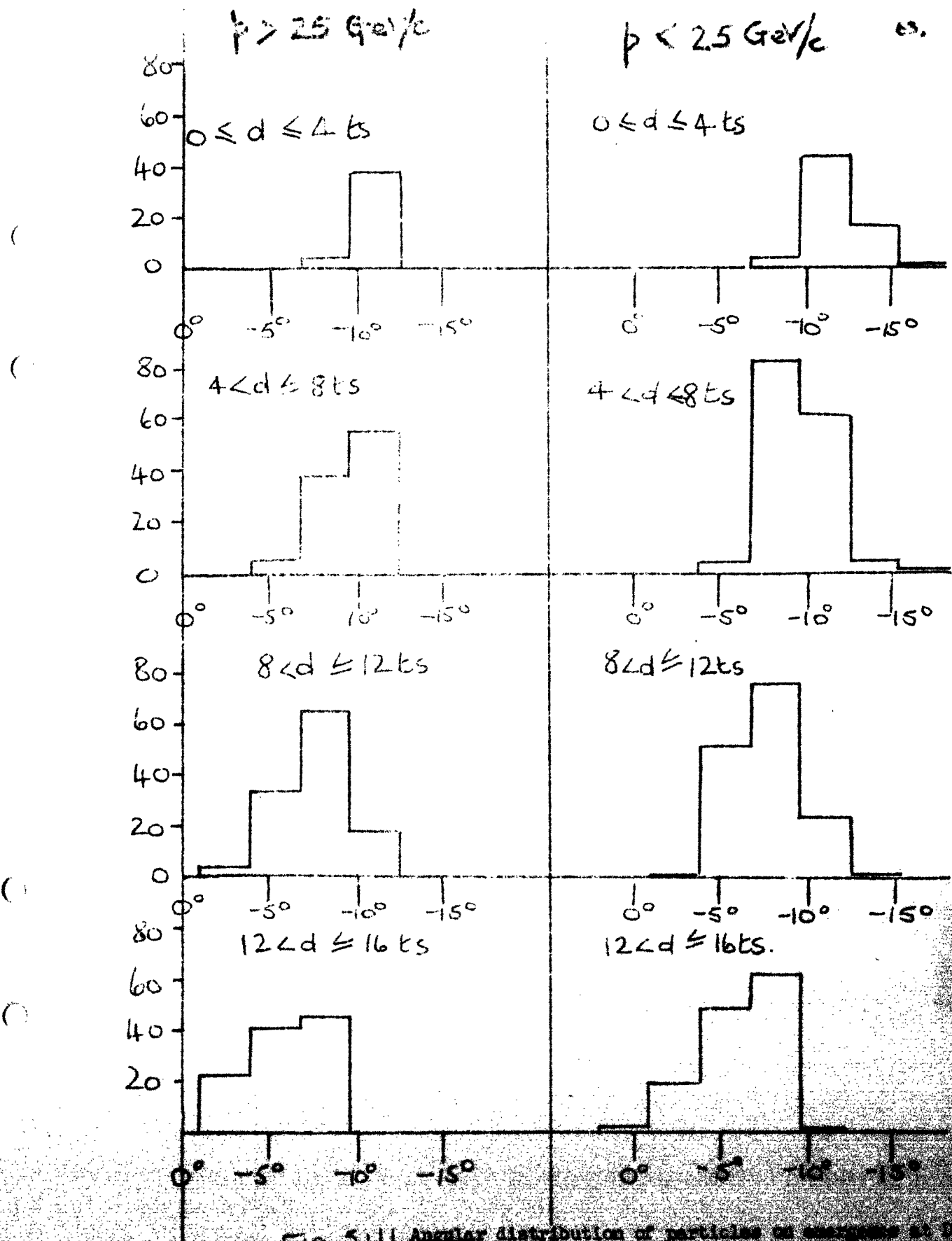
Fig 5·11 Angular distribution of particles at momenta ≷ 0 (a ≤ 16)
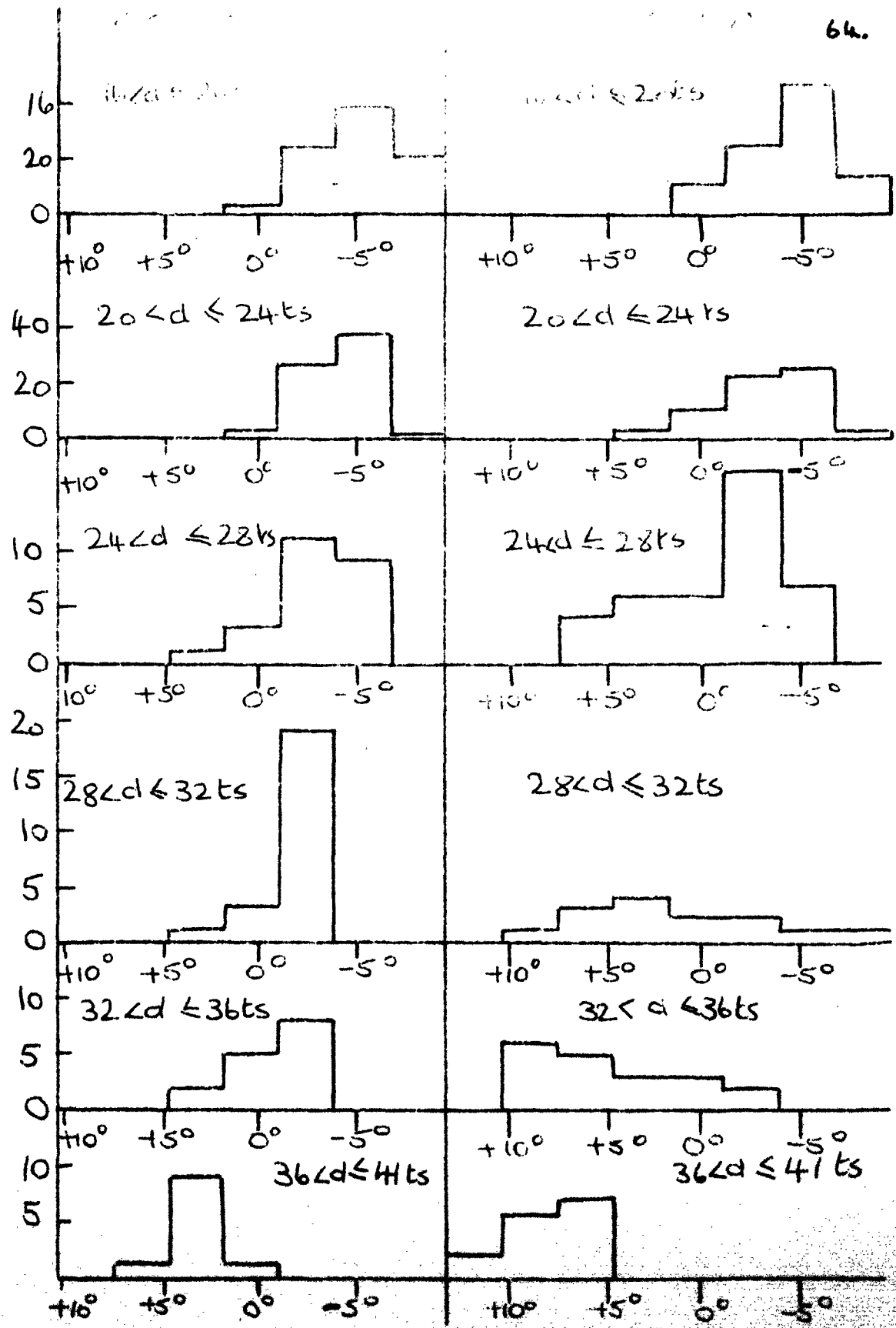
Fig 5.12 Angular distribution of particles on emergence at D
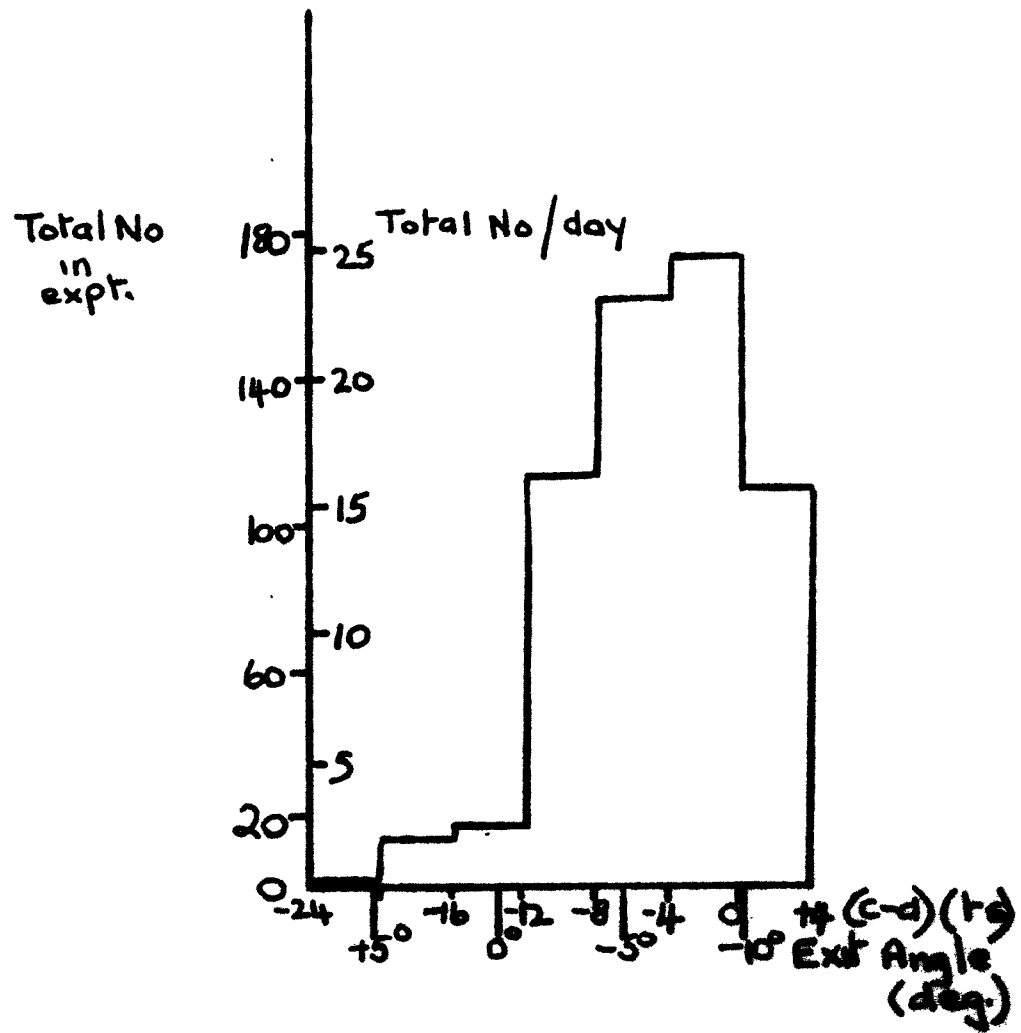
Fig. 5·13 Total angular distribution.

Table 5.5 Distribution of particles with exit angle at D
as a function of position in D

Position in D (t.o.s.)	$+7°39'$ $+4°47'$	$+4°47'$ $+1°53'$	$+1°53'$ $-1°0'$	$-1°0'$ $-3°54'$	$-3°54'$ $-6°47'$	$-6°47'$ $-9°37'$	$-9°37'$ $-12°25'$ Exit Angle
0 – 4						4	38
4 – 8					5	38	55
8 – 12				4	34	66	18
12 – 16				22	40	45	
16 – 20			3	24	38	21	
20 – 24			2	26	37	1	
24 – 28		1	3	11	9		
28 – 32		1	1	19			
32 – 36		2	5	8			
36 – 41	1	9	1				

6 THE MOMENTUM SPECTRUM OF MUONS IN THE ZENITH ANGLE RANGE $77.5^{\circ} - 90^{\circ}$

6.1 Acceptance Characteristics of the Spectrograph

The basic data for the spectrum measurements were given in §5. The calculation of the spectra as a function of zenith angle follows the method outlined in §4, i.e. spectra expected at sea level, on the basis of pions being the sole parents of muons, are used to calculate the expected rate of events as a function of zenith angle and momentum.

The expected spectra are given in Fig. 6.1.

The probability of a particle being accepted by the spectrograph has been found graphically. The quantity determined is the 'acceptance function', measured in units of cm^2 sterad; the rate of events recorded then follows as the product of the intensity and this function.

The acceptance function can be written as the product

$$A_o(p,\theta). \eta. G.$$

$A_o(p,\theta)$ is the geometrical function determined by the overall size of the counter trays and η is the probability of none of the appropriate counters in the instrument being quenched at the instant when the particle (of momentum p, at zenith angle θ) passes through them, G is the average probability of a particle not traversing an insensitive region in any counter tray on its passage through the instrument.

In the present case $\eta = 0.88$ and $G = 0.56$.

The function $A_o(p,\theta)$ is shown in Fig. 6.2.

10^{-5} 80°
82°
82°
84°
86°
88°
90°
90°

π production spectrum
$N(E_\pi) dE_\pi = 0.18 E_\pi^{-2.69}$

Dotted curves for 82°
and 90° uncorrected for
scattering.

Intensity (cm^{-2} sr^{-1} sec^{-1} GeV^{-1})

10^{-6}

10^{-7}

10^{-8}

10^{-9}

10^{-10}

1   10   100   1,000

Sea level energy (GeV)
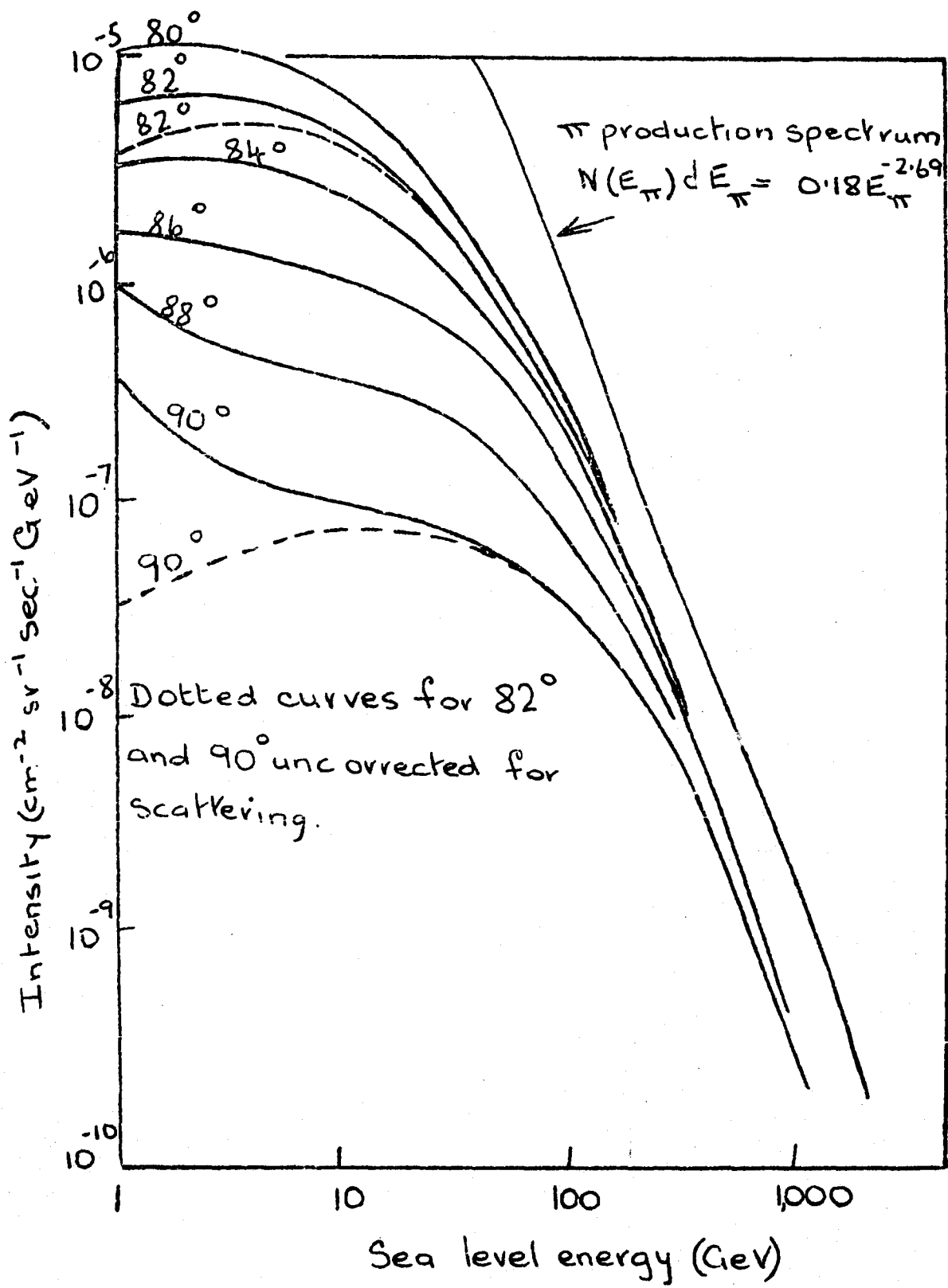
Fig. 6.1 The expected muon spectra at sea level as a
function of zenith angle
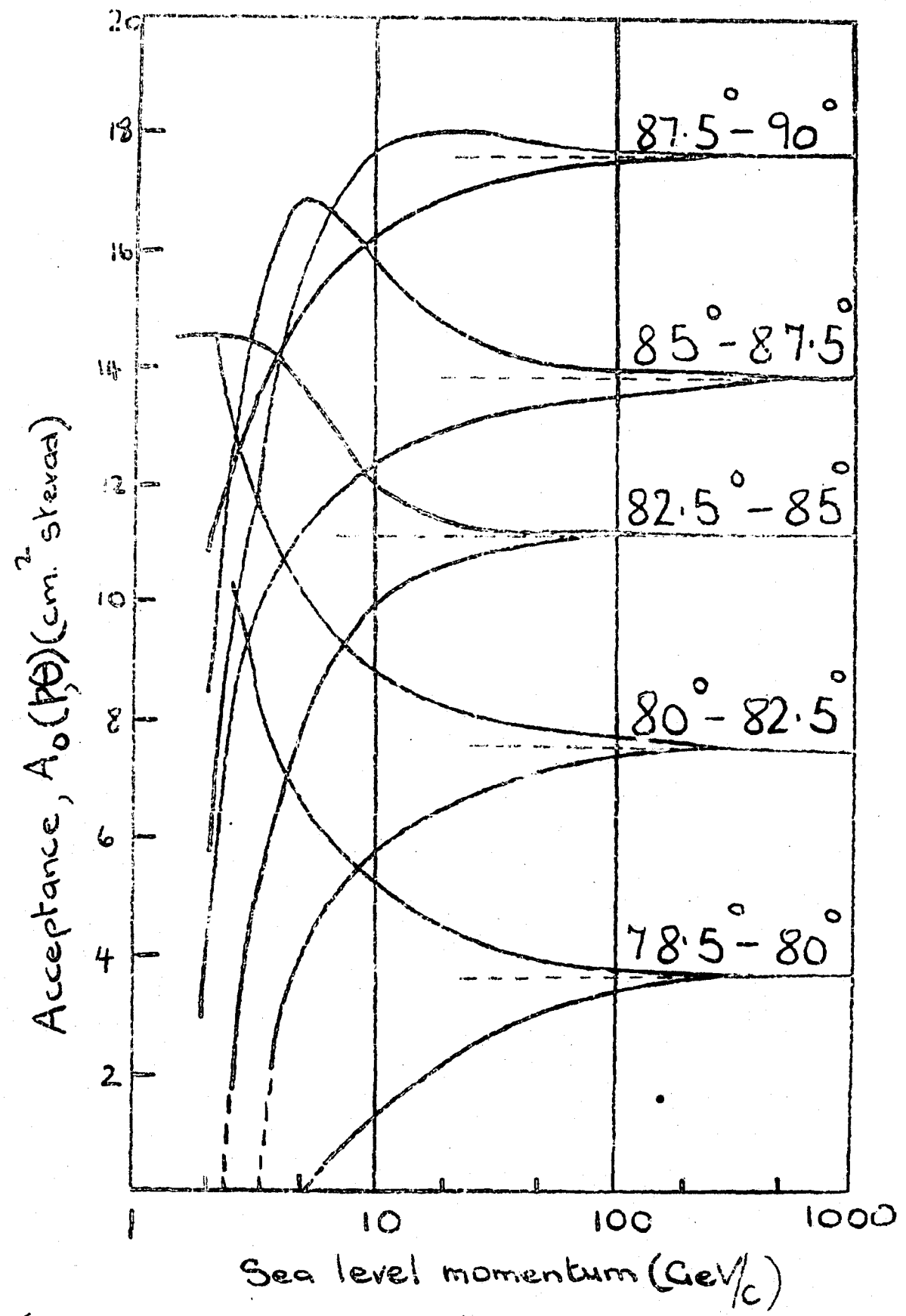
Fig. 6.2 The acceptance function $A_o(p, \theta)$

6.2 The Measured Momentum Spectra

The derived momentum spectra are shown in Figs. 6.3 - 6.7. In addition to the spectra expected for all pions as parents those for all kaons as parents are also shown.

In Fig. 6.8 the data for the whole zenith angle range are collected together and a histogram is plotted. The results show quite clearly that except at the lowest energies there is no evidence for a large fraction of the sea level muons being derived from kaons. Further discussion on this point is deferred until the next Chapter.

6.3 The Positive-Negative Ratio

The ratio of the numbers of positive to negative muons as a function of muon energy is an important parameter, bearing as it does on the multiplicity of particles produced in high energy collisions. The data from the present experiment has been combined and the measured ratios have been found as a function of muon energy at production.

The data are given in Table 6.1 and the ratios are plotted in Fig. 6.9. Also shown in the figure are the recent results of Hayman and Wolfendale (1962); these measurements were made with the Vertical Spectrograph at Durham and the measured energies have been converted to energies at production.

Although the statistical accuracy of the present data is low the results are of importance in that they confirm the conclusion of Hayman and Wolfendale that the ratio does not tend to unity, at least before several hundred GeV. This fact was interpreted by these authors as showing that the fluctuations in the multiplicity of high energy pions increases with increasing energy.
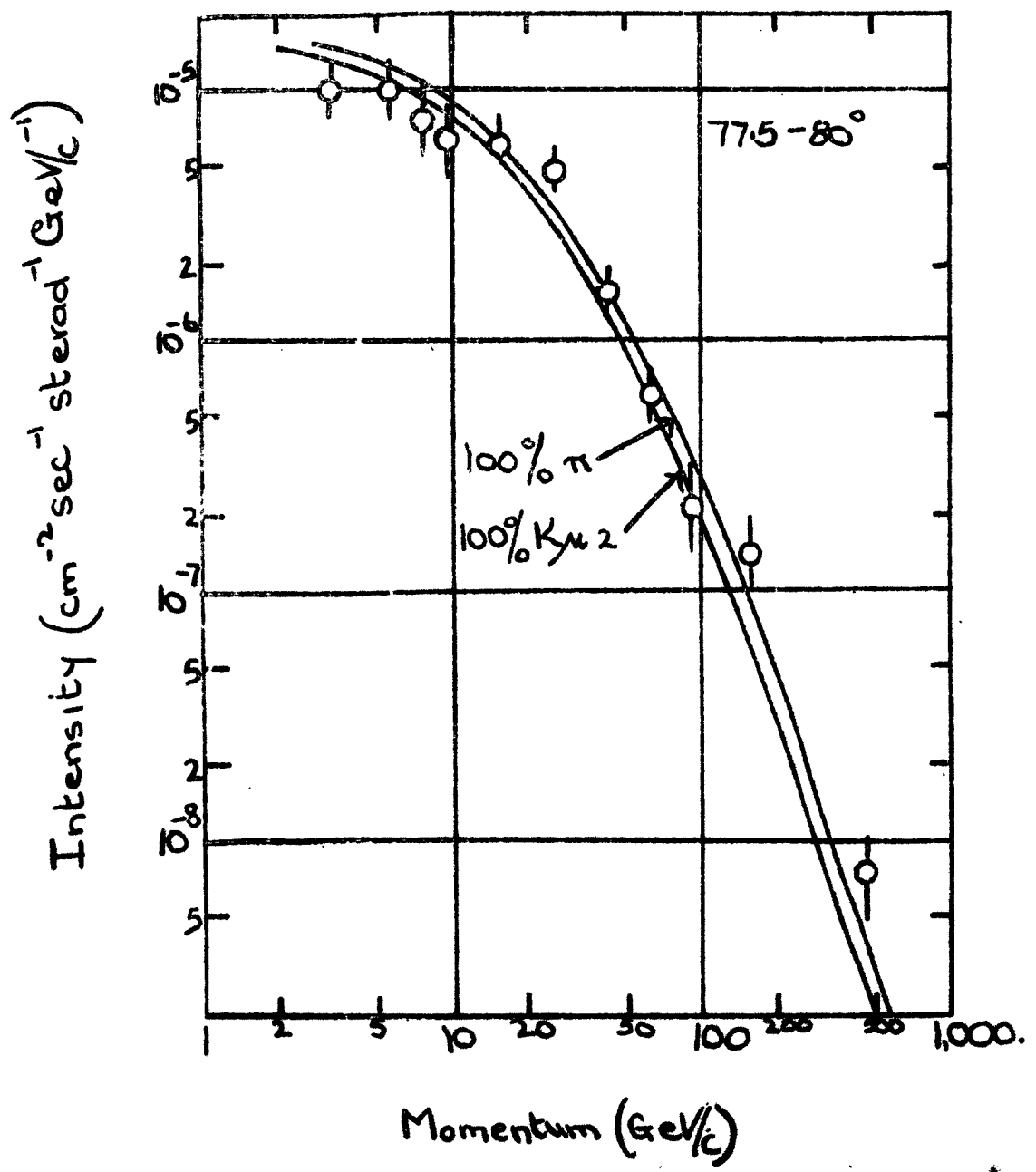
Fig 6.3 The Measured Momentum Spectrum in the range 77.5-80°

The graph shows Intensity (cm^{-2} sec^{-1} sterad^{-1} GeV/c^{-1}) plotted against Momentum (GeV/c), labelled 80 – 82.5°, with curves marked 100% π and 100% Kμ2.
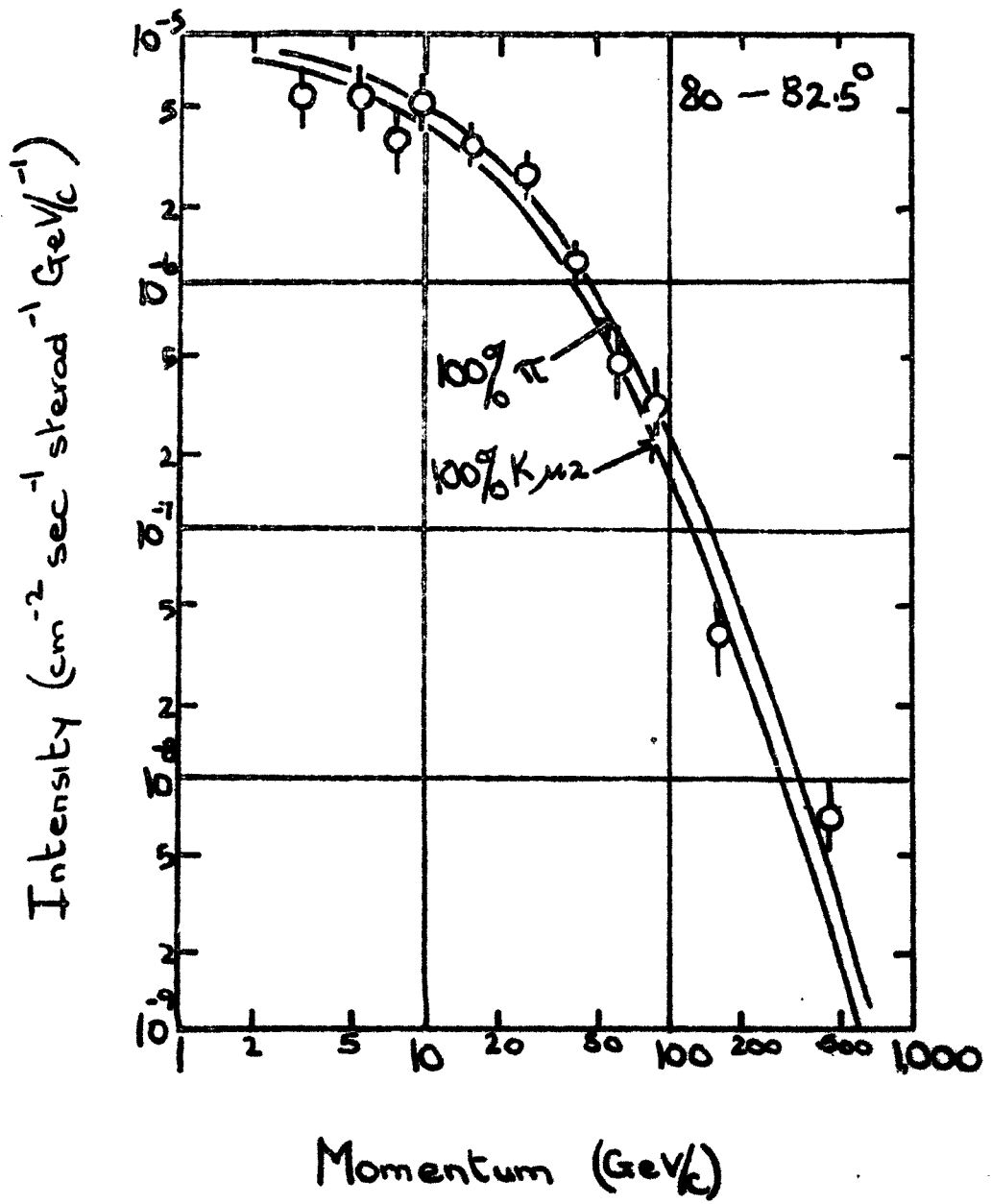
Fig 6.4 The Measured Momentum Spectrum in the range 80-82.5°
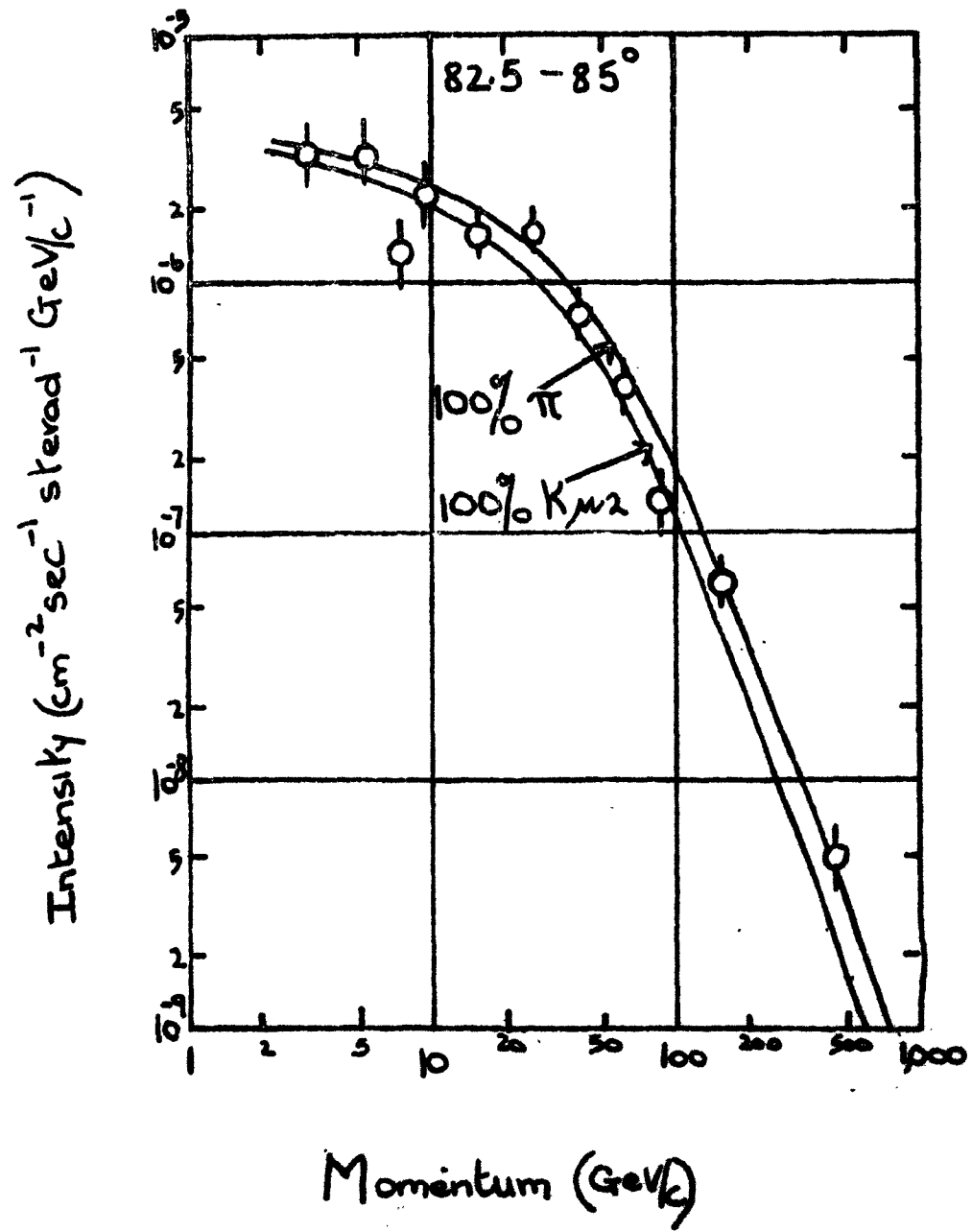
Fig. 6.5 The Measured Momentum Spectrum in the range 82.5-85°
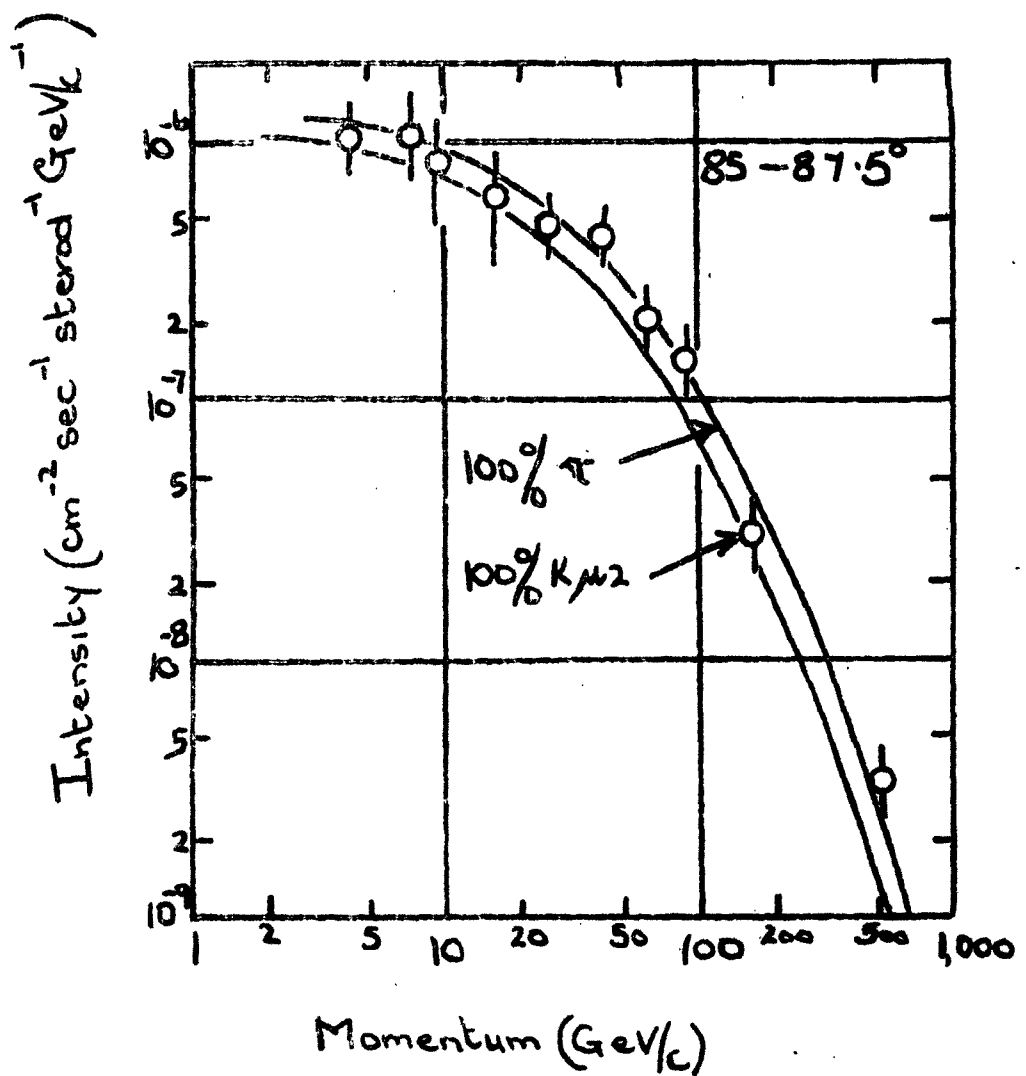
Fig 6.6 The Measured Momentum Spectrum in the range 85-87.5°
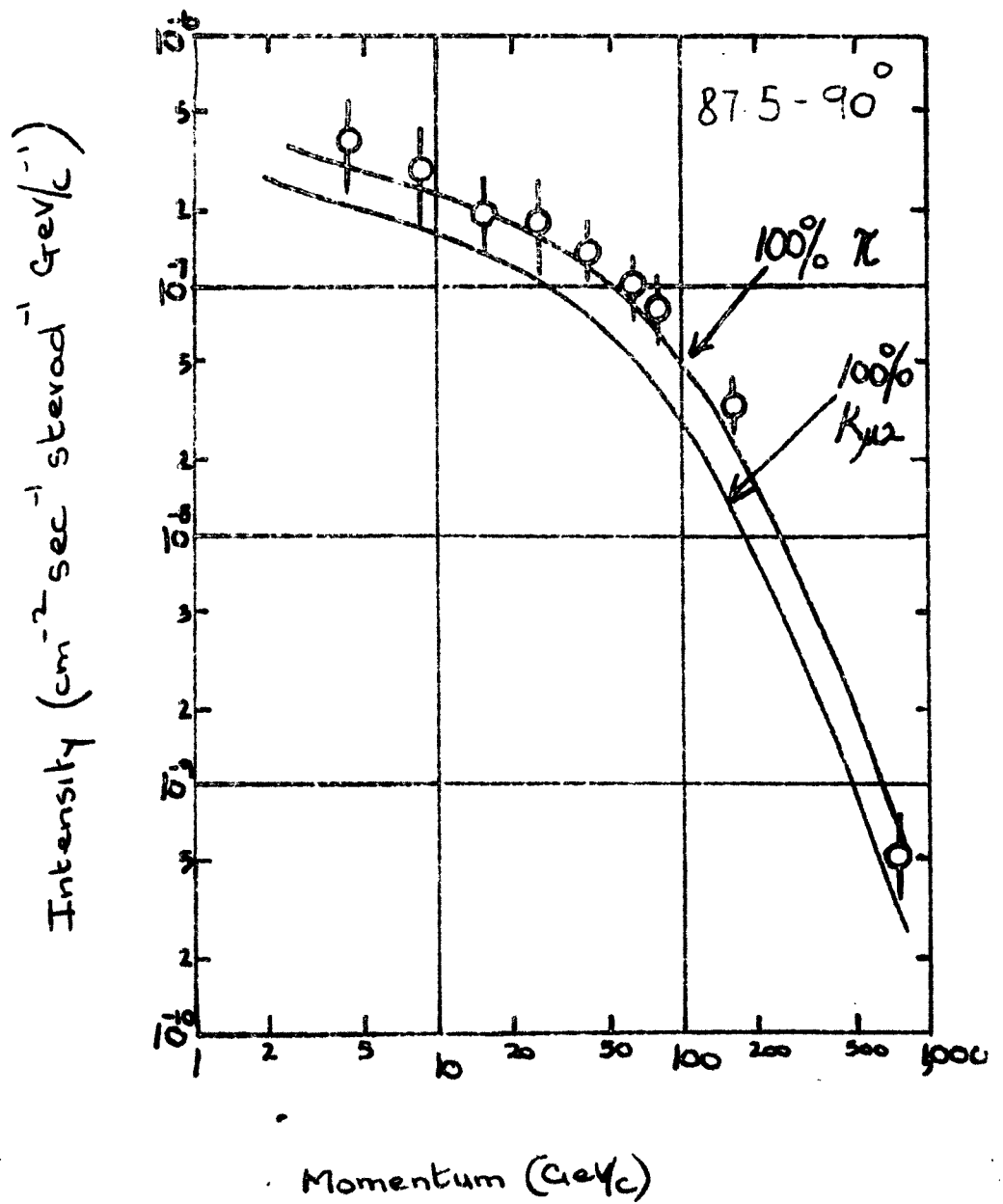
Fig. 6.7 The Measured Momentum Spectrum in the range 87.5-90°
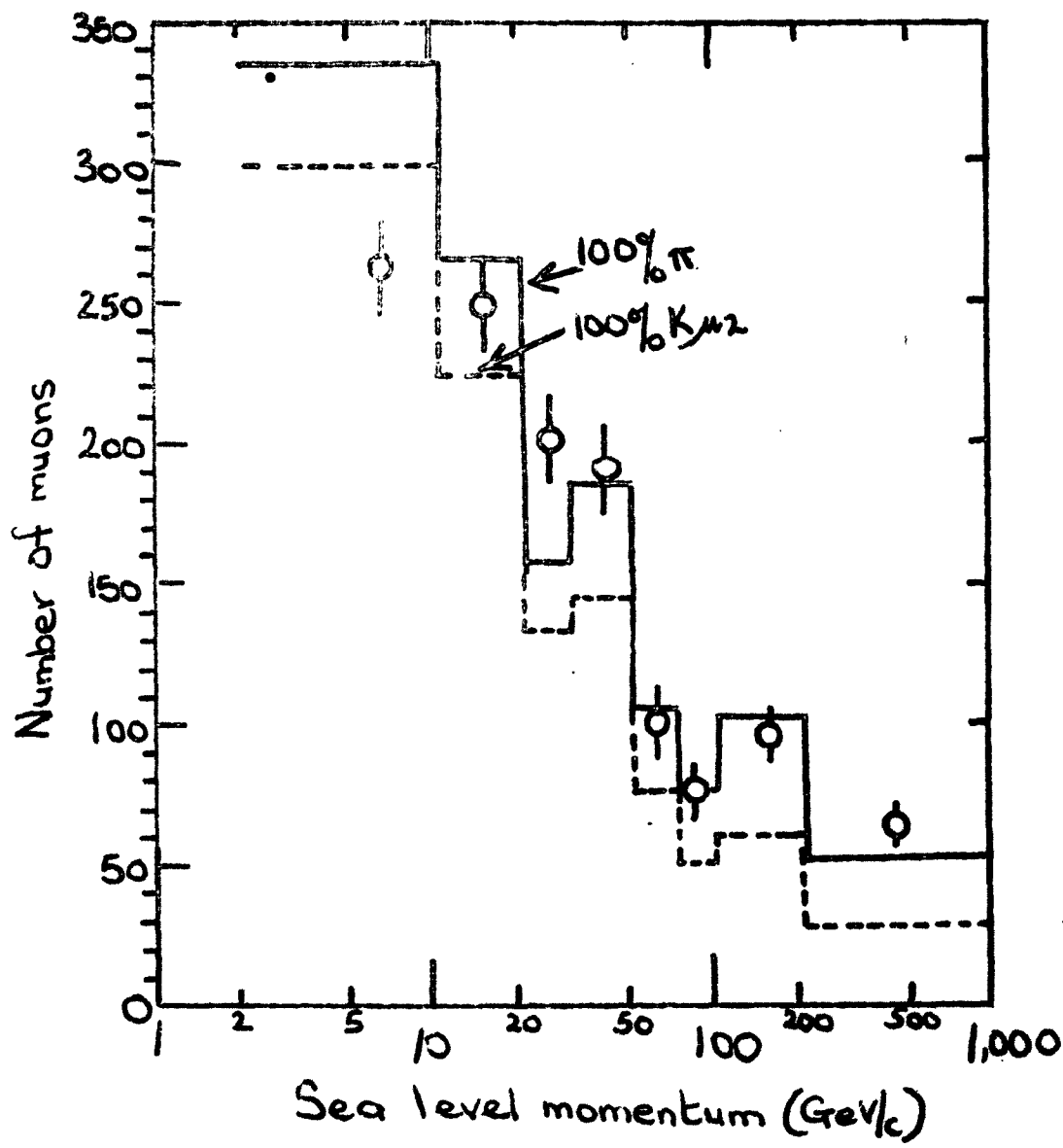
Fig 6.8 Collected Data for the range 77.5-90°

Energy Range at production GeV	Field A		Field B		Positive-Negative Ratio
	μ^+	μ^-	μ^+	μ^-	
10 - 20	3	67	96	1	2.07 ± 1.57
20 - 30	33	95	84	24	1.24 ± 0.17
30 - 40	43	44	67	40	1.29 ± 0.60
40 - 55	45	62	64	54	0.93 ± 0.40
55 - 75	46	41	54	36	1.30 ± 0.47
75 - 100	31	30	51	32	1.48 ± 0.26
100 - 150	28	23	40	16	1.74 ± 0.36
150 - 200	15	11	13	11	1.27 ± 0.11

Table 6.1   The Positive-Negative Ratio as a Function of Muon Energy at

Production

(A and B refer to opposite field directions)
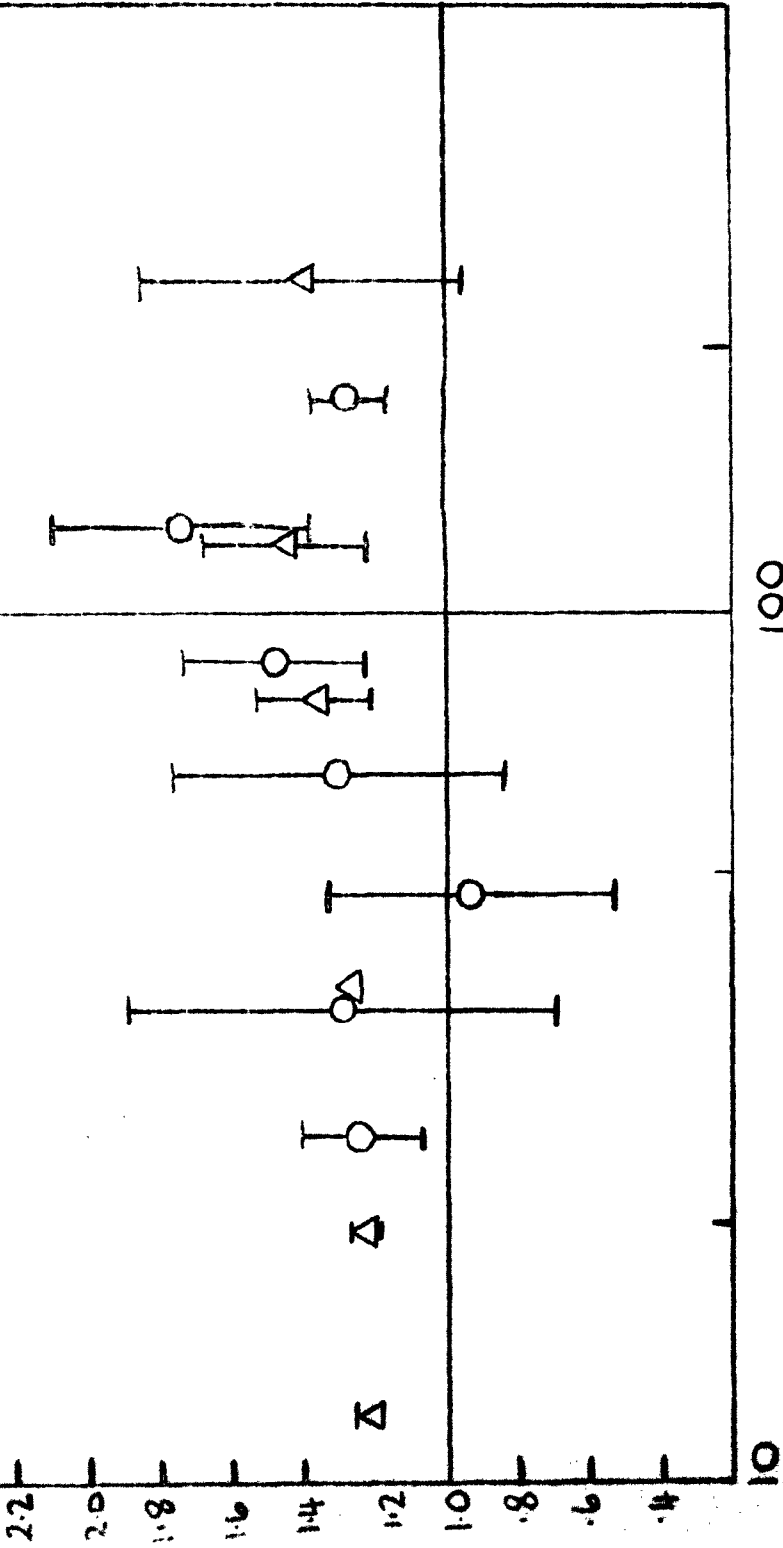
Fig. 6.9 The positive-negative ratio as a function of muon energy at production

7 INTERPRETATION OF RESULTS

7.1 Statement of the Problem

The basic problem is to derive information about the characteristics of high energy nuclear interactions from a comparison of the inclined and vertical muon spectra. Of the characteristics accessible to study, the most significant is the relative production in the high energy collisions of particles which give rise eventually to muons. The most convenient approach is to take the measured vertical spectrum as the starting point and from it to calculate the production spectra of the parent particles/different assumed masses of these particles. The spectra are then used to calculate predicted spectra at large zenith angles and, by comparison with the observed spectrum conclusions can, in principle, be drawn about the most likely parent particle (or combination of particles).

Prior to the present work being carried out it was not clear that the inclined muon spectrum was sensitive to the mass of the parent particle. The early work of Jakeman (1956) showed that a large sensitivity existed but the values taken for the masses and lifetimes of the relevant particles were, at that early time, necessarily imprecise. Pak et al. (1961) implied a sensitivity, but quantitative estimates were not given. The theoretical studies of Allen and Apostolakis (1961), however, showed that the inclined spectrum should be comparatively insensitive to the mass of the parent particle.

It is clear, then, that a detailed theoretical analysis of this problem is necessary.

7.2 The Vertical Muon Spectrum at Sea Level

The vertical spectrum is a key measurement and some attention will be given to the derivation of the best estimate.

It has been pointed out already (Chapter 1) that measurements of the momentum spectrum in the vertical direction have also been made by the Durham Cosmic Ray Group. Of the direct measurements made to date the Durham data (Gardener et al., 1962; Hayman and Wolfendale, 1962) are the most comprehensive and, it is hoped, the most accurate. The data on the intensities are given in Tables 7.1 and 7.2. It is necessary to point out that these data refer to single particles which pass unaccompanied through the spectrograph. It is likely that the fraction of muons lost through their being accompanied on arrival at the instrument is small at momentum below 100 GeV/c. At higher momenta some appreciable bias must result but the overlap of this momentum range with that covered by the present experiments is small.

7.3 The Production Spectrum of Muons in the Vertical Direction

Rather than calculate the production spectrum of the parent particles directly from the measured sea level spectrum it is convenient to introduce an intermediate stage, the 'muon production spectrum' $M(p)$ or $M(E)$ (Although momentum is the measured quantity it is conventional to work in terms of energy spectra; over the energy range considered where the particles are relativistic $E = pc$ and $M(E)$ is numerically equal to $M(p)$ if p is expressed in $\frac{1}{c} \times$ energy units).

In deriving $M(E)$ it is sufficiently accurate to assume that the muons are generated at a unique height in the atmosphere. This simplification is possible because first order errors cancel when the same assumption is made in going from the muon production spectrum in an inclined direction to the inclined muon spectrum at sea level. The resulting spectrum, $M(E)$, is given in Table 7.3; also given are the factors entering into the calculation, viz: the energy loss in the atmosphere from the production height (85 g.cm^{-2}, the medium height) to

Table 7.1 The Measured Differential Intensity of Vertical Cosmic Ray
Muons as a Function of Momentum over the Range 5-1000 GeV/c

Method of measurement	Momentum (GeV/c)	Differential Intensity $(cm^{-2}sec^{-1}sterad^{-1}(GeV/c)^{-1})$	Statistical error (%) (standard deviation)
I	5.45	$3.21 \cdot 10^{-4}$	4.2
*	6.3	$2.44 \cdot 10^{-4}$	3.5
	7.45	$1.95 \cdot 10^{-4}$	2.8
	9.15	$1.28 \cdot 10^{-4}$	2.4
	10.8	$8.51 \cdot 10^{-5}$	3.0
	12.4	$6.14 \cdot 10^{-5}$	2.7
	14.6	$4.35 \cdot 10^{-5}$	2.6
	17.8	$2.52 \cdot 10^{-5}$	2.6
	22.6	$1.35 \cdot 10^{-5}$	2.6
	31.3	$5.85 \cdot 10^{-6}$	2.6
	42.3	$2.88 \cdot 10^{-6}$	3.9
	56.1	$1.22 \cdot 10^{-6}$	4.5
II	72.5	$5.75 \cdot 10^{-7}$	8
	88.1	$3.27 \cdot 10^{-7}$	9
	112	$1.36 \cdot 10^{-7}$	10
III	153	$5.18 \cdot 10^{-8}$	18
	244	$1.14 \cdot 10^{-8}$	20
	413	$1.98 \cdot 10^{-9}$	+60/-37**
	854	$1.84 \cdot 10^{-10}$	+70/-42**

* Region of normalization to Geiger counter spectrum.
** Error according to the analysis of Regener (1951).
I   Projection method, m.d.m. = 273 ± 8 GeV/c
II Track simulator method, m.d.m. = 493 ± 84 GeV/c
III Track simulator method, m.d.m. = 657 ± 112 GeV/c

Footnote: after Hayman and Wolfendale, 1962.

Table 7.2 The Intensities and Values of γ_μ of the Differential Spectrum of
Vertical Cosmic Ray Muons at Standard Momenta over the Complete Range
0.4-1000 GeV/c

Momentum (GeV/c)	Differential Intensity ($cm^{-2}sec^{-1}sterad^{-1}(GeV/c)^{-1}$)	γ_μ
0.4	$2.58 . 10^{-3}$	-0.44
0.5	$2.85 . 10^{-3}$	-0.16
0.7	$2.80 . 10^{-3}$	+0.22
1.0	$*2.45 . 10^{-3}$	+0.56
1.5	$1.93 . 10^{-3}$	+0.90
2.0	$1.48 . 10^{-3}$	+1.14
3.0	$8.73 . 10^{-4}$	+1.42
5.0	$3.79 . 10^{-4}$	+1.76
7.0	$2.05 . 10^{-4}$	+1.96
10.0	$1.02 . 10^{-4}$	+2.14
15	$4.16 . 10^{-5}$	+2.35
20	$2.04 . 10^{-5}$	+2.48
30	$7.20 . 10^{-6}$	+2.65
50	$1.77 . 10^{-6}$	+2.85
70	$6.60 . 10^{-7}$	+2.98
100	$2.25 . 10^{-7}$	+3.10
150	$6.28 . 10^{-8}$	+3.22
200	$2.40 . 10^{-8}$	+3.30
300	$6.10 . 10^{-9}$	+3.38
500	$1.12 . 10^{-9}$	+3.47
700	$3.50 . 10^{-10}$	+3.51
1000	$9.70 . 10^{-11}$	+3.55

* Normalized to the intensity given by Rossi (1948). After Hayman & Wolfendale 1962

Table 7.3 The Vertical Muon Production Spectrum, M(E)

Energy at production (GeV)	Survival Probability S(E)	Energy Loss (GeV)	Correction Factor $F_c(E)$	Production Spectrum, M(E) ($cm^{-2}sec^{-1}steradian^{-1}GeV^{-1}$)
3.00	0.27	2.00	0.86	7.75×10^{-3}
3.55	0.36	2.05	0.89	4.76×10^{-3}
4.10	0.43	2.10	0.91	3.14×10^{-3}
5.15	0.52	2.15	0.94	1.57×10^{-3}
7.35	0.64	2.35	0.96	5.71×10^{-4}
9.40	0.72	2.40	0.97	2.76×10^{-4}
13.50	0.79	2.50	0.98	1.27×10^{-4}
17.60	0.84	2.60	1.00	4.95×10^{-5}
22.70	0.88	2.70	1.00	2.35×10^{-5}
32.80	0.92	2.80	1.00	7.84×10^{-6}
52.90	0.95	2.90	1.00	1.86×10^{-6}
73.00	0.96	3.00	1.00	6.87×10^{-7}
103.1	0.97	3.10	1.00	2.32×10^{-7}
153.3	0.98	3.25	1.00	6.40×10^{-8}
203.4	0.98	3.40	1.00	2.45×10^{-8}
303.8	0.99	3.75	1.00	6.16×10^{-9}
504.3	1.00	4.25	1.00	1.12×10^{-9}
704.8	1.00	4.75	1.00	3.50×10^{-10}
1,005.6	1.00	5.60	1.00	9.70×10^{-11}

sea level, the survival probability, $S(E)$, and the correction factor, $F_c(E)$, which allows for the variation of rate of energy loss with energy.

7.4 Unstable Particles giving rise to Muons

It was pointed out in §7.1 that the object is to obtain information on the relative frequencies of production of the various parents of the muons. Of the known unstable particles a large fraction give rise to one or more muons at some stage in their decay sequences. The most important decay schemes are listed in Table 7.4. Also given are the relative abundances of the decay modes and the characteristic energy (minimum, maximum and mean) of the resulting muons (The authors are indebted to Mr. J.L. Osborne for this Table).

It is clear from Table 7.4 that if the energy spectra of all the generated particles (pions, kaons, hyperons) were the same then the majority of the muons would come from pions, followed by a smaller contribution from kaons and a much smaller contribution from the hyperons. Consequently attention is directed to the evaluation of the relative frequencies of production of pions and kaons.

In the case of the charged kaon, the most frequent decay mode (58% abundance) is

$$K_{\mu2} \to \mu + \nu,$$ with a lifetime of 1.22×10^{-8} sec.,

and this is also the mode which gives rise to the muons of the highest energies.

The procedure to be followed is to derive the sea level muon spectra expected at large zenith angles for the two extreme cases of all pions and all kaons, decaying in the $K_{\mu2}$ mode, and then to estimate the relative importance of $K_{\mu2}$-production by comparison of the expected spectra with observation. The relative importance of charged kaons can then be found from the known abundance of the $K_{\mu2}$-mode.

Table 7.4 Decay Schemes giving rise to Muons

Particle	Decay Mode	Abundance	Total energy as fraction of Parent total energy		
			$E_{\mu max}$	$E_{\mu main}$	$\bar{E}_\mu$
(a) II body					
$\pi^\pm$	$\mu^\pm + \nu$	100%	1	.573	.787
$K^\pm$	$\mu^\pm + \nu$	58%	1	.046	.523
$K^\pm$	$\pi^\pm + \pi^0 \to \mu^\pm + \nu$	26%	0.918	.050	.396
K^0	$\pi^+ + \pi^-$, $\mu^+ + \nu$, $\mu^- + \bar\nu$	34.5%*	0.914	.049	.394
Λ^0	$p + \pi^- \to \mu^- + \bar\nu$	64%	.244	.037	.121
Σ^+	$n + \pi^+ \to \mu^- + \nu$	49%	.350	.023	.153
Σ^-	$n + \pi^+ \to \mu^- + \bar\nu$	100%	.358	.022	.156
+ the following 3 stage decays					
Σ^0	$\Lambda^0 + \gamma$, 64% $\to p + \pi^- \to \mu^- + \bar\nu$	100%**	.244	.032	~.1
Ξ^0	$\Lambda^0 + \pi^0$, 64% $\to p + \pi^- \to \mu^- + \bar\nu$	100%**	.233	.028	~.1
Ξ^-	$\Lambda^0 + \pi^- \to \mu^- + \nu$, 64% $\to p + \pi^- \to \mu^- + \bar\nu$	100%	2 stage μ .251 / 64% 3 stage μ .233	.026 / .027	.116 / ~.1
(b) III body					
$K^\pm$	$\mu^\pm + \pi^0 + \nu$	4%	.921	.050	.352
$K^\pm$	$\pi^\pm + \pi^0 + \pi^0 \to \mu^\pm + \nu$	2%	.659	.06?	.265
$K^\pm$	$2\pi^\pm + \pi^\pm \to \mu^\pm + \nu$	6%✓	.634	.072	.262
K^0	Branching ratios not known				

* Each parent gives 2 μs   ** each parent gives 0.64 μs
✓ each parent gives 1.64 μs   ✓✓ each parent gives 5 μs

7.5 Derivation of the Production Spectra of Pions and $K_{\mu 2}$-mesons

Since the expected inclined sea level muon spectrum on the assumption of all pions as parents has already been calculated, it is not necessary to carry through the $K_{\mu 2}$-calculations to sea level. Instead, all that is necessary is to evaluate the expected muon production spectra in inclined directions for the two cases of pions and $K_{\mu 2}$-mesons as parents and to translate their comparison to sea level.

Various approximations are made in the analysis, the most important being that the primary particles (protons) and the secondary nuclear inter-acting particles are absorbed exponentially in the atmosphere with the same absorption length ($\lambda = 120$ g. cm^{-2}). The justification for this value of λ comes from the reviews by Sitte (1961) and Perkins (1961) on the attenuation of the whole nuclear-active component in the atmosphere. The attenuation length is significantly greater than the interaction length of protons and pions, due to the comparative inelasticity of the high energy interactions. It is likely that the interaction length for charged kaons is closely similar to that for pions.

Use is made of the relation given by Barrett et al. (1952), between the muon production spectrum, $M_x(E)$, and the production spectrum of the parents $F_x(E/r)$, which assumes a unique correspondence between the energy of a muon and that of its parent particle (i.e. neglects the spread in energy on decay). This relation is

$$M_x(E) = \frac{F_x(E/r_x)}{r_x} \cdot \frac{1}{1 + E/B_x} \qquad \qquad \dots\dots (7.1)$$

where $B_x = \frac{m_x c^2 r_x H}{c T_x}$, T_x is the mean lifetime of the parent particle of mass m_x, H is the weighted scale height of the atmosphere, and E/r_x is the effective energy of the parent particles which give rise to muons of energy E. Small

corrections are applied to the derived relations for $F_x(E/r_x)$ to allow
more accurately for the spread in energies of the muons in the decay process.
The resulting relations are denoted as $F_x(E/r_x)_c$.

The adopted values for the various quantities are:

(i) pions : $r_\pi = 0.76$, $B_\pi = 90$ GeV

(ii) $K_{\mu2}$-mesons $r_K = 0.52$, $B_K = 517$ GeV.

The derived production spectra for pions and $K_{\mu2}$-mesons are given in
Fig. 7.1. Over limited regions of energy the spectra can be approximated by
straight lines of simple analytical form; thus, for the pion production
spectrum, $F_\pi(E)_c = 0.20E^{-2.7}$ for $10 < E < 1000$ GeV, and for the $K_{\mu2}$ production
spectrum, $F_K(E)_c = 0.64E^{-2.95}$ for $20 < E < 500$ GeV.

7.6 The Muon Production Spectra at Large Zenith Angles

The muon production spectra can be derived in a straightforward way,
using equation (7.1) modified to allow for the effect of obliquity by using
the value of B_x appropriate to the zenith angle θ. At small zenith angles
$B_x(\theta) = B_x \sec \theta$ but at angles above about 75° a more complicated expression
is necessary.

Neglecting decay spread, the ratio of the muon production spectra, for
the cases of all $K_{\mu2}$ mesons, and all pions, as parents of the muons, follows
directly as

$$\frac{M_K(E,\theta)}{M_\pi(E,\theta)} = \frac{F_K(E/r_K)}{F_\pi(E/r_\pi)} \cdot \frac{r_\pi}{r_K} \cdot \frac{(1 + E/B_\pi(\theta))}{(1 + E/B_K(\theta))} \qquad \dots\dots\dots (7.2)$$

under the same approximation as for equation (7.1). Small corrections are
applied for the effect of decay spread, and the ratio is plotted as a function
of E for various values of θ in Fig. 7.2. Since the subsequent history of the
muons does not depend on the character of their parents the ratios shown in
Fig. 7.2 are also the ratios of the sea level muon intensities expected in the
two cases.
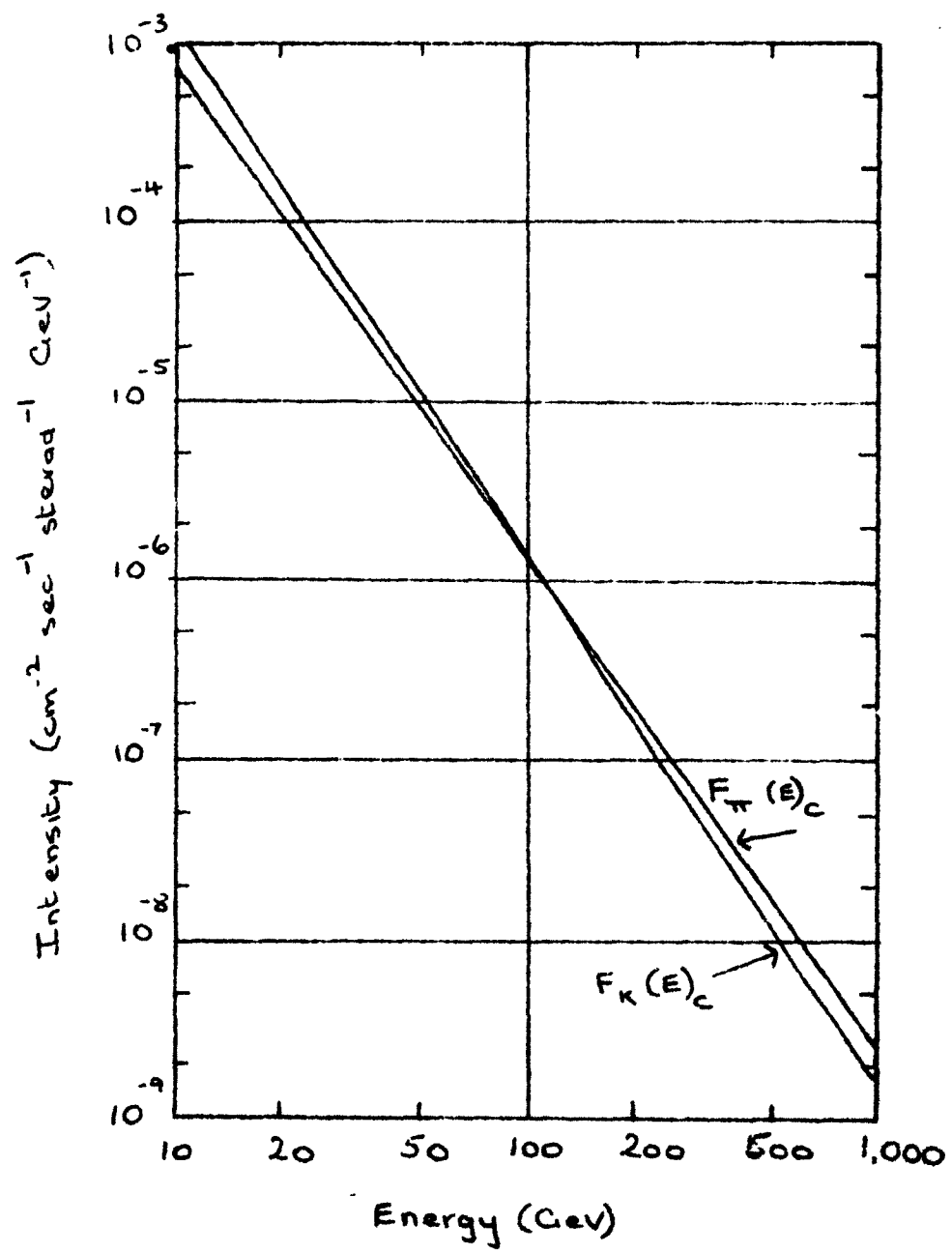
Fig. 7.1 Production for pions and $K_{\mu e}$ -mesons
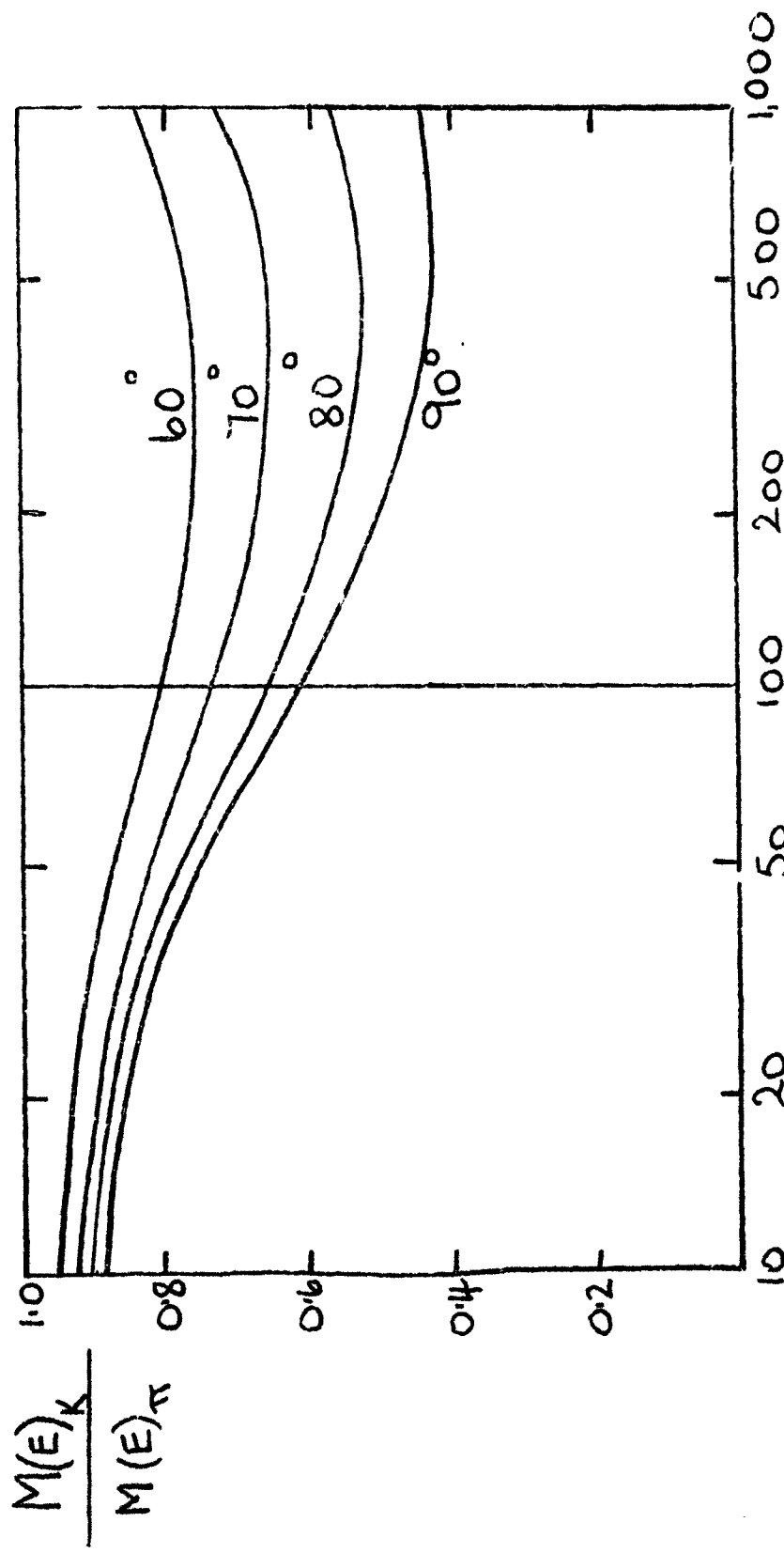
Fig. 7.2 Ratio of the muon production spectra vs energy

It is immediately apparent that the intensity of muons in inclined directions is sensitive to the nature of the parent particles, and, if adequate statistical accuracy is available, the fractions of muons derived from pions and kaons can be determined.

### 7.7 Determination of the K/π Ratio from the Measurements of Inclined Spectra

7.7.1 The measurements at 80°

The spectrum measured at 80° (Fig. 4.5, p 38) has been converted to a spectrum at production, and the intensities are compared in Fig. 7.3 with those expected on the basis of 100% pions or 100% $K_{\mu2}$-mesons as parents. Also shown in the figure is the curve corresponding to equal production of pions and $K_{\mu2}$-mesons.

It is possible, by interpolation, to determine the fraction of $K_{\mu2}$-mesons (F_K) required to give agreement with experiment. It is clear from the figure that there is no evidence for a large value of F_K, in fact, the results are not inconsistent with $F_K = 0$ throughout. The derived values of F_K have significance only for the two points of highest energy where the statistical accuracy is reasonable. The interpolated values are given in Table 7.5. In this table the errors in F_K have been increased to allow for the statistical errors ($\sim 3\%$) in the vertical muon spectrum on which the calculations are based.

7.7.2 The measurements in the range 77.5°-90°

A similar treatment has been carried out for the measurements made with the flash-tube spectrograph and the data of Figs. 6/have been combined to give
.3-6.7
the ratios of muon intensities at production given in Fig. 7.4. A feature of the results is that there is some anomalous behaviour of the ratio at energies below 20 GeV; however, this is just the region where there are large corrections for the effects of scattering in the atmosphere, energy loss in the magnet, etc.

Fig. 7.3 Ratio of the muon production spectra for the experiment at 80°
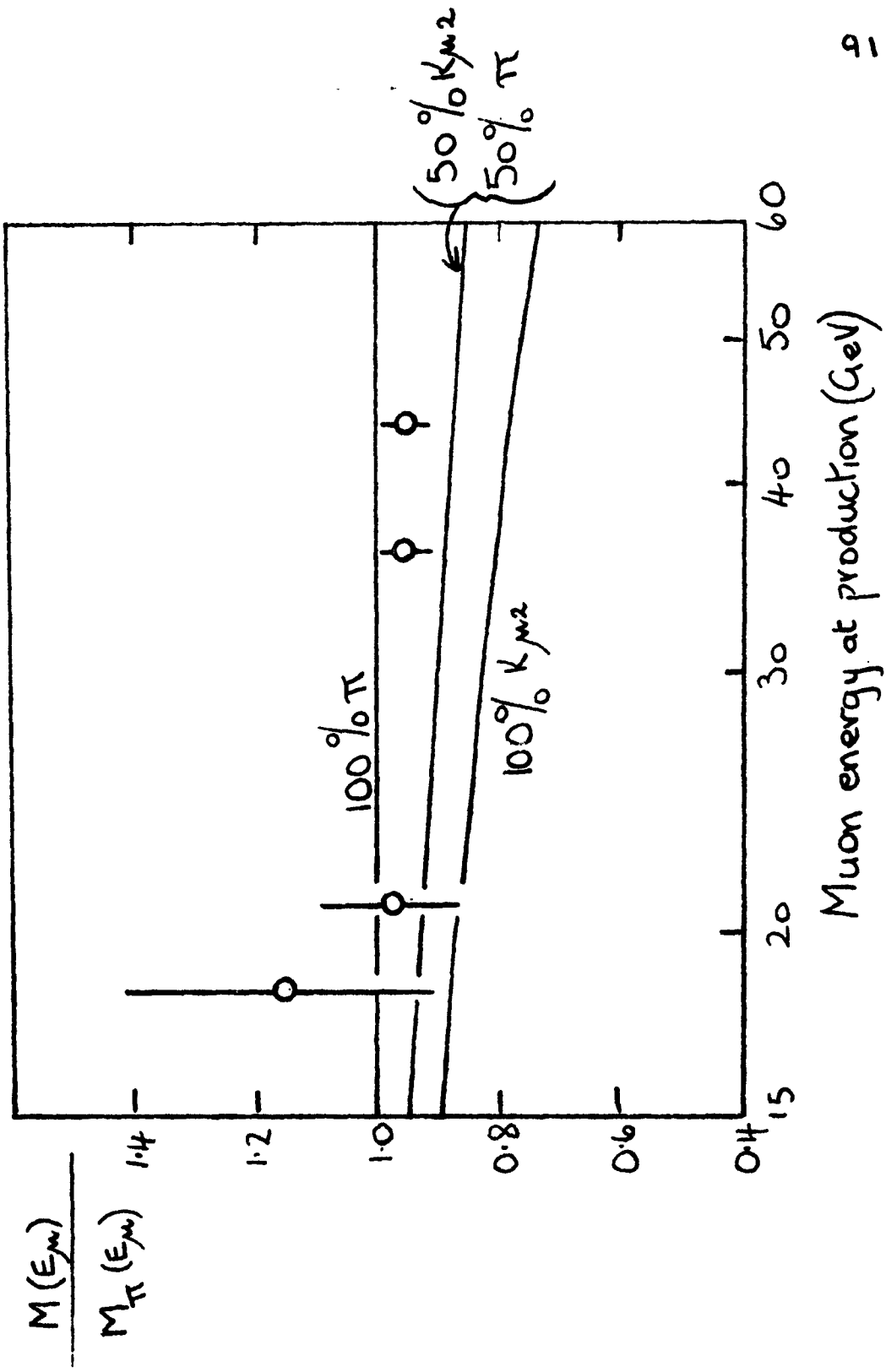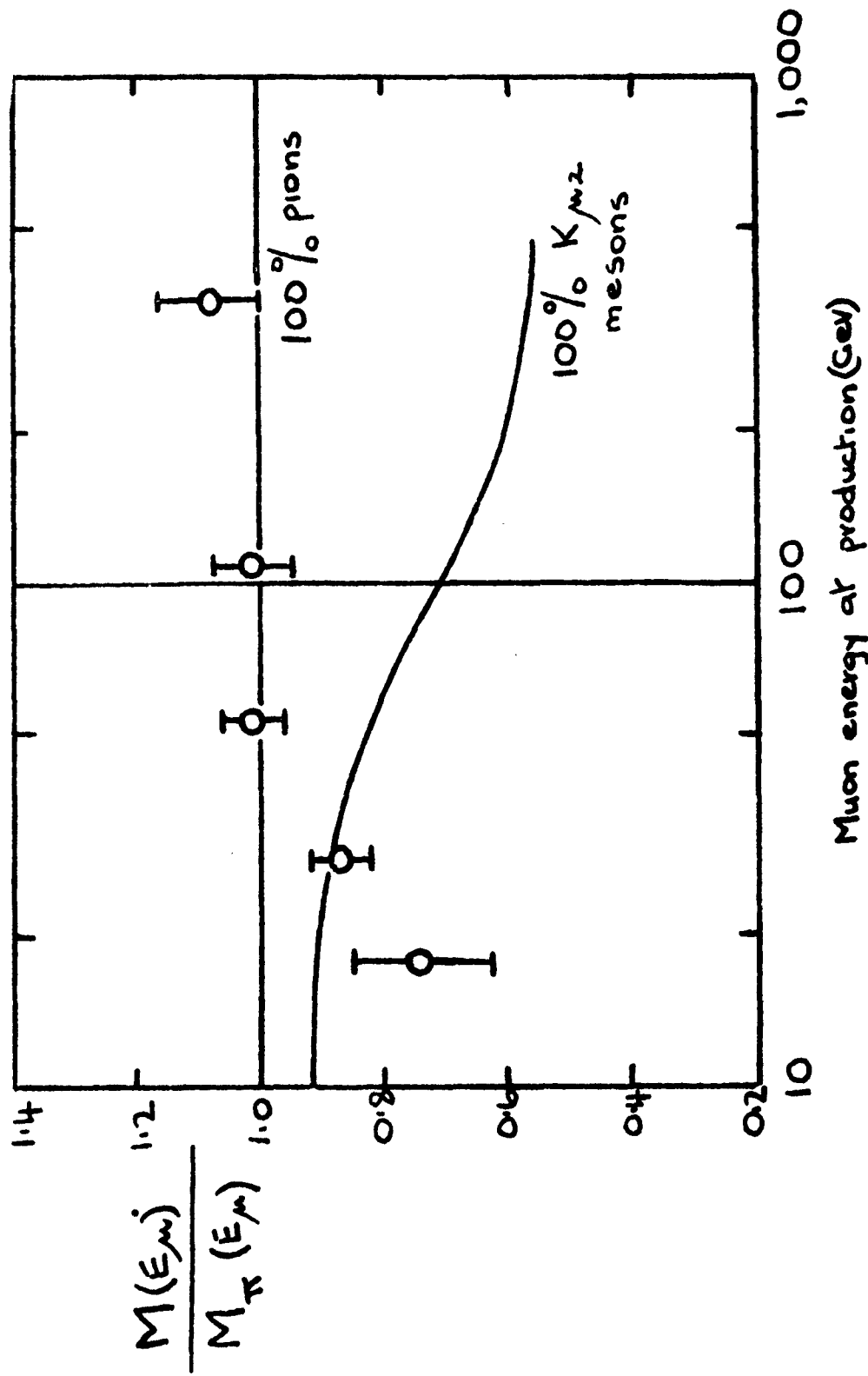
Fig. 7.4 Ratio of the muon production spectra for the experiment covering the range 77.5 - 90°

It is considered that these anomalous values do not invalidate the conclusions at high energies where only small corrections are applied to the data.

The interpolated values of F_K are given in Table 7.5

7.7.3 The Measurements of Allen and Apostolakis (1961)

It has been remarked already that the only other measurement of the momentum spectrum at very large zenith angles ($>70^{\circ}$) is that by Allen and Apostolakis (1961). Since their results have not been analysed with respect to the determination of the quantity F_K this analysis is carried out here. The data for the angular range $65^{\circ}-85^{\circ}$ have been combined and the ratios of observed to expected intensities of muons at production have been calculated as a function of muon energy. These results are presented in Fig. 7.5.

The values of F_K have been found in the usual way and these are given in Table 7.5.

7.7.4 Conclusions from the measurements of inclined spectra

The values of F_K found in the three experiments are plotted against muon energy, for energies above 20 GeV, in Fig. 7.6; under the assumption that F_K does not vary with muon energy over the range 20 - 400 GeV, the data can be combined with the result that F_K is less than ~0.25. This means that less than 25% of the sea level muons in this energy range are derived from kaons decaying in the $K_{\mu 2}$-mode.

The calculations can be pressed a stage further by determining the corresponding contribution from all charged kaons, from a knowledge of the relative abundance of charged kaons of decay modes other than $K_{\mu 2}$ and their relative efficiency of producing muons. The most important mode is the $K_{\pi 2}$-mode

Table 7.5 F_K as a function of muon energy at production

Experiment	Muon Energy (GeV)	F_K
Durham, 80°	36	0.25 ± 0.23
	44	0.22 ± 0.20
Durham, $77.5 - 90^\circ$	28	> 0.66
	53	< 0.22
	105	< 0.18
	361	< 0.02
Allen and Apostolakis	28	< 0.23
	55	< 0.72
	108	< 0.28
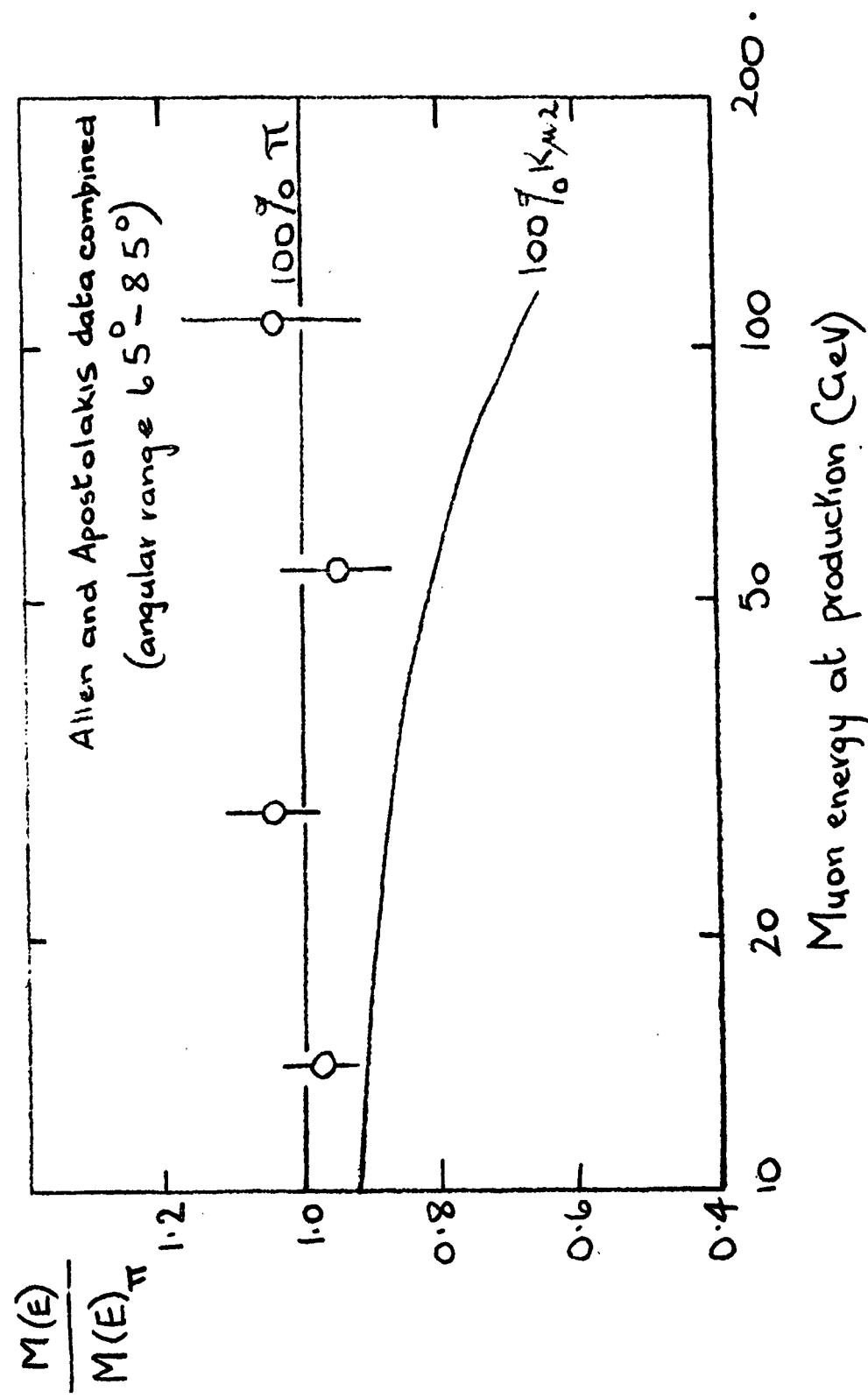
Fig. 7.5 Ratio of the muon production spectra for the experiment by Allen and Apostolakis (1961)

□ 80° spectrum (§4) O Allen + Apostdakis (1961)
◇ 77.5-90° spectrum (§7)

Muon energy at production $E_\mu \rightarrow$ (Gev)
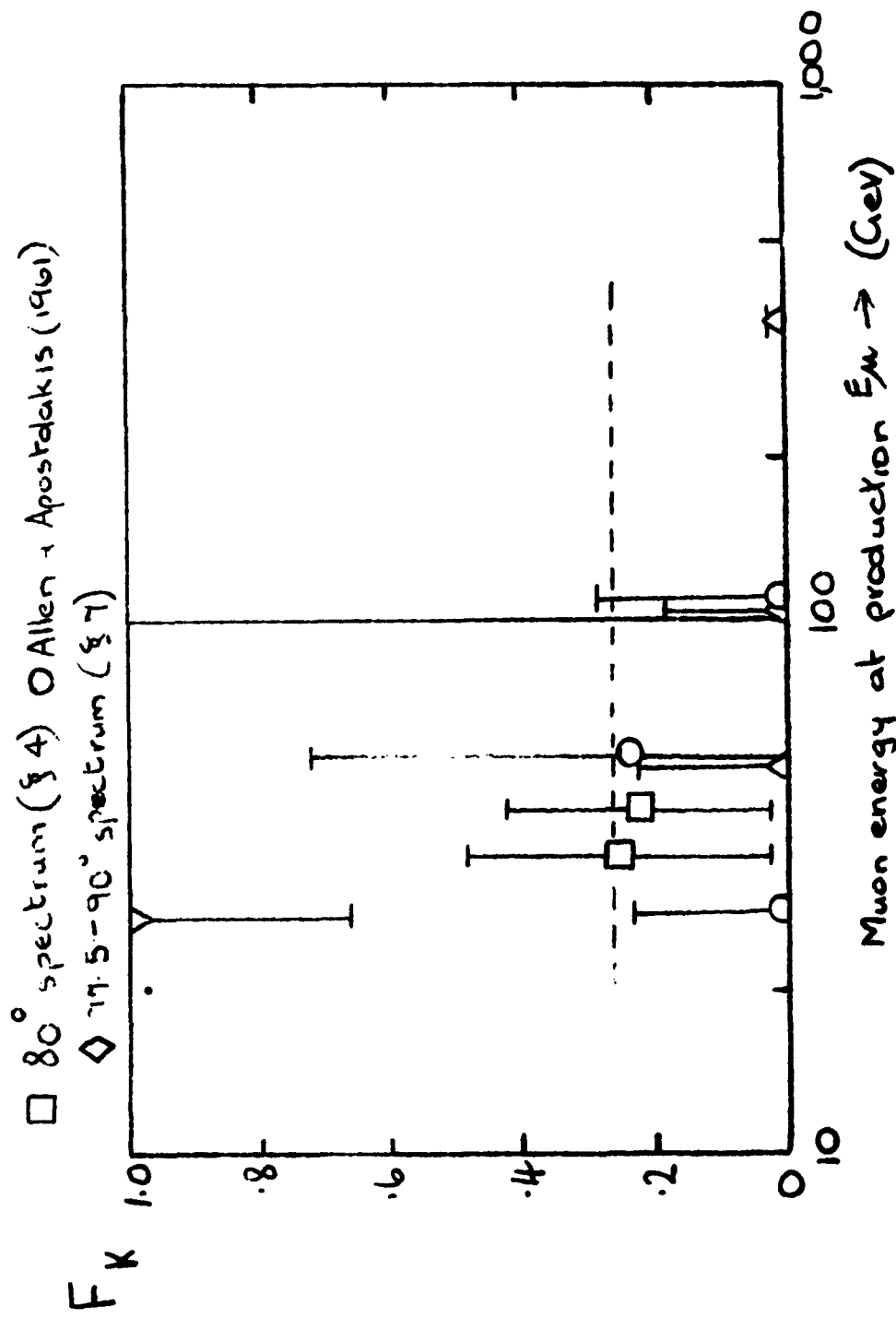
Fig 76.' The variation of F_K with muon energy for the experiments on inclined muon spectra

F_K

($K_{\pi 2} \to \pi^+ + \pi^0$; abundance 27%) which has an efficiency of about 65% for a production spectrum of the form E^{-3}. The effect is to increase the upper limit of F_K to ~0.3, that is, the ratio of all charged kaons to charged pions plus kaons has a value less than 0.3.

A further contribution to the muon flux is expected from neutral kaons, in particular through the K_1^0-mode:

$$K_1^0 \to \pi^+ + \pi^- \text{ (lifetime } 1.0 \times 10^{-10} \text{ sec)}$$
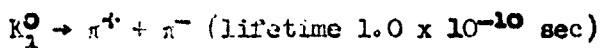
At high energies it is likely that the frequencies of production of the four states of the kaon, $K^+ K^- K^0 \bar{K}^0$, are equal and the result is that the upper limit to F_K is increased a little further.

The conclusion is that the ratio of the production of all (charged) kaons to all kaons plus pions is less than ~0.35 that is, the K/π ratio is less than ~0.55 for pion energies in the range 30-600 GeV, the corresponding range of the primary protons being approximately 700 - 30,000 GeV.

7.8 Comparison with other observations

Conclusions about the fraction of muons derived from kaons at lower energies have been made from studies of the polarization of muons at sea level and underground. A recent summary has been given by Wolfendale, (1962), leading to the conclusion that K/π ratio is <0.3 for pion energies below 16 GeV (muon energies <12 GeV), a conclusion that comes mainly from the work of Bradt and Clark (1962) and Alikhanyan et al. (1962). These indirect determinations of the K/π ratio are consistent with the direct measurement of this quantity in machine experiments. Thus, von Dardel et al. (1960), using 25 GeV protons from the CERN proton synchrotron, found a K^+/π^+ ratio in the range 0.2 - 0.3 and a K^-/π^- ratio in the range 0.04 - 0.07, the results referring to secondary particles of energies 5 to 18 GeV.
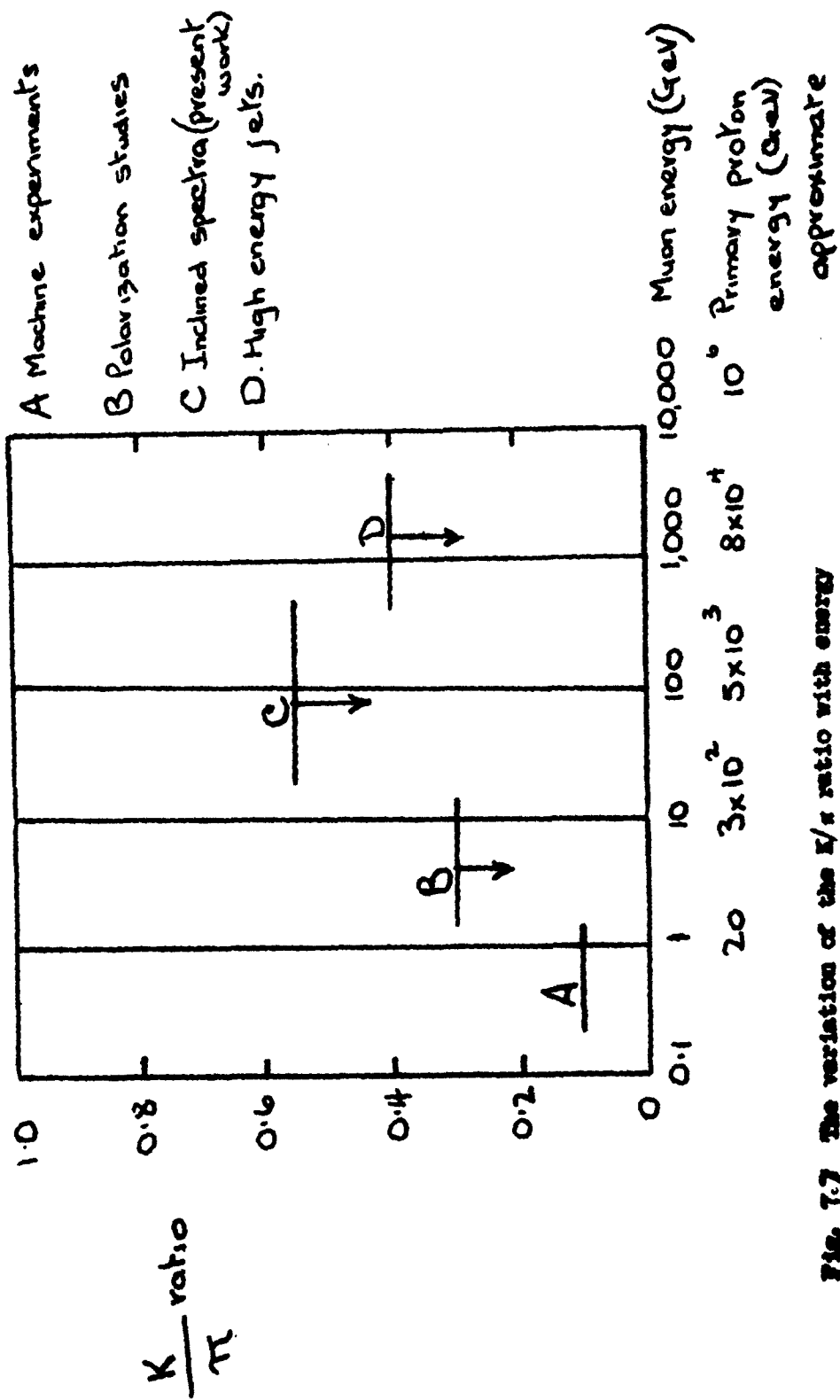
Fig. 7.7 The variation of the K/π ratio with energy

A Machine experiments

B Polarization studies

C Inclined spectra (present work)

D. High energy jets.

$\dfrac{K}{\pi}$ ratio

Muon energy (GeV)

Primary proton energy (GeV) approximate

At much higher energies studies of cosmic ray jets have shown that the K/π ratio is still comparatively low. Thus, Bowler et al. (1962) find K/π < 0.3 for the range of energy of produced particles 300 - 7,000 GeV.

Finally, in Fig. 7°7, the K/π ratios found by the various methods are shown. In addition to the energy scale for the resulting muons an estimate is made of that for the primary protons.

7.5 Conclusions

The conclusion to be drawn from this work is that the ratio of the numbers of kaons to pions (of the same energy) produced in proton-air nucleus collisions is less than 5% over the range of proton energy 700 - 50,000 GeV. Taken together with the results of other experiments it is clear that there is no evidence for a rapid increase in the K/π ratio over an energy range of primary protons extending from a few GeV to some 500,000 GeV.

The type of experiment described in this report is important in that the conclusion about the K/π ratio is made with a minimum of assumptions about nuclear processes. In this respect it is superior to both the polarization studies and the jet studies.

More extended measurements on both the inclined spectrum and the positive-negative ratio should enable closer limits to be put on the K/π ratio and an examination to be made of fluctuations in the multiplicity of produced particles at ultra-high energies.

APPENDIX 1   List of Technical Notes, with Abstracts

No. 1   Variations of the Sea Level Muon Flux

by P. V. O'Connor and A. W. Wolfendale, 26 January 1960

Abstract

The characteristics are described of a cosmic ray spectrograph which uses a solid iron magnet with Geiger counters as detecting elements. The instrument is being used to study the variations of the μ-meson flux at sea level, with direction and time, as a function of momentum.

Preliminary results are reported of the measurement of the pressure coefficient of the μ-meson flux for three bands of momenta having median values 2.9 GeV/c, 4.5 GeV/c and 8.6 GeV/c. Using a simple one-term regression formula the corresponding pressure coefficients are 0.25% mb^{-1}, 0.15% mb^{-1} and 0.11% mb^{-1}. These values bear a constant ratio to the expected coefficients, as would be expected from an analysis based on the known mechanism of the propagation of cosmic rays and the properties of the atmosphere.

No. 2   Correlation of Intensity Changes of the
Sea Level Muon Flux with Pressure Changes

by P. V. O'Connor and A. W. Wolfendale, 15 July, 1961

Abstract

A cosmic ray spectrograph has been operated near sea level for an extended period and intensity changes of the particle flux have been correlated with changes in the meteorological parameters. In particular, the variation of flux with atmospheric pressure has been examined as a function of particle momentum in the range 2 - 10 GeV/c. The results show no evidence for any appreciable departure from the theoretical predictions of Dorman (1957).

No. 3 Momentum Measurements with a Cosmic Ray Spectrograph

by F. Ashton, P.V.O'Connor and A.W. Wolfendale, 25 July, 1961.

Abstract

The characteristics of a cosmic ray spectrograph which uses a solid iron magnet as the deflecting element have already been described by O'Connor and Wolfendale (1960). The present work considers the problem of the accurate determination of the momenta of cosmic rays traversing the instrument. In particular, the magnetic and scattering deflections of muons are evaluated for the case in which momentum loss in the iron is important.

No. 4 Properties of the Earth s Atmosphere Relevant to the Interpretation

of Cosmic Ray Experiments

by F. Ashton 8 January, 1962

Appendix 2 Atmospheric mass as a function of zenith angle

A requirement of calculations on the propagation of cosmic rays in the atmosphere is the variation of atmospheric mass with zenith angle and distance from sea level.

Calculations have been made using the 'standard' atmosphere given by Rossi, (1952), which is sufficiently accurate for the range of atmospheric depths of importance to cosmic ray propagation, with the results shown in Figure A2.1 and A2.2. Figure A2.1 shows the mass of atmosphere traversed by a particle arriving at a point distance S from sea level in the direction θ, for a variety of zenith angles. Figure A2.2 gives the total mass traversed by a particle arriving at sea level; also shown is the result for the simplified case where the curvature of the earth is neglected (flat earth approximation. It is seen that the departure from the approximate result occurs at about 80°. In figure A2.3 the variation of the quantity $\frac{x}{\rho(x)}$ is plotted as a function of x, where $\rho(x)$ is the air density at atmospheric depth x. The weighted scale height of the atmosphere at zenith angle θ is given by

$$\bar{H} = \frac{\int_0^\infty \left(\frac{x}{\rho(x)}\right)_\theta \exp(-x/\lambda)dx}{\int_0^\infty \exp\left(-\frac{x}{\lambda}\right) dx}$$

and this value can be found with the aid of Fig. A2.3.
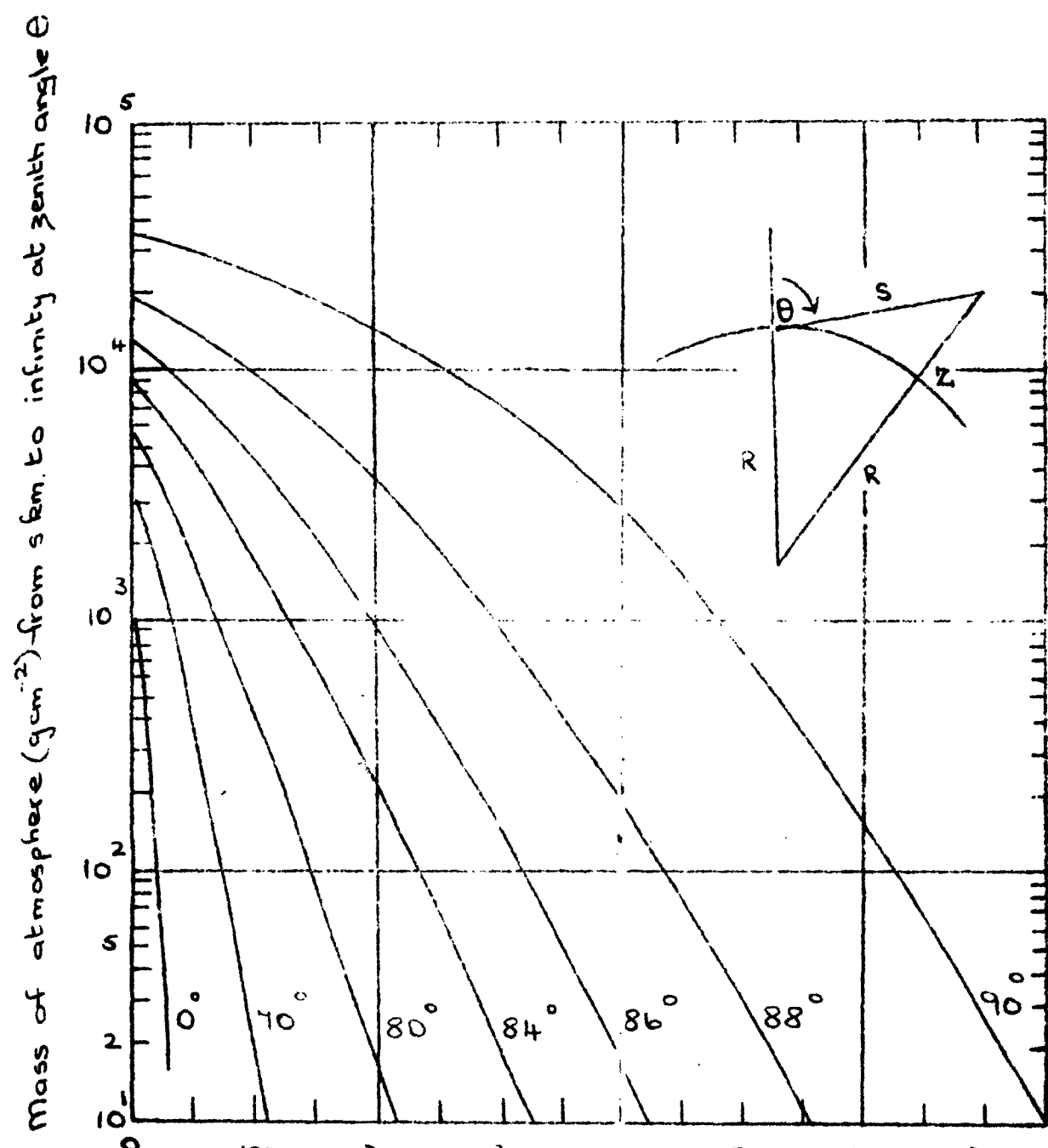
Fig. A2.1 The mass of atmosphere traversed as a function of zenith angle and distance from sea level
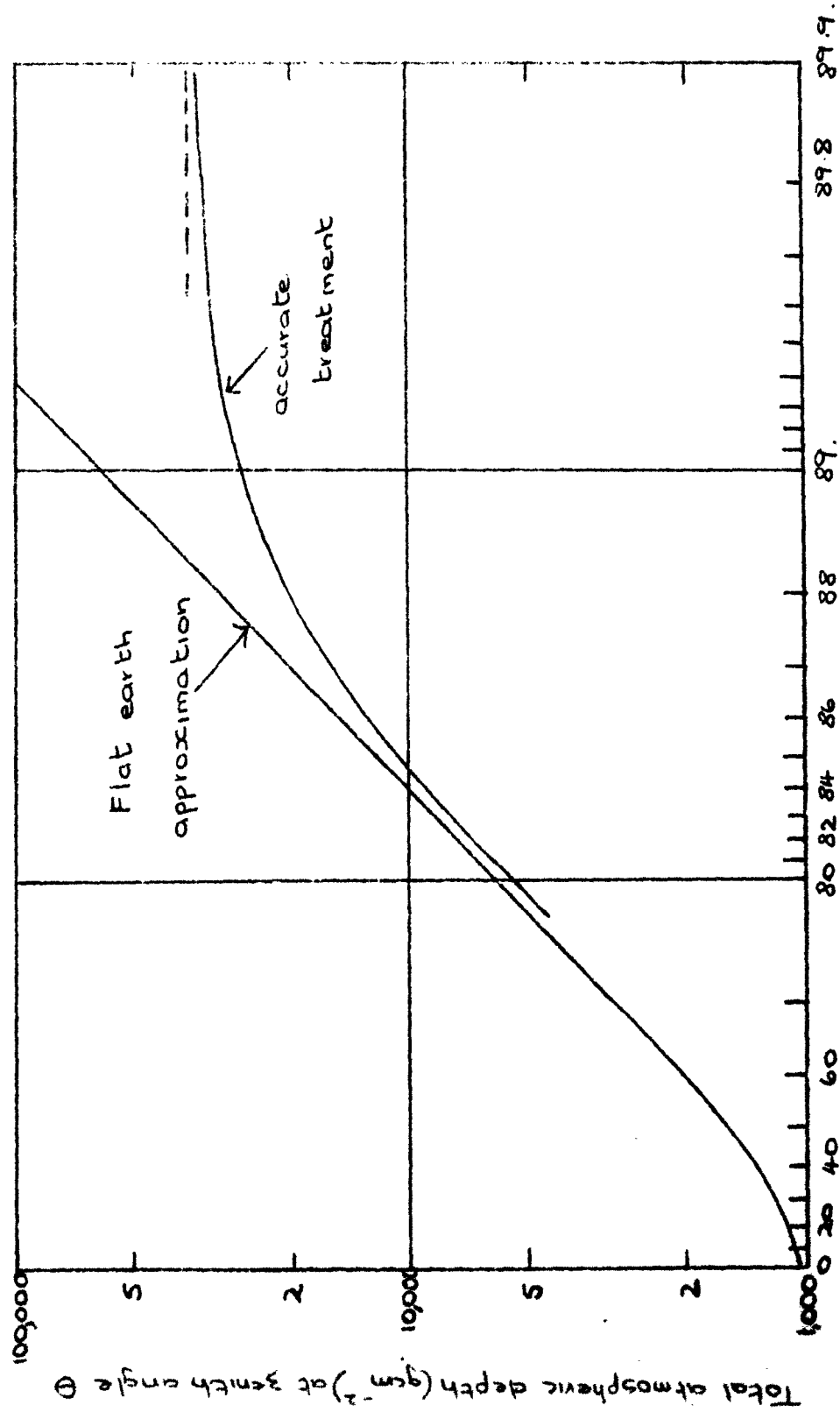
Fig. A2.2 The total atmospheric mass traversed as a function of zenith angle

Axis label (vertical): Total atmospheric depth ($g\,cm^{-2}$) at zenith angle Θ

Axis label (horizontal): Zenith angle Θ (degrees)

Curve labels: Flat earth approximation; accurate treatment
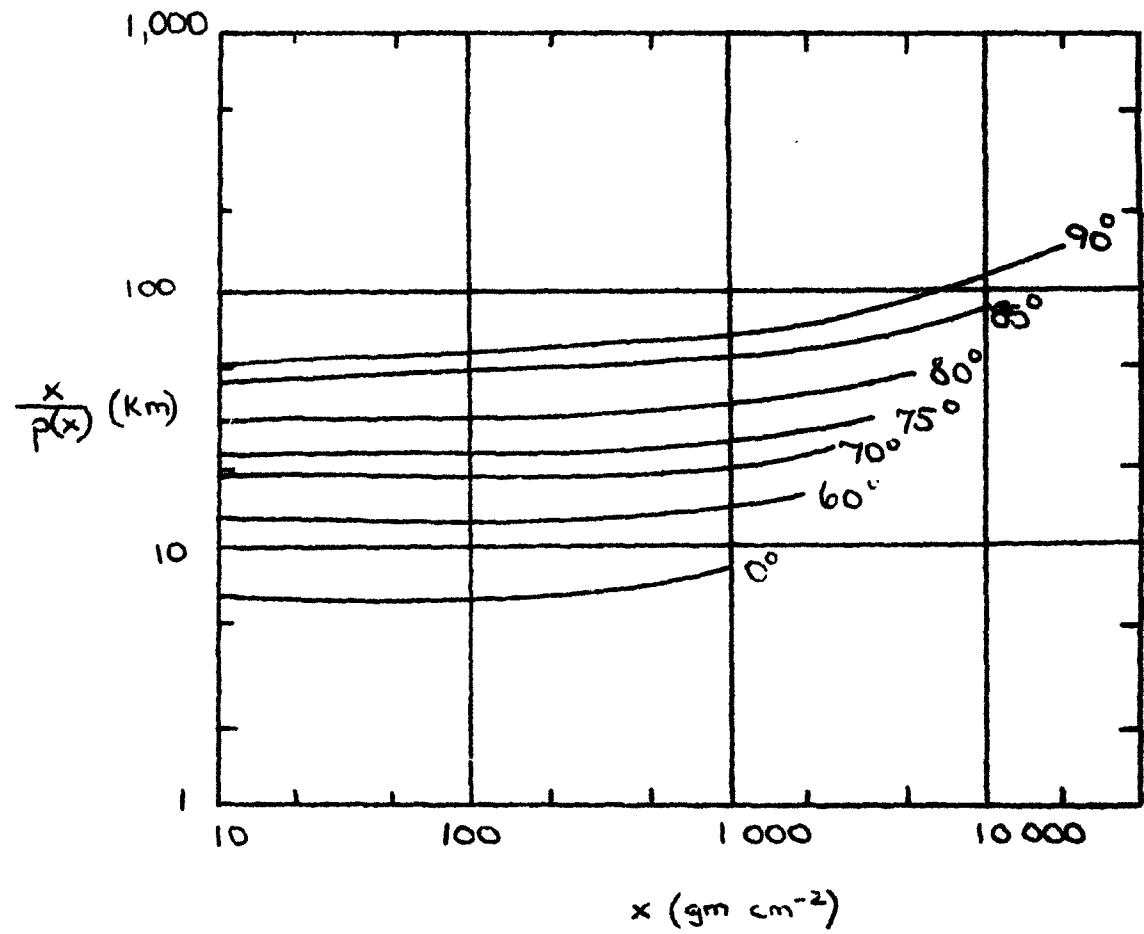
Fig. A2.3. The variation of the ratio of atmospheric depth to density with atmospheric depth.

Appendix 3 Energy Loss in the Atmosphere

If E_1 is the energy at ground level and E_2 the energy at the production level then $E_2 = E_1 + \int_o^X \frac{dE}{dx} \, dx$. The upper limit of this integral for a given zenith angle corresponds to an atmospheric depth of 120 gm cm^{-2} and can be found from figure A2.2. The variation of the energy loss of muons in air has been found by making appropriate modifications to the equation given by Ashton (1961) for the energy loss of muons in iron. In figure A3.1, $\frac{dE}{dx}$ is plotted as a function of E for three different air densities: corresponding to ground level, the production levels of muons in the vertical and in the horizontal directions.

The survival probability of a muon between atmospheric depths x_1 and x_2 at zenith angle θ is given by

$$\exp - \left\{ \int_{x_1}^{x_2} \frac{m_\mu c^2}{c \, T_o} \, \frac{1}{E(x)} \left\{ \frac{x}{\rho(x)} \right\}_\theta \frac{1}{x} \, dx \right\}$$

where m_μ and T_o are the mass and rest lifetime of the muon.

The equation has been integrated numerically and the resulting survival probability is given in Fig. A3.3.
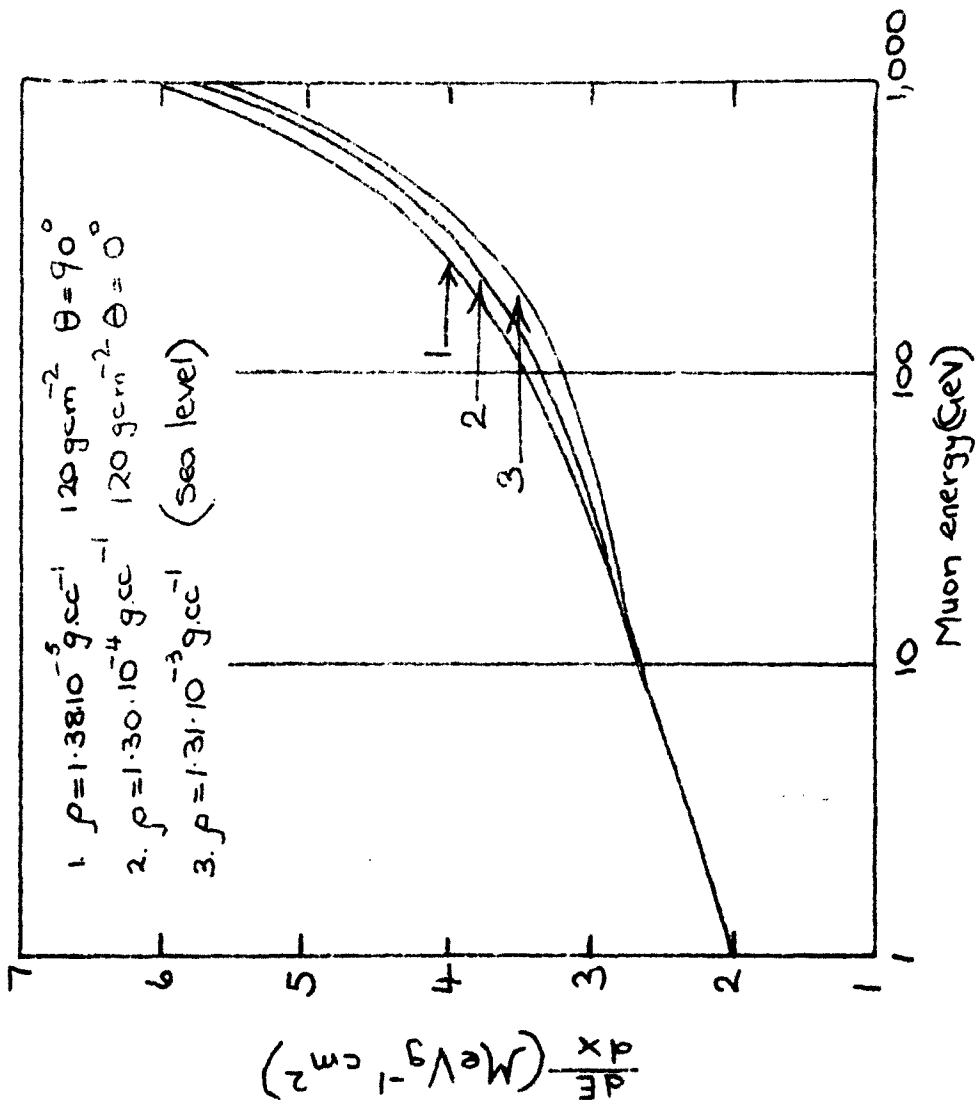
Fig. A3.1   The rate of energy loss for muons in the atmosphere.
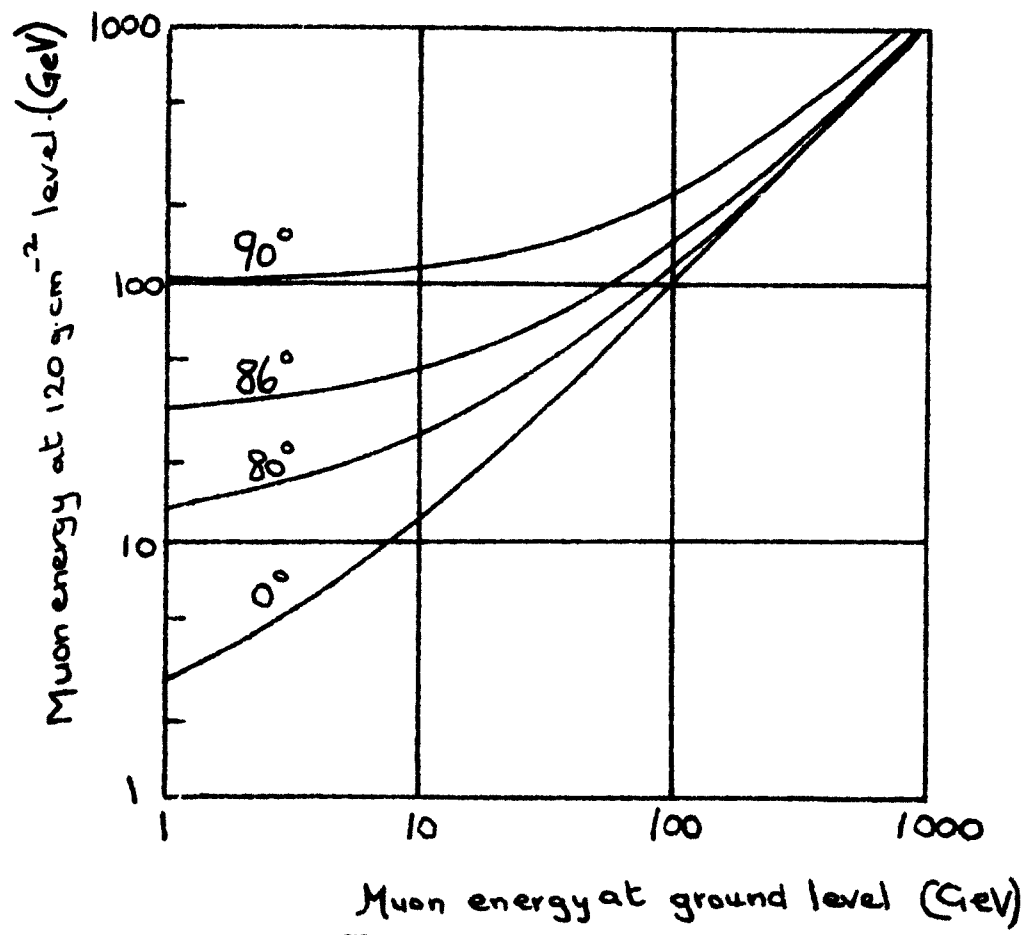
Fig. A3.2 Muon energy at production as a function of energy at ground level.
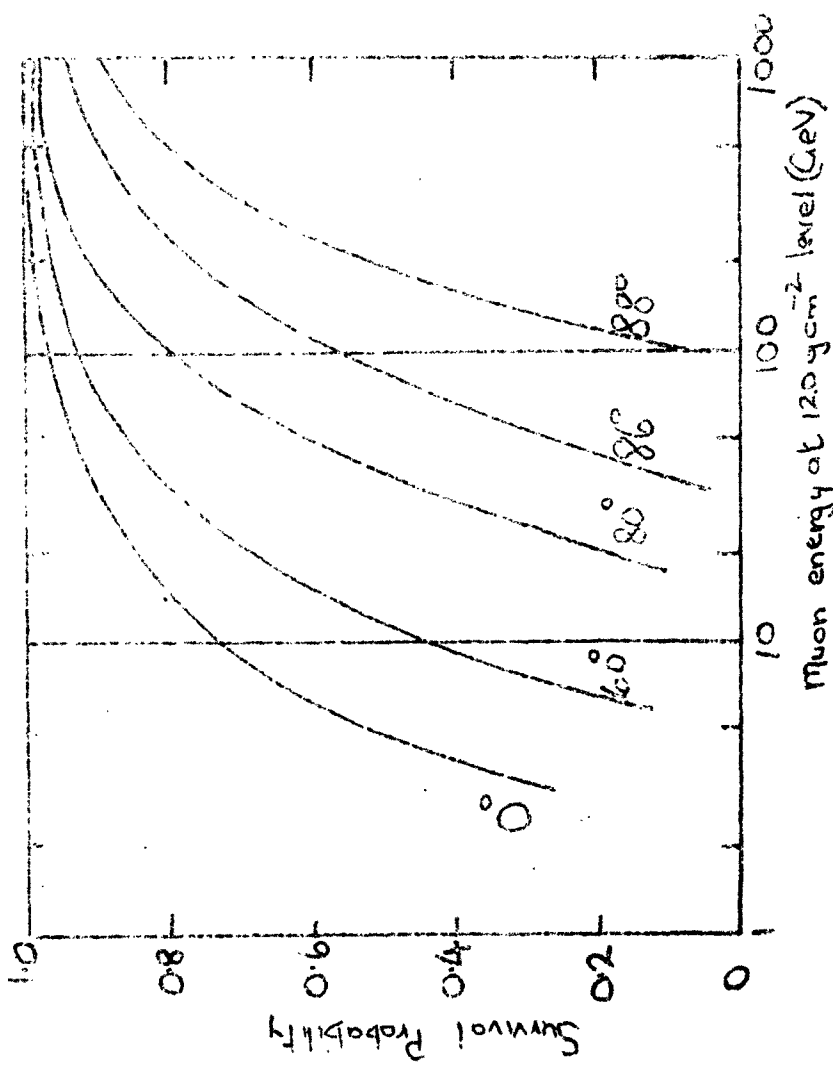
Fig A 3.3 Survival probability as a function of muon energy at production.

Appendix 4   Verification of the Scattering Constant

Consideration of the theory of the spectrograph (§4) shows that, for the magnetic induction used in the experiments, the ratio of r.m.s. scattering deflexion to magnetic deflexion is 0.30. As was mentioned in §5.7, it is possible to check this value, and to determine the magnitude of the accuracy of track location, by studying the variation of the r.m.s. value of the discrepancy, x, (Fig. A4.1) at the centre of the magnet, with momentum.

In Fig. A4.1, x is given by $x = \ell_1 \alpha_1 + \ell_1 \alpha_2 + (y - \frac{\ell \theta}{2})$ where the first two terms arise from scattering in the trays B and C and the final term arises from scattering in the magnet.

The distributions in α_1 and α_2 are Gaussians with standard deviation $7.7 \times 10^{-3} p^{-1}$ radians.

The distribution in $(y - \frac{\ell \theta}{2})$ follows from scattering theory: The probability that a particle of momentum p suffers an angular deflexion, θ (projected angle), and a projected displacement y in traversing t radiation lengths is given by:

$$P(t,y,\theta)dy d\theta = \frac{\sqrt{3}}{2\pi} \cdot \frac{\omega^2}{t^2} \exp\left\{ -\omega^2\left(\frac{\theta^2}{t} - \frac{3y\theta}{t^2} + \frac{3y^2\theta}{t^3} \right)\right\} dy d\theta$$

where $\omega = \frac{2\pi \theta}{E_s}$ and $E_s = 21$ MeV/c. (Rossi and Greisen, 1941).

From this equation the distribution in $y - \frac{\ell \theta}{2}$ is found to be a Gaussian with standard deviation $\frac{\ell}{\sqrt{12}} \langle \theta \rangle$, where $\langle \theta \rangle$ is the r.m.s. projected angle of scattering in the magnet.

It follows that the distribution in x is Gaussian, with standard deviation
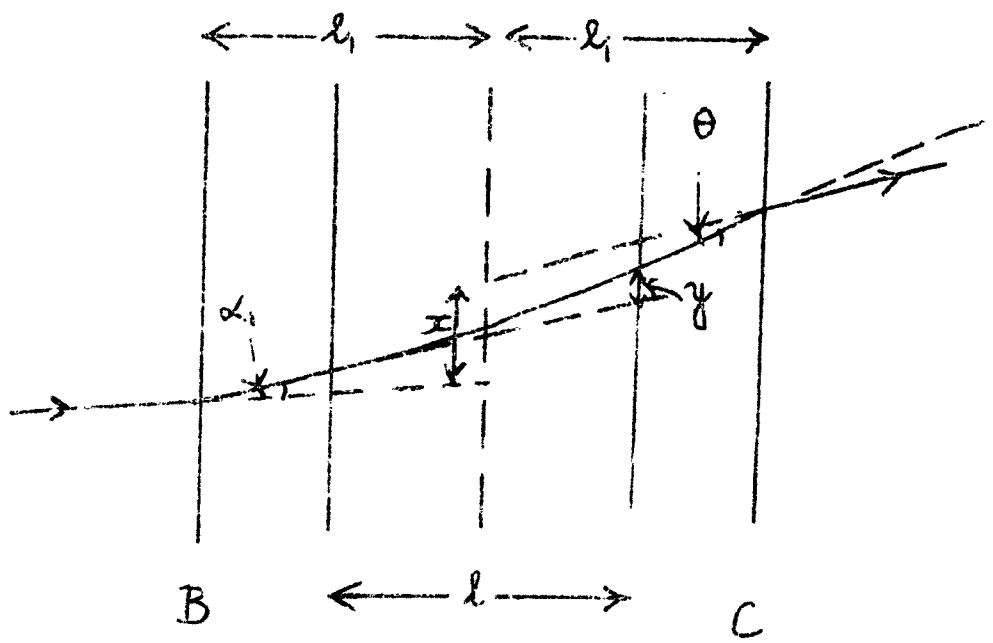
Fig. A4.1   Scattering of a particle in the magnet and flash-tube trays.

$$\langle x_{\Delta+\Delta_o} \rangle^2 = 2l_1^2 \, \sigma_\alpha^2 + \frac{l^2}{12} \langle \theta^2 \rangle + x_o^2$$

$$= (\Delta+\Delta_o)^2 \left\{ 0.0157 \, K^2 + 0.00032 \right\} + x_o^2$$

$$(\text{in units of } t.s.^2)$$

where x_o is, as in §5.7, the contribution from errors in track location.

The variation of $\langle x^2 \rangle$ with $(\Delta+\Delta_o)^2$, for particles of sufficient energy for the energy loss in the magnet to be neglected, is shown in Fig. A4.2. Also shown is the theoretical line, drawn through the weighted mean value, found assuming $K = 0.30$. The fit to the experimental points is regarded as satisfactory.

Fig. A4. 2 The variation of mean square discrepancy with mean square deflexion.
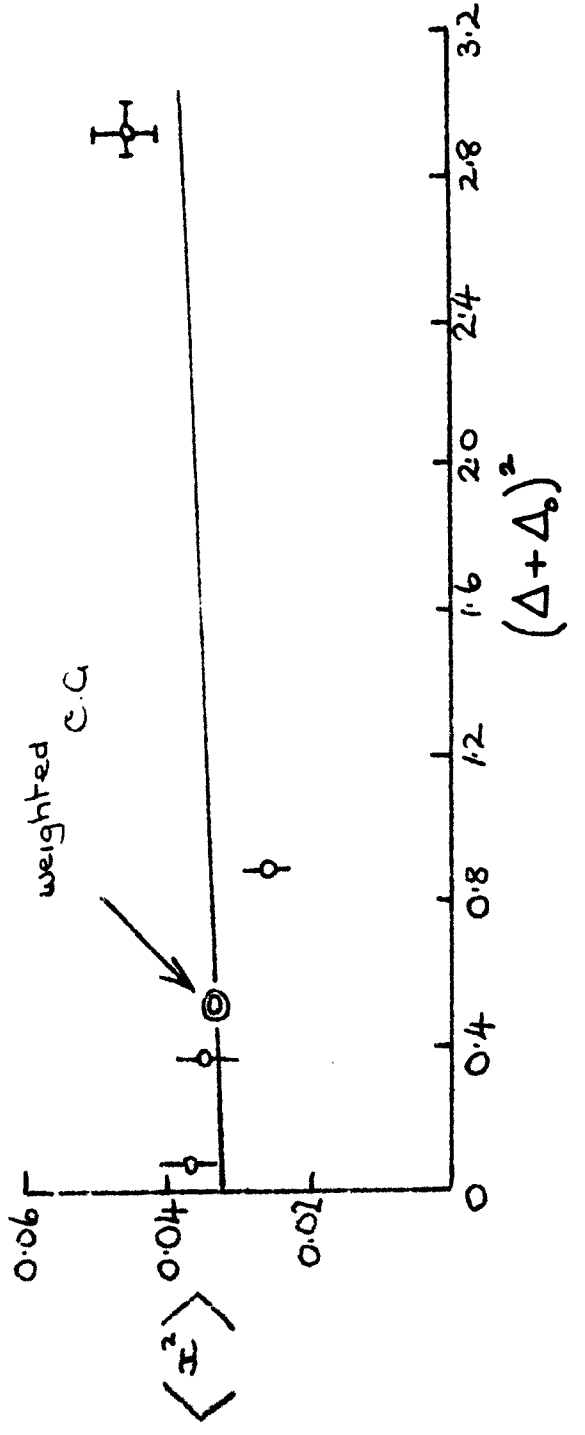
References

Alikhanyan, A.L., Asatiani, T.L., Krishchyan, V.M., Matevosyan, E.M., and
Sharkhatunyan, O.C., 1962, Proc. Int. Conf. on Cosmic Rays and the
Earth Storm, Kyoto, 1961, J. Phys. Soc. Japan, (Suppl. AIII), 17, 304.

Allen, J.E. and Apostolakis, A.J., 1961, Proc. Roy. Soc. A, 265, 117.

Ashton, F., 1961, Proc. Phys. Soc., 77, 587.

Ashton, F., Nash, W.F. and Wolfendale, A.W., 1959, Proc. Roy. Soc., 253, 163.

Ashton, F. and Wolfendale A.W., 1962, Proc. Int. Conf. on Cosmic Rays and the
Earth Storm, Kyoto, 1961, J. Phys. Soc. Japan, 17, Suppl. AIII, 313.

Bachelet, F. and Conforto, A.M., 1956, Nuovo Cim., 14, 6, 1479.

Barrett, P.H., Bollinger, L.M., Cocconi, G., Eisenberg, Y. and Greisen, K.,
1952, Rev. Mod. Phys., 24, 133.

Bennett, H.W., and Nash, W.F., 1959, Nuovo Cim., Suppl. 15, 193.

Bernadini, G., Conversi, M., Pancini, E., Scrocco, E. and Wick, G.C., 1945,
Phys. Rev., 68, 109.

Bowler, M., Duthie, J., Fowler, P., Kaddoura, A., Perkins, D.H., Pinkau, K.
and Wolter, W., 1962, Proc. Int. Conf. on Cosmic Rays and the Earth Storm,
Kyoto, 1961, J. Phys. Soc. Japan (Suppl. A III), 17, 424.

Bradt, H.V., and Clark, G.W., 1962, Proc. Int. Conf. on Cosmic Rays and the
Earth Storm, Kyoto, Japan, 1961, J. Phys. Soc. Japan (Suppl. A III) 17, 300.

Conversi, M., Pancini, E. and Piccioni, O., 1945, Phys. Rev., 68, 3.

Coxell, H., 1961, Ph.D. Thesis, University of Durham.

Coxell, H., and Wolfendale, A.W., 1960, Proc. Phys. Soc., 75, 578.

von Daruell, G., Mermal, R.M., Weber, J., and Winter, K., 1961, Proc. 10th
High Energy Nuclear Physics Conf., Rochester, 1960 (New York: Interscience)
p. 857.

Dorman, L. I., 1957, Cosmic Ray Variations (Moscow, State Publishing House).

Duperier, A., 1949, Proc. Phys. Soc., A62, 684.

Elliot, H., 1952, Progress in Cosmic Ray Physics, Ed. J.G. Wilson, (London, Pergamon Press).

Gardener, M., Jones, D.G., Taylor, F.E., and Wolfendale, A.W., 1962, Proc. Phys. Soc., 80, 697.

Hayman, P.J. and Wolfendale, A.W., 1962a, Proc. Phys. Soc., 80, 710.

1962b, Nature, London, 195, 166.

Jakeman, D., 1956, Canad. J. Phys., 34, 432.

Mathews, P.M., 1959, Canad. J. Phys., 37, 85.

Moroney, J.R., and Parry, J.K., 1954, Aust. J. Phys., 7, 423.

Myssowsky, L., and Tuwin, L., 1927, Zeits. f. Phys., 44, 369.

O'Connor, P.V., and Wolfendale, A.W., 1960, Nuovo Cim., Suppl. 2, 15, 202.

Olbert, S., 1953, Phys. Rev., 92, 454 - Phys. Rev., 96, 1400.

Pak, W., Ozaki, S., Roe, B.P., and Greisen, K., 1961, Phys. Rev., 121, 905.

Pine, J., Davisson, R.J., and Greisen, K., 1959, Nuovo Cim., 14, 1181.

Rossi, B., 1931, Nature, London, 128, 300.

1948, Rev. Mod. Phys., 20, 537.

1952, High Energy Particles (New York, Prentice Hall).

Rossi, B. and Greisen, K., 1941, Rev. Mod. Phys., 13, 240.

Sarabhai, V., Merurar, N.W., and Bhavsar, P.D., 1953, Proc. Ind. Acad. Sci., A41, 245.

Sheldon, W.R. and Duller, N.M., 1962, Nuovo Cim., 23, 63.

Sitte, K., 1961, Handbuch der Physik, 46/1, 157 (Berlin, Springer).

Perkins, D.H., 1961, CERN Conference on Very High Energy Phenomena, (Geneva, CERN), 99.

Wilson, B.G., 1959, Canad. J. Phys., 37, 19.

Wolfendale, A.W., 1962, Proc. Int. Conf. on Cosmic Rays and the Earth

Storm, Kyoto, 1961, J. Phys. Soc., Japan (Suppl. A III) 17, 358.

AF 61(052)-27

DURHAM COLLEGES,
DURHAM, ENGLAND.
REPORT
20 JAN 63

VARIATIONS OF THE SEA LEVEL MUON FLUX

F. ASHTON, J.B.M. PATTISON and A.W. WOLFENDALE

ABSTRACT: Studies of cosmic ray muons have been made with a spectrograph. The characteristics of the instrument are described. Time variations in the vertical direction are attributed to meteorological changes. Momentum spectra have been measured in the range 2-500 GeV/c for zenith angles 77.5-90°. The K/π ratio is inferred to be <0.55 for proton-air nucleus collisions of 700-20,000 GeV. The positive-

negative ratio has been confirmed at 1.2 for the muon energy range 10-200 GeV.

negative ratio has been confirmed at 1.2 for the muon energy range 10-200 GeV.

negative ratio has been confirmed at 1.2 for the muon energy range 10-200 GeV.

negative ratio has been confirmed at 1.2 for the muon energy range 10-200 GeV.